

ROLE OF COVALENT MODIFICATION OF HYALURONAN WITH INTER-ALPHA
INHIBITOR HEAVY CHAINS DURING ACUTE LUNG INJURY

Kevin Chen Ni

Submitted to the faculty of the University Graduate School
in partial fulfillment of the requirements
for the degree
Doctor of Philosophy
in the Department of Biochemistry and Molecular Biology,
Indiana University

April 2019

Accepted by the Graduate Faculty, Indiana University, in partial fulfillment of the requirements for the degree of Doctor of Philosophy.

Doctoral Committee

Irina Petrache, M.D., Co-Chair

Carmella Evans-Molina, M.D., Ph.D., Co-Chair

X. Charlie Dong, Ph.D.

October 22, 2018

Mark G. Goebel, Ph.D.

Ronald C. Wek, Ph.D.

© 2019

Kevin Chen Ni

Dedication

This thesis is dedicated to my grandparents (爷爷倪友兰, 奶奶邱克勤, 外公汤福坤, and 外婆张雪珍) and parents (Hua Ni and Bo Tang) for their work ethic and belief in education as first generation Asian-American immigrants that allowed me to grow up in USA, thrive in public schools, graduate from college, and pursue a MD/PhD degree. I also dedicate this thesis to my wife Yiting Hao, who I met just before I started my PhD journey, for how much we have grown tackling new challenges and supporting each other along the entire way.

I am indebted to many people who have provided invaluable support. I am especially indebted to my K-12 and Harvard College teachers who taught so much and challenged me in so many different ways. I am especially grateful for my math teacher Ms. Croft at Skyline High School for helping me find a lab position at University of Utah through one of her previous students, where I ended up working with two MD/PhD graduate students. I am grateful to Dean Yaw Li (now Senior VP at Merck Research) for believing in me and investing in my training. I am grateful to Aubrey Chan and Matt Smith for their patience and time with training an undergraduate with no lab experience and made countless mistakes.

Many thanks to Rachelle Gaudet at Harvard for welcoming me to such a warm and fun lab environment at a junction in my life when I did not know whether medical school and PhD admissions were still within reach. I am grateful to Dr. Gaudet for helping me fall in love with research, developing my interest in protein biochemistry, and guiding me through a rewarding two-year senior thesis journey.

Many individuals at Harvard helped me into med school. Many thanks to Jong Lee, James Michel, Jill Constantino, Barbara Cone, resident tutors, and friends (Johnny,

Sophie, and Rachel) at Cabot House and in lab (Jessica) who helped me get into med school.

Lastly, I am indebted to Raghu Mirmira, Maureen Harrington, and Jan Receveur for taking the risk in accepting and training a MSTP student who had no publications and track record for biomedical research.

Acknowledgements

This thesis would not be possible without the thoughtful support and guidance of my PhD mentor Irina Petrache, who has invested so much of her time and funds to train me and provide the nurturing environment for which I have been able to grow and thrive as a scientist. I feel very blessed to have received her support for over the course of five years, during which I put together three first-author papers and four predoctoral grant submissions. The origins of this thesis came from my efforts to secure predoctoral funding, for which Dr. Petrache provided invaluable advice and direction. I have been fortunate to have the opportunity to pursue a PhD in a lab located at one of the best lung research hospitals in the country, which Dr. Petrache made possible with her move to National Jewish Health.

I am grateful to my Biochemistry PhD committee members at IUSM (Ron Wek, Carmella Evans-Molina, X. Charlie Dong, and Mark G. Goebel) and former members (Maria B. Grant and Keith L. March) for their time, advice, support, and confidence in me. We would not have pursued and completed the endotoxic shock experiments had it not been for their feedback. I am grateful to my National Jewish Research Mentoring Committee consisting of William J. Janssen, Peter M. Henson, and Dennis R. Voelker who made available so many resources that I utilized to develop this thesis.

Numerable people at Indiana University School of Medicine and National Jewish Health have helped me greatly in lab. I would like to first thank everyone in Petrache Lab, especially Erica Beatman, Danting Cao, Kengo Koike, Andrew Mikosz, Matt Justice, Karina Serban, and Kelly Schweitzer for helping me every step of my PhD. I learned a great deal from members of the William Janssen and Lee Reinhardt labs. I am also indebted to my students who assisted me and taught me as much as much as I tried to teach them: Amar Gill, Muhammad Umair Mukhtar, Catherine Meador, and Simi Abraham. Lastly, I want to thank Jie Xie, who was co-mentored by Dr. Petrache, for his

beautiful PhD work that was the initial impetus for us to investigate the endogenous enzymatic role of TSG-6 during acute lung injury.

I am grateful to all my MSTP classmates for their advice, support, and challenging me to grow, especially Lauren Maurussich, Thao Trinh, Sherri Huang, and Jenny Lin. I am also indebted to all the upper classmates who shared their advice on everything including classes to grants.

My training would have not been possible had it not been for the generous support of T32HL091816-07 (IUSM Lung Diseases Training), 5T32GM077229-03 (IUSM MSTP), and 1F30HL136169-01A1 (NRSA to KN).

Kevin Chen Ni

ROLE OF COVALENT MODIFICATION OF HYALURONAN WITH INTER-ALPHA
INHIBITOR HEAVY CHAINS DURING ACUTE LUNG INJURY

The extracellular matrix (ECM) provides a structural and signaling platform for cells that comprise various organs, playing a critical role in tissue maintenance, injury, and repair. Hyaluronan (also known as hyaluronic acid, HA) is a ubiquitous ECM polysaccharide consisting of a repeating disaccharide backbone that can be covalently modified by the heavy chains (HC) of the serum protein inter-alpha-inhibitor (IaI) during inflammation. Known as the only covalent modification of HA, the HC linking of HA is exclusively mediated by the inflammation-induced secreted enzyme TNF α -stimulated gene-6 (TSG-6). Mice deficient for HC-HA formation, due to the lack of either TSG-6 or IaI, display reduced survival during systemic lipopolysaccharide (LPS)-induced endotoxic shock and its associated acute lung injury. We therefore hypothesized that HC-HA should play an important protective role against acute lung injury induced by intratracheal LPS or *Pseudomonas aeruginosa* (PA) gram-negative bacteria. We also identified that lung instillation of LPS or PA caused rapid induction of lung parenchymal HC-HA that was largely cleared during resolution of injury, indicative of a high rate of HA turnover and remodeling during reversible lung injury. However, using TSG-6 knockout mice, we determined that HC-HA exerted minimal protective effects against intratracheal LPS or PA-induced acute lung injury. To better address the differential roles of HC-HA during systemic versus localized intratracheal exposure to LPS, we characterized and compared the induction of HC-HA in plasma and lung in these two models. While lung parenchymal HC-HA formed in both injury models, intravascular HC-HA and TSG-6 were exclusively induced during systemic LPS exposure and were associated with improved outcomes, including decreased number of circulating neutrophils and plasma

TNF α levels. Our results suggest that LPS induces HC-HA formation in various tissues depending on the route of exposure and that the specific intravascular induction of HC-HA during systemic LPS exposure may have a protective role during endotoxic shock.

Irina Petrache, M.D., Co-Chair

Carmella Evans-Molina, M.D., Ph.D., Co-Chair

Table of Contents

List of Tables.....	xiv
List of Figures.....	xv
List of Abbreviations.....	xvi
Chapter 1. Introduction.....	1
1.1 Hyaluronan	1
1.1.1 Extracellular matrix	1
1.1.2 HA structure and synthesis	2
1.1.3 HA renewal	5
1.2 Heavy-chain modified hyaluronan	8
1.2.1 Structure	8
1.2.2 TNF α Stimulated Gene-6	11
1.3 Acute lung injury and endotoxic shock	16
1.3.1 Acute respiratory distress syndrome and acute lung injury.....	16
1.3.2 Sepsis and endotoxic shock	16
1.3.3 Mice models of ALI and endotoxic shock.....	17
1.4 Role of HA during inflammation.....	18
1.4.1 HA fragmentation	18
1.4.2 HA in inflammatory trafficking	19
1.4.3 HA in bone marrow	20
1.4.4 HC-HA in chronic lung diseases	20
1.4.5 HC-HA in endotoxic shock	21
Chapter 2. Sources of TSG-6 during ALI and endotoxic shock.....	23
2.1 Introduction.....	23
2.2 Methods.....	24
2.2.1 Reagents.....	24

2.2.2 Cell culture	24
2.2.3 Human TSG-6 (hTSG-6) western blot	27
2.2.4 hTSG-6 ELISA	27
2.2.5 Statistics.....	28
2.2.6 Measurements of messenger RNA (mRNA).....	31
2.2.7 Time-course of macrophage expression of TSG-6 in LPS-instilled mice.....	31
2.3 Results.....	31
2.3.1 TSG-6 secretion by lung resident cells	31
2.3.2 Microvascular endothelial TSG-6 expression and secretion	37
2.4 Discussion	39
Chapter 3. Rapid clearance of HC-HA during resolving ALI	41
3.1 Introduction.....	41
3.2 Methods.....	41
3.2.1 Animal husbandry	41
3.2.2 Mouse IT LPS- and PA- induced ALI	44
3.2.3 Lung parenchymal HC-HA formation	44
3.2.4 Measurements of whole lung messenger RNA (mRNA).....	45
3.2.5 HA histology.....	46
3.2.6 Histologic ALI scoring	47
3.2.7 Expression time-course of genes implicated in HA breakdown in LPS- challenged mice	48
3.2.8 HA fragmentation assessment in whole lung.....	48
3.2.9 Lung tissue HA staining and discontinuity quantification	49
3.2.10 Bronchoalveolar lavage fluid (BALF) collection and flow cytometry.....	49
3.2.11 ELISA.....	50
3.3 Results.....	53

3.3.1 Lung parenchymal HC-HA induction and clearance	53
3.3.2 HA turnover and remodeling during ALI.....	58
3.3.3 Effect of HC-HA on ALI outcomes.....	70
3.4 Discussion	77
Chapter 4. Intravascular HC-modification of HA during endotoxic shock.....	83
4.1 Introduction.....	83
4.2 Methods.....	83
4.2.1 Animal husbandry	83
4.2.2 Mouse endotoxic shock model.....	83
4.2.3 Mouse IT LPS-induced ALI model	84
4.2.4 Plasma collection and lung perfusion	84
4.2.5 Lung parenchymal and plasma HC-HA levels	84
4.2.6 Whole lung mRNA analysis	84
4.2.7 TSG-6 activity assay	85
4.2.8 Analysis of plasma by flow cytometry	85
4.2.9 Mouse TNF α ELISA.....	86
4.3 Results.....	86
4.3.1 Effect of TSG-6 on survival during endotoxic shock	86
4.3.2 Lung parenchymal HC-HA formation after endotoxic shock	86
4.3.3 Intravascular HC-HA and TSG-6 induction after endotoxic shock	91
4.3.4 Vascular markers of inflammation in <i>TSG-6</i> KO mice.....	91
4.4 Discussion	97
Chapter 5. Conclusion.....	103
5.1 Summary	103
5.2 Future directions.....	111
References	115

Curriculum vitae

List of Tables

Table 1-1. Offspring of <i>TSG-6</i> breeding pairs	15
Table 3-1. Genotyping of <i>TSG-6</i> mice	43

List of Figures

Figure 1.1. HA structure	3
Figure 1.2. TSG-6 transesterification reactions.....	10
Figure 1.3. Conservation of TSG-6 serine residue that catalyzes HC-HA formation	14
Figure 2.1. hTSG-6 ELISA standard curves.....	30
Figure 2.2. TNF α or LPS induction of TSG-6 in lung cells	34
Figure 2.3. TSG-6 expression in mouse AM during ALI.....	36
Figure 2.4. Inflammatory induction of HMVEC-L TSG-6 secretion and expression	38
Figure 3.1. Flow cytometry analysis of broncholarveolar lavaged leukocytes.....	52
Figure 3.2. Lung parenchymal HC-HA formation after LPS or PA injury.....	55
Figure 3.3. Distribution of HC and HA staining after PA injury	57
Figure 3.4. Lung HA molecular weight distribution after LPS injury	60
Figure 3.5. Effect of TSG-6 on lung HA molecular weight and lavage levels.....	62
Figure 3.6. Morphological changes in interstitial HA staining after LPS injury	63
Figure 3.7. HA staining after LPS injury	65
Figure 3.8. Effect of ALI on genes implicated in HA synthesis and breakdown	69
Figure 3.9. Effect of TSG-6 on severity and resolution of LPS-induced ALI	72
Figure 3.10. Effect of TSG-6 on histological injury scores of LPS-induced ALI	75
Figure 3.11. Effect of TSG-6 on severity and resolution of PA induced ALI.....	76
Figure 4.1. Effect of TSG-6 on survival during endotoxic shock	88
Figure 4.2. Lung parenchymal HC-HA after IP and IT LPS injury	89
Figure 4.3. Plasma HC-HA and TSG-6 activity after IP and IT LPS injury	93
Figure 4.4. Effect of TSG-6 on circulating PMN and plasma TNF α	95
Figure 5.1. Sources of TSG-6 during respiratory infection and sepsis.....	108
Figure 5.2. Schematic of PMN trafficking during localized vs. systemic infection.....	109
Figure 5.3. Potential mechanisms of HC-HA's protective effects during sepsis/shock .	110

List of Abbreviations

ALI acute lung injury

AM alveolar macrophage

ARDS acute respiratory distress syndrome

ASC adipose stem and progenitor cell

BALF bronchoalveolar lavage fluid

BSA bovine serum albumin

CEMIP cell migration inducing and HA binding protein

CFU colony forming unit

CUB complement C1r/C1s, Uegf, and bone morphogenetic protein

DAMP damage-associated molecular pattern

DAPI 4',6-diamidino-2-phenylindole

DMEM Dulbecco's Modified Eagle Medium

dpi days post injury

E. coli *Escherichia coli*

ECM extracellular matrix

EDTA ethylenediaminetetraacetic acid

ELISA enzyme-linked immunosorbent assay

FBS fetal bovine serum

g g-force

GAG glycosaminoglycan

GlcNAc N-acetylglucosamine

GlcUA D-glucuronic acid

h hour

HA hyaluronan

HA₁₀ 10-oligosaccharide HA

hAM human alveolar macrophage
HARE HA receptor for endocytosis
HAS hyaluronan synthase
HAse hyaluronidase treatment
HC heavy chain
HC-HA HC-modified HA
HMW high molecular weight
HRP horseradish peroxidase
HT heterozygote
HYAL hyaluronidase
IACUC Institutional Animal Care and Use Committee
IL1 β interleukin 1 β
IP intraperitoneal
IRB institutional review board
IT intratracheal
I α I Inter-alpha-inhibitor
kDa kiloDalton
KO knockout
LMW low molecular weight
LPS lipopolysaccharide
min minute
MSC mesenchymal stem cell
OCT optimal cutting temperature
PA Pseudomonas aeruginosa
PAMP pathogen-associated molecular pattern
PBDM peripheral blood monocyte-derived macrophage

PBMC peripheral blood monocyte cell

PBS phosphate buffered saline

PFA paraformaldehyde

PMN polymorphonuclear cells

PTX3 pentraxin-related protein 3

RAGE receptor for advanced glycation end products

RNA-seq RNA-sequencing

ROS reactive oxygen species

RPMI Roswell Park Memorial Institute

S. hyaluronolyticus *Streptomyces hyaluronolyticus*

SDS-PAGE sodium dodecyl sulfate polyacrylamide gel electrophoresis

TBS tris-buffered saline

TBW total body weight

TLR4 toll-like receptor 4

TMEM2 transmembrane protein 2

TNF α tumor necrosis factor α

TRU turbidity reducing unit

TSG-6 TNF α stimulated gene-6

U unit

vWA von Willebrand type A

WT wildtype

Chapter 1. Introduction

1.1 Hyaluronan

1.1.1 Extracellular matrix

The extracellular matrix (ECM) is the meshwork of proteins and polysaccharides secreted and maintained by cells. The function of the ECM is not only to provide structural support, but also to supply an interface for the intricate cell-to-cell communications and interactions that have allowed multicellular organisms to evolve into highly advanced vertebrates. An essential component of the ECM is a family of large unbranched polysaccharides known as glycosaminoglycans (GAG) consisting of a repeating disaccharide sequence [1].

GAGs are present in most organisms within the kingdom Animalia, and these polysaccharides have affected evolution at both the cellular and organismal levels. The glycotransferase enzymatic machinery capable of synthesizing GAG polymer chains [1] appeared early during the inception of invertebrate animals [1, 2]. These proteins are typically transmembrane proteins anchored at the Golgi apparatus, which would append GAG chains to proteins headed to the plasma membrane or secreted extracellularly. With the evolution of the earliest chordate predecessors of vertebrates, the transmembrane protein encoding an enzyme capable of synthesizing hyaluronan (also known as hyaluronic acid, HA) is thought to have evolved from a preexisting GAG glycotransferase [3]. HA synthase was unique for also encoding the machinery for concomitantly extruding HA out of the plasma membrane into the extracellular space as HA was being synthesized [4]. With the advent of the earliest vertebrates, a number of proteins emerged with Link protein domains that bind HA [3]. The Link domain consists of two anti-parallel triple-stranded β -sheets and two α -helices that form a compact fold with a hydrophobic core and surface HA-binding groove [5-7]. This structure is present in each of the key vertebrate HA-binding proteins including the cartilage proteoglycan

aggrecan, lymphatic vessel endothelial HA receptor 1 (LYVE1), scavenger receptor stabilin-2, and cell-surface adhesion receptor CD44. With the Link domain's ability to bind HA, the earliest vertebrates were able to utilize HA and co-evolve specialized functions with these Link bearing proteins, allowing HA to serve a range of essential structural [8], developmental [9, 10], and immunological [11] roles that feature cell-cell and cell-ECM interactions [12]. An example of HA acquiring indispensable roles is the developmental requirement of hyaluronan synthase 2 (HAS2) in mice, where cell-HA interactions facilitate cell migration and cell-fate specification events required for cardiac morphogenesis [10].

1.1.2 HA structure and synthesis

The GAG family of unbranched polysaccharides consists of alternating sequence of a uronic sugar or galactose (glycos) and an amino sugar (aminoglycan) as implied by its name [1]. The repeating disaccharide of HA (**Figure 1.1A**) consists of the uronic sugar, D-glucuronic acid (GlcUA), and the amino sugar, N-acetylglucosamine (GlcNAc), joined by a β -(1→3) glycosidic link. GlcNAc and the next GlcUA are joined by a β -(1→4) glycosidic link [1]. High molecular weight (HMW) HA as large as 10 megaDalton in size is found in the synovial fluid with the large HA containing upwards of 30,000 of the disaccharide repeats [13, 14]. When mixed with water, HA forms a viscoelastic solution occupying enormous hydrodynamic volume. The water uptake has been attributed to the amino and carboxylate side groups present on the amino sugar and hexuronic acid, respectively, which function together to bind and retain water (**Figure 1.1B**). Because of these unique biochemical properties, HA makes important contributions to essential cellular processes that require the ECM, such as cell migration, differentiation, and proliferation [15].

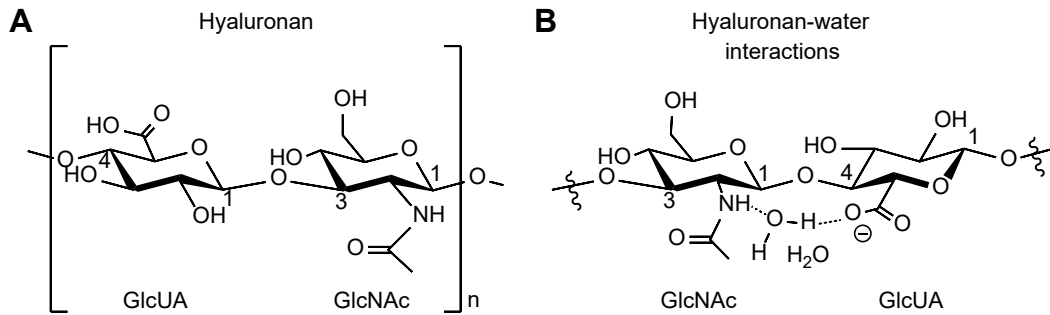


Figure 1.1. HA structure

A. As a GAG, HA is a linear (unbranched) polysaccharide chain consisting of a repeating disaccharide sequence. The HA disaccharide sequence consists of D-glucuronic acid (GlcUA) and N-acetylglucosamine (GlcNAc) joined by a β -(1 \rightarrow 3) glycosidic link. The glycosidic links alternate between β -(1 \rightarrow 3) and β -(1 \rightarrow 4) along the chain. Note the absence of sulfate modification on the free hydroxyl groups. **B.** In the presence of water, HA forms hydrogen bonds with water through its amide and carboxylate side chains.

Besides HA, the other four members of the GAG family of polysaccharides are heparin sulfate, chondroitin sulfate, dermatan sulfate, and keratan sulfate. As their names suggest, the hydroxyl side groups at different positions on the saccharide units of these GAGs can be modified by a sulfate group [1]. Additionally, these GAGs are typically covalently linked to a core protein and exist as proteoglycans throughout the body. Since the sulfation can vary appreciably between any two chains, these GAGs encode tremendous molecular heterogeneity. Further diversity and functionality are achieved when multiple GAGs are attached the same core protein. In striking contrast, HA is homogenous with the only variable being the size of the polysaccharide, because the saccharides of HA are not sulfated and are not linked to any core protein. The reason for this has to do with how HA polysaccharide is not synthesized within the endoplasmic reticulum and Golgi apparatus like other GAGs, but rather HA is uniquely synthesized at the inner plasma membrane and extruded into the extracellular space as it is being made [12]. This unique HA property allowed cells to bypass the size constraints of synthesizing GAGs within endoplasmic reticulum and Golgi apparatus. Consequently, HA is the largest GAG macromolecule in the ECM. Whereas the typical size of HMW HA present in uninjured tissue is greater than 1 megaDalton, all other GAGs are less than 50 kiloDalton (kDa) [16].

In mammals, there are three homologous membrane proteins encoding HA synthases (HAS1-3) that synthesize and extrude HA at the plasma membrane [17]. The disaccharide repeat sequence is generated by sequential transfer of an intracellular pool of nucleotide activated GlcUA and GlcNAc to the growing polysaccharide chain. The three HAS have different rates of synthesis and generate HA of different size distributions with HAS2 generating the largest HA (>2 megaDalton) [18, 19] and HAS3 generating the smallest HA (100-100 kDa) [18]. Whereas all three HAS are expressed in mice during development and postpartum [17, 20], only HAS2 deficiency is

embryonically lethal due to defects in cardiac morphogenesis [10]. Additionally, *HAS3* knockout (KO) mice and tissue-specific *HAS2* KO mice that bypass the earlier *HAS2*-KO cardiac lethality have defects in other organs [21, 22], which implicate cell-HA interactions in a diverse range of developmental processes. In contrast, the developmental and physiological roles of *HAS1* remain undefined, likely because *HAS1* is the least physiologically active of the three requiring very high intracellular concentrations of nucleotide activated GlcNAc for synthesizing HA [19].

Bacterial glycosyltransferases capable of synthesizing specific GAG have been found in various microbes [2]. Bacterial glycosyltransferases are present for all GAGs except keratan and they are more likely to have emerged by convergent evolution rather than by horizontal genetic transfer of GAG synthases from animals. Typically, bacterial-synthesized GAG are different from their animal-synthesized counterparts, because they do not undergo sulfation and epimerization modifications. However, due to the lack of modifications in vertebrate HA, bacterial-synthesized HA is biochemically identical to their vertebrate-counterparts and thus non-immunogenic, which likely provided the selection pressure in various *Pasteurella* and *Streptococcus* strains for synthesizing HA capsules to evade the host immune system [23].

1.1.3 HA renewal

HA is notable for its continuous synthesis and degradation during homeostasis that allows each tissue to achieve its characteristic molecular weight size distribution and level of HA. It has been estimated that up to a third of the total HA mass in the human body undergoes turnover every day [24]. In the lung, an estimated 5% of interstitial HA is turned over each day, which can increase with *Escherichia coli* (*E. coli*) bacteremia [25, 26]. Continuous turnover occurs locally in peripheral tissues and also systemically when interstitial HA in peripheral tissues is drained as lymph to lymph nodes and systemic circulation, where it is primarily catabolized by the liver, but also taken up in smaller

amounts by the kidney and spleen [24]. The clearance of circulating HA is rapid with a half-life of only 2.5-5 min [27, 28] and is primarily mediated by liver sinusoidal endothelial cells that efficiently endocytose and catabolize HA in lysosomes [29]. In contrast, the turnover of HA in peripheral tissues is several magnitudes slower [30] and varies with location [31].

Hyaluronidases 1 and 2 (HYAL1-2) are the key hyaluronidases expressed in mammalian somatic tissue [32]. *HYAL1-2* encode endoglycosidases that cleave internal β -(1 \rightarrow 4) glycosidic links between disaccharide repeats. Comparative analyses of *HYAL1* and *HYAL2* KO mice implicate both enzymes as critically important for homeostatic HA turnover [29]. *HYAL2* is a membrane glycosylphosphatidylinositol-linked hyaluronidase essential for clearing HMW HA by degrading HMW HA into smaller 20 kDa fragments that can be readily endocytosed by liver sinusoidal endothelial cells for lysosomal breakdown into monosaccharides [29, 33]. The exact mechanism of *HYAL2*-mediated cleavage has been debated, but likely involves several plasma membrane proteins working in concert to degrade HA: CD44 for binding HA [34-36] and a Na⁺-H⁺ exchanger that acidifies the local environment for optimal *HYAL2* activity [33]. With *HYAL2* deficiency, HA is not broken down into the 20 kDa fragments that can be readily endocytosed and lysosomally degraded by hepatic sinusoidal endothelium, which causes the accumulation of HMW HA in peripheral tissues and especially overloads the lymph nodes and systemic circulation that drain the HA in peripheral tissue [29, 33]. *In utero*, this abnormal accumulation of oversized HA leads to craniofacial and heart developmental defects in both *HYAL2* KO mice and humans [37-39], which implicates proper HA input in these morphogenetic processes [10].

In contrast, *HYAL1* is a secreted and endocytosed hyaluronidase that has optimal activity in acidic lysosomes when the pH is 3.8 [40, 41]. *HYAL1* deficiency leads to a lysosomal storage disorder [42] characterized by significant HA accumulation in the

liver sinusoids and minor increases in peripheral tissue, lymph nodes, and plasma [29]. In both mice and humans, the typical presentation of HYAL1 deficiency is joint inflammation due to abnormal joint macrophages and fibroblasts that have lysosomes overloaded with HA [43, 44]. With the relative absence of developmental defects in both mice and humans and less HA accumulation outside the liver as compared to HYAL2 deficiency [42, 43, 45], it has been suggested that HYAL1 deficiency can be partially compensated for by lysosomal exoglycosidases β -hexosaminidase and β -glucuronidase, which catabolize HA by removing terminal saccharides instead of targeting the internal glycoside links, as in the case of HYAL1-2 [46].

It was recently discovered that there are two related proteins in humans that can degrade HMW HA: transmembrane protein 2 (TMEM2) and cell migration-inducing and HA binding protein (CEMIP, also known as KIAA1199), which feature domains homologous to bacterial polysaccharide lyases, but have no homology to *HYAL1-2* and other hyaluronidase-like genes, can promote HA breakdown [47]. While TMEM2 is a membrane protein that can directly cleave extracellular HMW HA [47], CEMIP is a secreted HA-binding protein that promotes HA-binding and endocytosis [48, 49]. During development, TMEM2-mediated HA degradation has been implicated in angiogenesis in zebrafish [50], and mutations in the *CEMIP* gene that impair the ability of its encoded product to endocytose and clear HA lead to hearing defects in humans [48]. The role of these two proteins in HA turnover in adult tissues is unclear, but CEMIP may play a role in homeostatic HA turnover in human skin fibroblasts [48]. Another protein implicated in HA-binding and endocytosis is the scavenger receptor stabilin-2 (also known as HA receptor for endocytosis, HARE) [51]. Highly expressed in liver sinusoidal endothelial cells for systemic HA clearance by endocytosis, *Stabilin-2* KO mice exhibited an increased accumulation of HA in plasma [52].

1.2 Heavy-chain modified hyaluronan

1.2.1 Structure

The repeating disaccharide backbone of HA is unique for its ability to be modified with a polypeptide. While the other glycosaminoglycans are attached to proteoglycan core proteins *via* a saccharide linker, their disaccharide backbone cannot be modified by peptide and instead obtain their unique functionality through sulfation. The modification of HA with the heavy-chains (HC) of the serum protein inter-alpha-inhibitor (IαI) is the only known covalent modification of HA (**Figure 1.2A**). The discovery of the addition of the HC polypeptide to HA was first made when HA isolated from the synovial fluid of inflamed joints was found to be complexed with protein matching serum IαI, which was noticeably absent in healthy joints [53]. This specific presentation of HC-modified HA (HC-HA) in tissue during inflammation coincides with two events typically associated with inflammation and both of these events are critical for the catalysis of this HC-HA covalent modification. The first event required for forming the HC-HA modification is the induction of the tumor necrosis factor α (TNF α) stimulated gene-6 (TSG-6) enzyme responsible for catalyzing the modification (**Figure 1.2B**). The second required event is the inflammation-induced vascular leak of the serum IαI that serves as the enzymatic substrate.

TSG-6 catalyzes the covalent modification *via* two transesterification reactions (**Figure 1.2C**). During the first reaction, TSG-6 removes a HC from the serum protein inter-alpha-inhibitor (IαI) to form a TSG-6-HC intermediate. In the presence of HA, TSG-6 then transfers the HC to HA to form HC-modified HA and TSG-6 is regenerated and available to catalyze another covalent modification [54]. This covalent modification specifically occurs at the C6 hydroxyl group of the GlcNAc saccharide of HA [55].

Figure 1.2. TSG-6 transesterification reactions

A-B. HA is a linear polysaccharide with a repeating disaccharide sequence: GlcUA (green) and GlcNAc (orange). HA can be covalently modified with the heavy-chains (HC; blue ovals) of inter-alpha-inhibitor (Ial). The covalent modification is exclusively mediated by the enzyme TNF α stimulated gene-6 (TSG-6). TSG-6 is a secreted protein consisting of HA-binding Link and CUB domains. Ial contains a chondroitin sulfate polysaccharide chain that is covalently linked with a HC1, HC2, and light chain protein known as bikunin. Cartoon by Ni et al. [56], open source. **C.** Schematic representation of the two transesterification reactions mediated by TSG-6 enzyme, adapted from [54]. A conserved serine residue on TSG-6 is responsible for carrying out the two reactions. In the first reaction, the TSG-6 serine removes a HC from Ial by forming an ester bond with the terminal aspartate of HC. In the second reaction, the TSG-6-HC intermediate modifies the C6 hydroxyl of a GlcNAc present in HA with HC and regenerates TSG-6, so that it can catalyze another modification. Besides TSG-6 enzyme and Ial substrate, the two transesterifications only require the presence of divalent metal cations (Mg²⁺ and Ca²⁺) [57-59]. The energy for the reaction is stored in Ial at the HC-chondroitin sulfate bond [57].

IaI is a serum protein consisting of two HC (HC1 and HC2) proteins and a light chain protein known as bikunin attached to the same chondroitin sulfate polysaccharide chain [60]. Like most serum proteins, IaI is assembled inside hepatocytes and secreted by the liver. IaI was initially recognized as a protease inhibitor due to bikunin being a Kunitz-type serine protease inhibitor. However, interest has turned to the characterization of HC-ECM interactions and the systemic role of the two HCs, because bikunin's physiologic role as a protease inhibitor role is likely relatively minor [61]. HCs contain one von Willebrand type A (vWA) domain, also seen in many other ECM proteins [60, 62], that allow it to bind various other ECM components like vitronectin [63]. The finding that HC regulates complement [64, 65] and neutrophil [66] activation suggests that HC has important roles during systemic inflammation. In this context, HC-HA may provide a scaffold that binds inflammatory cells expressing the HA receptor CD44 and promotes their undergoing HC-mediated effects.

1.2.2 TNF α Stimulated Gene-6

TSG-6 was first discovered in TNF α -treated foreskin fibroblasts [67] as an inflammation-induced secreted protein. The proinflammatory cytokines TNF α and interleukin 1 β (IL1 β) were soon identified as the key inflammatory stimuli for *TSG-6* gene transcription in non-hematopoietic cells [68]. Both cytokines promote transcriptional factor binding at essential NF-IL6 binding sites and a secondary AP-1 site in the *TSG-6* promoter, which collectively serve to enhance *TSG-6* transcriptional expression [69, 70]. The TSG-6 protein consists of a HA-binding Link domain and a complement C1r/C1s, uegf urchin epidermal growth factor, and bone morphogenetic protein 1 (CUB) domain. Like other proteins bearing a Link domain for binding HA, TSG-6 appeared in the earliest vertebrate ancestor [3]. TSG-6 features a serine residue, which is adjacent to the Link domain, that is responsible for removing HC from IaI. The importance of the association of HC with TSG-6 is emphasized by the finding that the catalytic TSG-6 serine is

evolutionarily conserved in all vertebrates from fish to mammals (**Figure 1.3**) [71, 72].

The Link domain in TSG-6 has an extremely high affinity for HA, much higher than the Link domain in the cell-surface adhesion receptor CD44 [73], which may allow TSG-6 to effectively bind HA and repeatedly modify it during inflammation [74].

Like the Link domain, the CUB domain of TSG-6 is also well conserved and essential for HC-HA formation [75]. Specifically, the TSG-6 CUB domain promotes the Ca^{2+} -dependent non-covalent interaction of TSG-6 with the Mg^{2+} -binding vWA domains present on *Ial*'s HCs. This TSG-6 engagement with the vWA domain, which is the first step in forming the TSG-6-HC covalent intermediate [58], is the likely reason for the TSG-6 enzymatic requirement for the divalent metals Mg^{2+} and Ca^{2+} . It has also been proposed that the CUB domain may facilitate dimerization of HA-bound TSG-6, which has implications on how TSG-6-binding of HA can potentially reorganize HA ultrastructure [75].

The evolutionarily conserved role of TSG-6 in covalently modifying HA was established in mice with the discovery that oocyte release from the ovary required its surrounding HA-rich matrix to be covalently modified with HC. Both TSG-6 and *Ial* deficiency led to identical phenotypes of complete infertility due to lack of HC-HA in the cumulus ECM surrounding the oocyte [76, 77]. Lack of pentraxin-related protein 3 (PTX3, also known as TSG-14), which is localized non-covalently to the HC-HA-enriched cumulus matrix and binds TSG-6, was found to only cause subfertility [78, 79]. These findings show that HC-HA modification can orchestrate large-scale reorganization of ECM to perform specific functions.

It was recently reported in chickens and mice that HC-HA plays a key developmental role in vertebrate midgut rotation and intestinal left-right asymmetry that was similarly impaired in *TSG-6* KO mice and *Ial* KO mice [80]. Since cumulus cell-directed oocyte release is limited to mammals [81], this discovery was very important in

that it established a developmental role of HC-HA that is likely evolutionarily conserved across all vertebrates. Specifically, HC-modification of HA potentiated a HA-enriched ECM expansion that was critical for initiating midgut rotation and inhibiting vascular development in the right dorsal mesentery [80]. While it was suggested that *TSG-6* KO embryos may exhibit reduced viability due to midgut malrotation, which can give rise to life-threatening intestinal strangulation, we have not observed any non-Mendelian inheritance trends among our pups from heterozygote (HT) x KO and HT x HT breeding schemes that would suggest reduced viability in *TSG-6* KO mice (**Table 1-1**).

Additionally, two other research groups have independently confirmed that *lal* breeding schemes lead to Mendelian inheritance trends, which argues against any viability deficits due to HC-HA deficiency [76, 82]. These observations were consistent with how we have not observed any deficits from pup to adulthood and the clinical observation that most cases of intestinal malrotation do not lead to life-threatening volvulus and strangulation [83, 84].

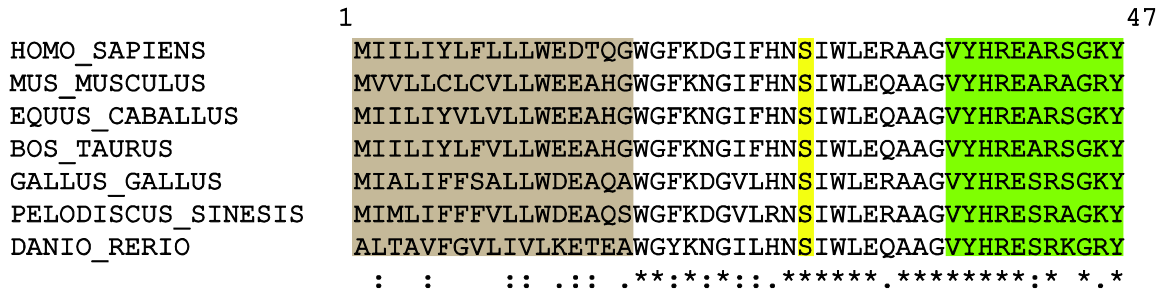


Figure 1.3. Conservation of TSG-6 serine residue that catalyzes HC-HA formation

Sequence alignment of TSG-6 pro-protein in vertebrates (residues 1-47 shown, numbering based on human TSG-6) containing the signal peptide (highlighted in brown) and first few residues of the HA-binding Link domain (highlighted in green). The serine residue responsible for removing HC from IαI (highlighted in yellow) is evolutionarily conserved across all vertebrates from fish to mammals. Species analyzed: *Homo sapiens* (human), *Mus musculus* (mouse), *Equus caballus* (horse), *Bos taurus* (cattle), *Pelodiscus sinensis* (chinese softshell turtle), and *Danio rerio* (zebrafish). CLUSTAL multiple sequence alignment was completed using MUSCLE 3.8 (Multiple Sequence Comparison by Log-Expectation); “*” (asterisk) denotes fully conserved residue. “:” (colon) denotes residues with strongly similar properties (>0.5 in Gonnet PAM 250); “.” (period) denotes residues with weakly similar properties (≤0.5 in Gonnet PAM 250). Alignment from Ni et al. [56], open source.

HT (female) x HT (male) viable pups				
	WT	HT	KO	Total
Female	40	56	33	129
Male	24	45	28	97
Observed Total	64	101	61	226
Expected Total	32.25	64.5	32.25	129
Observed %	28.3185841	44.69027	26.99115	
Expected %	25	50	25	

HT (female) x KO (male) viable pups			
	HT	KO	Total
Female	85	71	156
Male	55	67	122
Observed Total	140	138	278
Expected Total	139	139	278
Observed %	50.3597122	49.64029	
Expected %	50.00	50.00	

Table 1-1. Offspring of *TSG-6* breeding pairs

Genotypes of mice pups from our two *TSG-6* mating pairs: HT (female) x HT (male) and HT (female) x KO (male). Expected total counts were calculated using Mendelian inheritance ratios of 1:2:1 (WT:HT:KO) and 1:1 (HT:KO) for HT x HT and HT x KO breeding schemes. WT, wildtype. HT, heterozygote. KO, knockout.

1.3 Acute lung injury and endotoxic shock

1.3.1 Acute respiratory distress syndrome and acute lung injury

Acute lung injury (ALI) and its corresponding clinically defined condition acute respiratory distress syndrome (ARDS) are the leading causes of morbidity and mortality in the critical care setting. ARDS describes an acute, non-cardiogenic condition in the lungs where alveolar endothelial and epithelial barriers become permeable and allow the vascular leak of protein, fluid, and leukocytes into the lung, which severely impair gas exchange. Underlying infections, either systemic (sepsis) or local (pneumonia), are the leading causes of ARDS and carry an increased mortality risk compared to ARDS triggered by non-infectious causes [85-87]. Although recent advances in ARDS have been achieved with lung protective approaches to mechanical ventilation, after thirty years of clinical trials, no therapeutic breakthroughs in pharmacological interventions have been developed, likely due to the heterogeneity of ARDS [88].

1.3.2 Sepsis and endotoxic shock

Sepsis is defined clinically as an infection, typically bacterial, that causes systemic inflammatory response, which is characterized by life-threatening microvascular inflammation and permeability that can cause multiple organ dysfunction, including ARDS in the lungs. Pneumonia is the leading cause of sepsis, accounting for 40-60% of cases, followed by intra-abdominal and urinary tract infections [89]. This significant overlap of pneumonia, sepsis, and ARDS highlights the common pathophysiological disruption of the alveolar microvascular endothelial and epithelial barrier function that is driven by lung and systemic inflammatory cross-talk.

Endotoxic shock from endotoxemia refers to severe systemic inflammatory response that follows exposure to circulating endotoxin, a component of the bacterial outer membrane. The prototypical endotoxin is lipopolysaccharide (LPS), a hallmark gram negative bacterial pathogen-associated molecular pattern (PAMP) used to

experimentally study the innate immune response to gram negative bacteria. Endotoxic shock is often used interchangeably with septic shock, but septic shock specifically refers to severe systemic inflammatory response with persistent hypotension that is generated in response to circulating microbial organisms in the bloodstream.

Like ARDS, clinical trials for sepsis have not yielded any breakthroughs in targeted pharmacological interventions [90]. Since Toll-like receptor 4 (TLR4) and inflammatory cytokines TNF α and IL1 β have been implicated in endothelial microvasculature instability, therapies were developed to block the effects of these proteins during sepsis. While showing promise in animal studies, none of these therapies were found to be effective in phase III clinical trials [91-93]. Therefore, treatment of sepsis remains primarily supportive including antibiotics for bacterial infection and conservative fluid resuscitation for septic shock.

1.3.3 Mice models of ALI and endotoxic shock

ALI can be modeled in mice by direct delivery via trachea (intracheal instillation, IT) of live bacteria or LPS extracted from gram negative bacteria. A single IT instillation of bacteria or LPS elicits a neutrophilic inflammatory response in the lung and disrupts the alveolar microvascular barrier [94]. The rapid neutrophil recruitment that follows IT instillation of live gram negative bacteria including *Pseudomonas aeruginosa* (*PA*) is essential for controlling bacterial proliferation in the respiratory tract [95-97]. The initial neutrophilic response is followed by recruitment of macrophages and lymphocytes that promote clearance of apoptotic neutrophils and resolution of inflammation [98, 99]. Either IT LPS- or *PA*- induced ALI in mice resolves without the late fibroproliferative responses of ARDS that may be a consequence of continuous airway epithelial insult by mechanical ventilation, combined with maladaptive host responses [100, 101].

Intraperitoneal (IP) administration of a high LPS dose in mice induces life-threatening endotoxic shock and ALI driven by lung microvascular permeability [94].

Both the IP LPS-induced endotoxic shock model and the cecal ligation and puncture (gram negative peritoneal and systemic infection) model cause neutrophilic accumulation in lung microvasculature and interstitium, but the neutrophil recruitment to the intra-alveolar spaces is minimal due to the maintenance of a largely intact alveolar epithelial barrier. The innate immune response to sequester neutrophils in the lung microvasculature following systemic LPS or bacteremia in mice contributes to acute lung respiratory failure similar to that seen with ARDS septic patients. While these sequestered neutrophils clear circulating gram negative bacteria [102, 103], a disproportionate neutrophil response in the lung during sepsis may cause more harm than benefit. Experimentally, lung sequestration diverts neutrophils from other organs, which was found in mice to be detrimental when bacterial infection was seeded intraperitoneally [104]. During the hyperactive innate immune response of endotoxic shock and sepsis, neutrophil trafficking and effector responses may be impaired and contribute to excessive vascular instability and tissue injury. Therefore, understanding how the ECM regulates neutrophil activation and directs their trafficking during experimental models of endotoxic shock and sepsis may yield new therapeutic targets.

1.4 Role of HA during inflammation

1.4.1 HA fragmentation

Inflammation is characterized by enhanced degradation and turnover of tissue HA. The relative contributions of hyaluronidases and reactive oxygen species (ROS) in HA breakdown remain unclear, but both likely contribute during inflammation [16]. It has been hypothesized that the low molecular weight (LMW) HA fragments generated during inflammation may act as damage-associated molecular pattern molecules (DAMPs) stimulating pro-inflammatory responses in the injured tissue. On the other hand, the generation of HA fragments may be important for proper clearance and resolution of

inflammation. For example, IT hyaluronidase administration after influenza A-induced respiratory infection in mice accelerated recovery [105].

A caveat of the pro-inflammatory effects of LMW HA reported in many studies is the potential endotoxin contamination. A recent study showed that non-pharmaceutical grade HA and hyaluronidase reagents contained significant endotoxin contamination that cannot be effectively removed by polymyxin B treatment [106]. Additionally, the study reported that endotoxin-free pharmaceutical grade HA did not have any inflammatory effects on bone marrow-derived macrophages and dendritic cells. Therefore, one should be cautious when interpreting results obtained with exogenous HA or hyaluronidase treatments.

1.4.2 HA in inflammatory trafficking

Interactions between HA and its CD44 receptor have been implicated in hematopoietic cell trafficking during inflammation. CD44 antibody blockade can interfere with monocyte [107] and macrophage [108] recruitment. Neutrophil adhesion in the liver sinusoids after either IP LPS or gram negative *E. coli* administration is similarly abolished with CD44 antibody blockade [109], which places HA at the center of the hepatic inflammatory response to gram negative bacterial sepsis. This neutrophil sequestration in the liver sinusoids can serve a protective role in trapping and removing circulating bacteria [102]. Macrophage efferocytosis of damaged or apoptotic neutrophils can induce reprogramming that suppresses production of proinflammatory cytokines [110, 111]. Since neutrophil activation and destruction of circulating bacteria can also lead to damage to underlying endothelial cells, such as hepatotoxicity in the liver and ALI in the lung, careful modulation of neutrophil sequestration and trafficking is needed to counter sepsis-induced mortality.

1.4.3 HA in bone marrow

Mortality from sepsis is greatest among elderly and infants, and post-mortem findings frequently uncover unresolved infectious foci suggestive of immunosuppression or immunological derangements [112, 113]. Experimental sepsis can cause hematopoietic stem and progenitor cell exhaustion and myelosuppression that presents as life-threatening neutropenia and inability to control bacterial infection [114, 115]. Neutropenia due to leukemia or other hematologic malignancies is a leading risk factor for sepsis [116]. The role of HA and HC-HA in the bone marrow remains largely undefined, but there is increasing evidence that they may be critical during systemic conditions that stress and mobilize the bone marrow compartment such as sepsis. A recent mouse study demonstrated the role of CD44-HA interactions in enhancing hematopoietic progenitor cell proliferation and improving progenitor engraftment after irradiation [117]. Our lab has previously shown that exogenous TSG-6 supplementation in mice improves hematopoietic progenitor cell function after cigarette smoke-induced myelosuppression [118]. Other labs have shown that *TSG-6* KO mice or exogenous TSG-6 supplementation can alter bone marrow stromal cell differentiation [119-121]. These studies underscore the possibility that HC-HA may act in the bone marrow during sepsis.

1.4.4 HC-HA in chronic lung diseases

Chronic lung inflammation is characterized by tissue remodeling processes that promote aberrant extracellular collagen synthesis and deposition that lead to the generation of pathological lesions. A hallmark of many chronic lung diseases such as pulmonary arterial hypertension [122], asthma [123], cystic fibrosis [124], and idiopathic pulmonary fibrosis [125] is the accumulation of HC-HA in these histopathological lesions. The accumulation of HC-HA in the lung has been suggested to have a pro-inflammatory role. The strongest evidence for pro-inflammatory HC-HA is from mouse models of

reactive airway disease. Specifically, mice lacking the ability to form HC-HA, either *TSG-6* or *Ial* KO, were found to exhibit decreased airway hyperresponsiveness after ovalbumin [126] or ozone injury [127, 128].

However, with other chronic lung diseases, it remains unclear whether the presence of HC-HA directly contributes to inflammation, as association does not imply causation. During chronic lung inflammation, HA deposits can co-localize with collagen deposits in the peri-broncho-vascular interstitium [129]. Adhesion and contact with HA is thought to regulate fibroblast and myofibroblast programming [130], which is especially important during bleomycin-induced lung fibrosis [131, 132]. The role of HC-HA during bleomycin-induced fibrotic reprogramming remains unclear. While HC-HA deficiency (*Ial* KO mice) did not alter key bleomycin-induced fibrosis and collagen deposition outcomes, differences in neovascularization and bronchoalveolar lavage inflammatory cell counts were noted [125].

It is important to acknowledge that HC-HA may also have protective effects in the lung. In particular, mice lacking the ability to form HC-HA, *Ial*-KO, exhibited impaired bronchial epithelial repair responses [63]. These diverse findings highlight how HC-HA may have complex roles during lung injury and repair and underscore the need for additional mechanistic studies.

1.4.5 HC-HA in endotoxic shock

Although HA can be found in the lung microvasculature, its levels are much higher, by 500-600 fold, in the liver sinusoid vasculature, which contains the highest systemic concentration of HA due to its role as the filter for circulating HA [133]. During endotoxic shock, liver sinusoidal HA is extensively covalently modified with HCs from *Ial* [134]. This formation of HC-HA was found to promote neutrophil adhesion in the liver sinusoids during endotoxic shock. Mice that lack HC-HA, such as *TSG-6* [135] or *Ial* [136] KO mice, exhibited more rapid onset of mortality during IP LPS-induced endotoxic

shock. The precise role of trapping neutrophils in liver during bacteremia is not known, but may play a protective role in clearing bacteria [102]. Experimentally, neutrophils can work in concert with Kupffer cells, which are specialized macrophages lining the walls of liver sinusoids, to eliminate systemic bacterial infections [137]. Additionally, Kupffer cells have been implicated as part of the mononuclear phagocyte system responsible for clearing circulating neutrophils [107]. This clearance of apoptotic neutrophils during sepsis may have a protective role in limiting excessive neutrophil-mediated endothelial injury.

Taken together, these findings highlight a key role of HC-HA during endotoxic shock. However, the exact mechanisms of HC-HA's protective effects remain unclear. Moreover, the role of HC-HA on injury severity and alveolar barrier repair during ALI caused by localized exposure to LPS (*via* IT) remains unexplored. To address these knowledge gaps, we first sought to determine the potential sources of TSG-6 enzyme that would catalyze HC-HA formation during ALI and endotoxic shock (Chapter 2). We then characterized the kinetics of HC-HA formation during IT LPS and *PA*-induced ALI and examined the role of HC-HA during these models of localized ALI using *TSG-6* KO mice (Chapter 3). Lastly, we characterized the differential HC-HA formation in the systemic vs. lung compartments between IP and IT LPS models and, in this context, we examined the role of HC-HA during IP LPS-induced endotoxic shock using *TSG-6* KO mice (Chapter 4).

Chapter 2. Sources of TSG-6 during ALI and endotoxic shock

2.1 Introduction

To obtain a spatiotemporal understanding of HC-HA production during LPS-induced acute inflammation, we focused on identifying the potential cellular sources of TSG-6 that would catalyze HC-HA formation in the lung and vasculature. As an inflammation-induced secreted enzyme, TSG-6 was originally identified as a protein secreted by TNF α -stimulated foreskin fibroblasts [67] and prolifically secreted by mesoderm-derived stromal cells including mesenchymal stem cells (MSC) [138] and adipose stem and progenitor cell (ASC) [118]. While the lung contains a multitude of mesoderm-derived stromal cells in the interstitium including lung fibroblasts and smooth muscle cells [139], the respiratory tract and alveoli are lined by endoderm-derived epithelial cells and myeloid-derived alveolar macrophages (AM). Additionally, the vasculature is lined with non-stromal endothelial cells and circulating throughout the blood are hematopoietic cells that can be divided into myeloid and lymphoid lineages.

Despite advances regarding the potential cellular sources of TSG-6 in the body, many questions still remain regarding the relative secretory contributions of inflammatory and stromal cells, especially in the context of lung and vasculature during ALI and endotoxic shock. In the lung, the documentation of TSG-6 expression and secretion from stromal and airway epithelial cells has been limited to gene expression studies [140]. While peripheral blood monocytes and peripheral blood monocyte-derived cells have been shown to express and secrete TSG-6 [68, 140], we could not find any published data whether terminally differentiated alveolar macrophages exhibited this function. Also, in the vasculature, while TSG-6 secretion from circulating myeloid cells including neutrophils and monocytes are likely contributors to circulating TSG-6 [68, 140], the role of endothelial cells as a source of circulating TSG-6 is limited to gene expression data from human umbilical vein endothelial cells [140]. These gaps in knowledge highlight a

strikingly incomplete understanding of the physiological lung and vascular sources of TSG-6 during health and disease.

It has been established that non-hematopoietic cells, especially stromal cells, can respond to the inflammatory cytokines TNF α and IL1 β by secreting TSG-6 [68]. In contrast, hematopoietic cells of myeloid lineage have been found to secrete TSG-6 in response to either TNF α or LPS with the latter being the more powerful inducer [68]. In vascular cells, IL1 β was identified as a potent stimuli of *TSG-6* transcriptional expression in human umbilical vein endothelial cells [140].

With this scientific premise, we addressed the secretory capabilities of potential cellular sources of TSG-6 in the lung and vasculature. Focusing on the inflammatory signals present during ALI and endotoxic shock, we treated various types of cells with LPS, TNF α , and/or IL1 β and quantitatively assessed their ability to secrete TSG-6 by enzyme-linked immunosorbent assay (ELISA). We additionally analyzed TSG-6 secretion into conditioned media by western blot and extracted RNA to measure *TSG-6* gene expression.

2.2 Methods

2.2.1 Reagents

All materials and reagents described in Chapters 2-4 were from ThermoFisher (Waltham, MA, USA), unless otherwise specified. Cell culture reagents were from Gibco (ThermoFisher), unless otherwise specified.

2.2.2 Cell culture

Primary human alveolar macrophages (hAM) were obtained by bronchoalveolar lavage of de-identified non-diseased human explanted lungs not used for transplantation and allowed to attach to tissue culture treated plastic in Roswell Park Memorial Institute (RPMI) media with 1X penicillin/streptomycin (100X at 10,000 U/mL) for 2 h.

Bronchoalveolar lavage was performed by the donor lung tissue core at National Jewish

Health following Institutional Review Board (IRB) approved protocol. Non-adherent cells were collected and discarded by phosphate buffered saline (PBS) wash. Indicated treatments were performed in RPMI media with 2% fetal bovine serum (FBS, HyClone, GE Healthcare, Marlborough, MA, USA) and 1X penicillin-streptomycin. Treatments included adding 20 ng/mL TNF α (R&D Systems, Minneapolis, MN, USA), 50 ng/mL ultrapure *E. coli* K12 LPS (LPS-EK, InvivoGen, San Diego, CA, USA), or vehicle (0.1% bovine serum albumin in PBS) for either 6 h or 24 h. After the collection of conditioned media supernatant (1000 g, 10 min) mixed with protease inhibitors (complete Protease Inhibitor Cocktail, Roche Diagnostics, Mannheim, Germany), cells were rinsed once with PBS and then lysed for RNA extraction per below.

Peripheral blood monocyte cell (PBMC)-derived macrophages (PBDM) were enriched from whole blood by negative selection (DynaBeads untouched human monocyte kit) and by adherence to tissue culture plastic. Incubation with macrophage colony stimulating factor (20 ng/mL MCSF, R&D Systems) over six days was used to differentiate PBMC into macrophage-like cells. Macrophage differentiation was achieved in serum-free RPMI supplemented with 1X non-essential amino acids, 1 mM sodium pyruvate, 2 mM glutamine, and 1X penicillin-streptomycin for days 1-3 and with additional 10% FBS for days 4-6. Treatments were performed in RPMI media with 2% FBS and indicated stimuli for 24 h.

BEAS-2B immortalized human bronchial epithelial cells were cultured in submerged conditions using Dulbecco's Modified Eagle Medium (DMEM), high glucose (4500 mg/L) media with 10% FBS, and 1X penicillin/streptomycin. Treatments were performed by rinsing once with PBS and then incubating in basal DMEM media with 2% FBS and indicated stimuli for 24 h.

Wi38 primary human fetal lung fibroblasts were grown in Minimum Essential Media (MEM) media with 10% FBS and 1X penicillin/streptomycin. Cells were used

between passages 8-12 for experiments. Treatments were performed by rinsing once with PBS and then incubating in basal MEM media with 2% FBS and indicated stimuli for 24 h.

Human adipose stromal/progenitor cells (ASC) isolation, expansion, and characterization were previously described [118, 141, 142]. All ASC isolation was performed by Dr. Keith March's lab at Indiana University School of Medicine following IRB approved protocol. Briefly, ASC were collected by liposuction of three human donors (two abdominal and one flank lipoaspirate). ASC isolation involved digestion using collagenase I (Worthington, Lakewood, NJ, USA) under mechanical agitation (2 h, 37 °C) and centrifugation (300 g, 8 min) to obtain a pellet containing the stromal vascular fraction. The stromal vascular fraction was filtered (250 µm Nitex filters, Sefar America, Buffalo, NY, USA), and red blood cells were lysed using ammonium chloride potassium (ACK) lysis buffer (154 mM NH₄Cl, 10 mM KHCO₃, and 0.1 mM ethylenediaminetetraacetic acid or EDTA). The stromal cells were cultured on tissue culture plastic using microvascular endothelial cell growth medium (EGM-2-MV) media (Lonza, Allendale, NJ, USA), and ASC between passages 4-6 were used for experiments. Treatments involved rinsing once with PBS to remove residual FBS and incubating in basal Endothelial Basal Medium-2 (EBM-2) media (Lonza) with indicated stimuli for 24 h. Demographic information of the ASC donors was described previously [143].

Primary human lung microvascular endothelial cells (HMVEC-L) from Lonza were cultured in microvascular endothelial growth medium (EGM-2-MV) following manufacturer's instructions. HMVEC-L were cultured and seeded between passages 6-7. Treatments involved rinsing once with PBS and incubating for 24 h in EGM-2-MV with the following: vehicle containing 0.1% bovine serum albumin (BSA, MilliporeSigma,

Burlington, MA, USA) in PBS, 20 ng/mL TNF α (R&D Systems), 20 ng/mL IL1 β (R&D Systems), or 20 ng/mL ultrapure *E. coli* K12 LPS (LPS-EK, InvivoGen).

2.2.3 Human TSG-6 (hTSG-6) western blot

Conditioned media supernatant (1000 g, 5 min) was mixed with Laemmli buffer. Proteins were separated by their molecular weight by sodium dodecyl sulfate polyacrylamide gel electrophoresis (SDS-PAGE) on Stain-Free Criterion TGX 4-20% gradient gels (Biorad, Hercules, CA, USA) and transferred to Immobilon-P PVDF membrane (MilliporeSigma) using TransBlot Semi-Dry (Biorad). All blot processing steps were performed with rocking and at room temperature unless otherwise specified. The blot was blocked in Tris-buffered saline (TBS) with 5% milk dissolved and 0.1% TWEEN-20 (MilliporeSigma) and probed using goat-anti-hTSG-6 antibody (AF2104, R&D Systems) in PBS buffer with 4% BSA (overnight, 4 °C). TBS with 0.1% TWEEN-20 (4 x 10 min) was used to wash the blots. Bovine anti-goat IgG-HRP (sc-2350, Santa Cruz Biotechnology, Dallas, TX, USA) secondary was used at 1:5000 in TBS with 5% milk and 0.1% TWEEN-20. Chemiluminescent horseradish peroxidase (HRP) substrate Immobilon Forte (MilliporeSigma) was added and imaged using ChemiDoc MP (Biorad). Total protein images of the Stain-free gels were also imaged using ChemiDoc MP. Densitometry was calculated using Image Studio Lite (Licor, Lincoln, NE, USA). HMVEC-L conditioned media was concentrated four-fold using 10 kDa cutoff centrifugal filters (Microcon-10, MilliporeSigma).

2.2.4 hTSG-6 ELISA

Human TSG-6 (hTSG-6) levels in conditioned media supernatant (600 g, 5 min) were measured as previously described [118] using a sandwich ELISA that had previously been validated by TSG-6 small interfering RNA (siRNA) in human MSC [138] and ASC [118]. 96-well plates (Nunc MaxiSorp) were coated with rat anti-hTSG-6 antibody (clone A38.1.20; Santa Cruz Biotechnology) diluted in 0.2 M sodium

bicarbonate buffer (pH 9.4) overnight. All steps including antibody coating were performed at room temperature with rocking. Plates were washed with buffered surfactant (WA126, R&D Systems) between each step. Blocking was performed by adding PBS with 0.25% BSA and 0.05% TWEEN-20 and rocking (1 h). Samples were then incubated for 2 h. HMVEC-L conditioned media was concentrated eight-fold using 10 kDa cutoff centrifugal filters (Microcon-10). Detection was performed by adding biotinylated goat anti-hTSG-6 antibody (BAF2104, R&D Systems) for 2 h, Streptavidin-HRP (DY998, R&D Systems) for 30 min, HRP substrate (DY999, R&D Systems) for 30 min, and quenched using 1 M H₂SO₄. Absorbance at 450 nm (HRP activity) and 584 nm (background) were measured using a 96-well plate reader (Molecular Devices, San Jose, CA, USA).

To normalize TSG-6 secretion relative to cell number, viable cell numbers were obtained by trypan blue exclusion and cell counting by hemocytometer. Standard curves were obtained using recombinant human TSG-6 (2104-TS-050, R&D Systems) mixed with the same FBS content present in the conditioned media. Standard curve calculated in the absence and presence of FBS (2%) (**Figure 2.1**) showed that addition of FBS reduced the magnitude of HRP activity. This observation may be due to the formation of TSG-6-HC covalent intermediate in the presence of FBS, an Ial source. Since Ial's ~80 kDa HCs are very large compared to 35 kDa TSG-6, formation of TSG-6-HC may sterically hinder binding by the capture or detection antibodies used in the sandwich ELISA. This steric hindrance may help explain why efforts to directly assay TSG-6 levels in human serum have been difficult [144].

2.2.5 Statistics

In Chapters 2-4, ANOVA and Tukey's multiple comparison tests were performed to determine statistical significance (GraphPad 6 Prism, GraphPad Software, La Jolla, CA, USA) unless a different test was specified. Data points from independent

experiments or individual mice ($n \geq 3$), median, or mean \pm SD were graphed unless otherwise specified. Results were considered significant at $P < 0.05$.

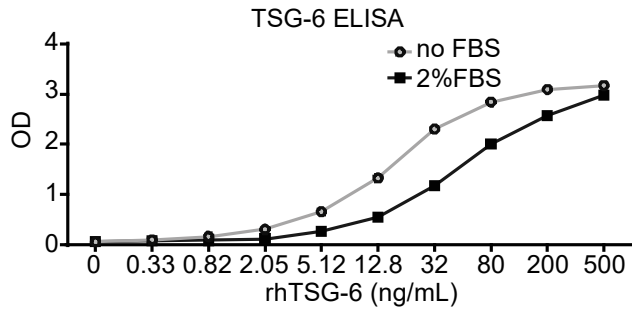


Figure 2.1. hTSG-6 ELISA standard curves

hTSG-6 standard curves were obtained using recombinant hTSG-6 with or without the addition of FBS (2% FBS). FBS reduced the magnitude of HRP substrate color development. The presence of FBS, an I₁ source, results in the formation of TSG-6-HC covalent intermediate. Our data suggests that the covalent linking to the large 80 kDa protein moiety may sterically hinder the binding of capture and detection antibodies, which would explain the reduction in HRP substrate color change. OD, optical density. Figure from Ni et al. [56], open source.

2.2.6 Measurements of messenger RNA (mRNA)

Total ribonucleic acid (RNA) was extracted from cultured cells as previously described using Buffer RLT Plus lysis buffer and RNeasy Plus Mini Kit (Qiagen) [56]. 1000-2000 ng of extracted RNA was used to synthesize complementary DNA (High-Capacity cDNA Reverse Transcription Kit). To measure the levels of specific mRNAs, real-time quantitative polymerase chain reaction (qPCR) reactions were performed using the StepOnePlus platform with Taqman Universal PCR Master Mix and Taqman probe *hTSG-6* (Hs01113602_m1). Relative mRNA expression was determined by the double delta comparative ($\Delta\Delta C_t$) method with *18s* RNA as the loading control (Taqman Hs99999901_s1).

2.2.7 Time-course of macrophage expression of TSG-6 in LPS-instilled mice

Expression of mouse *TSG-6* (*msTSG-6*), also known as *TNF α -induced-protein 6* (*TNFAIP6*), was obtained by Ensembl gene annotation in a previously published dataset. The detailed methods for generating the dataset, along with the analysis of the RNA-sequencing (RNA-seq) dataset, and National Center for Biotechnology Information (NCBI) deposition were discussed previously [145]. RNA-seq analysis was performed on resident and bone marrow-derived, recruited alveolar macrophages obtained by flow cytometry sorting of bronchoalveolar lavage of IT LPS (20 μ g / mouse) treated mice (C57BL/6, 10-12 week old; 0, 3, 6, 9, and 12 days post injury). Each of these murine alveolar macrophage studies were completed by Dr. William Janssen's lab at National Jewish Health following Institutional Animal Care and Use Committee (IACUC) approved protocol.

2.3 Results

2.3.1 TSG-6 secretion by lung resident cells

To determine which lung cells can produce TSG-6 during ALI, we investigated TSG-6 secretion by cultured lung macrophages, bronchoepithelial cells, and fibroblasts

(Figure 2.2). Since LPS was identified as a potent stimuli of TSG-6 secretion in myeloid cells [68, 140] and is encountered in the respiratory tract following instillation, we first measured TSG-6 secretion by human peripheral blood monocyte-derived macrophage (hPBDM) and alveolar macrophage (hAM) in response to vehicle or LPS stimulation by TSG-6 western blot analysis of conditioned media. We noted that LPS (50 ng/ml, 24 h) induced TSG-6 (38 kDa) and TSG-6-HC covalent intermediate (120 kDa) in both types of macrophages (**Figure 2.2A**). TSG-6-HC covalent intermediate readily formed in the presence of FBS, an Ial source, and was notably absent when FBS was omitted. Addition of either TNF α (20 ng/mL, 24 h), the eponymous TSG-6 stimulus, or LPS (50 ng/mL, 24 h) upregulated TSG-6 secretion in hAM (**Figure 2.2B**) in a manner that paralleled the induction of *TSG-6* transcript (**Figure 2.2C**). *TSG-6* expression was induced ~4 fold with TNF α stimulation and ~25 fold with LPS.

To ascertain whether the different lung cell types can secrete physiologically relevant amounts of TSG-6 in response to TNF α or LPS stimulus, we quantitatively compared levels of TSG-6 secretion by the different lung cell types with human ASC (hASC), which are known to prolifically secrete TSG-6 (**Figure 2.2D**). We noted a strikingly different pattern of TSG-6 induction between the myeloid hAM and the non-hematopoietic bronchoepithelial (BEAS-2B), lung fibroblast (Wi38), and stromal hASC. While hAM secreted substantially more TSG-6 in response to LPS than TNF α (LPS ~61 ng/mL vs. TNF α ~23 ng/mL), all three non-hematopoietic cells were more responsive to TNF α than to LPS. With the exception of hASC, LPS failed to induce any TSG-6 secretion in bronchoepithelial cells and lung fibroblasts. Of note, LPS-treated hAM secreted a substantial amount of TSG-6 (~61 ng/mL vs. ~11 ng/mL; LPS vs. veh, $P < 0.001$) that was comparable to LPS-treated ASC (~49 ng/mL) and to TNF α -treated lung fibroblast (~47 ng/mL).

To assess whether AM also upregulate *TSG-6* *in vivo* and to determine the relative difference in *TSG-6* expression in resident AM vs. bone marrow-derived, recruited AM, we examined a previously published RNA-seq gene expression dataset of resident and recruited AM collected by bronchoalveolar lavage of IT LPS-treated mice (**Figure 2.3**) [145]. We found that *TSG-6* expression was highest initially following injury at day 3 following LPS instillation in both types of AM and more robustly induced in recruited AM as compared to resident AM.

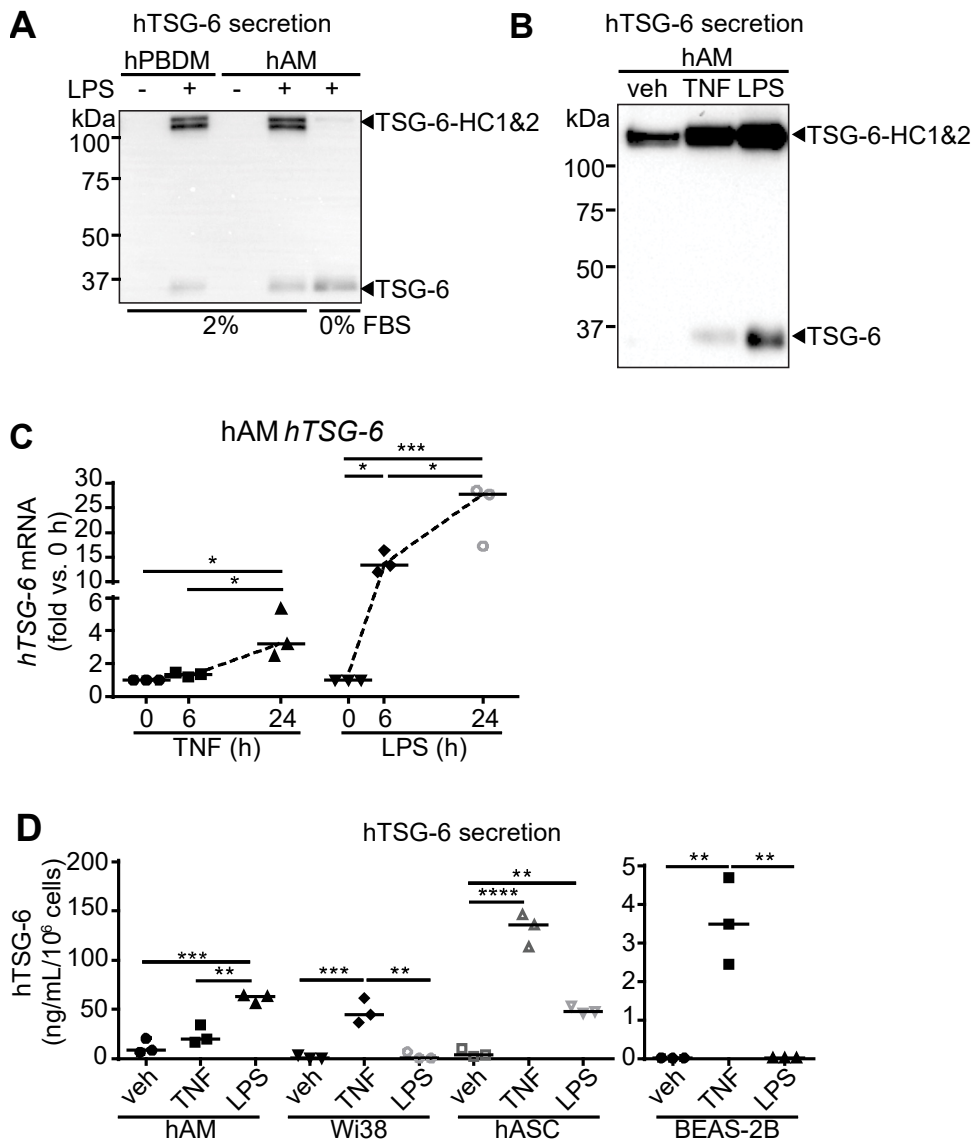


Figure 2.2. TNF α or LPS induction of TSG-6 in lung cells

A. LPS (50 ng/mL, 24 h) stimulation of TSG-6 secretion into conditioned media by human peripheral blood monocyte-derived macrophages (hPBDM) and alveolar macrophages (hAM) were detected by TSG-6 western blot. TSG-6 (35 kDa) readily formed TSG-6-HC covalent intermediate (120 kDa) only in the presence of FBS (an lal source), which was absent with 0% FBS. **B-C.** Stimulation of hAM TSG-6 secretion (**B**, 24 h) and gene expression (**C**, 6 or 24 h) by vehicle (veh), TNF α (20 ng/mL), or LPS (50

ng/mL) was assessed by western blot and qPCR, respectively. **D.** Levels of secreted TSG-6 by hAM, lung fibroblast Wi38 cells, and bronchoepithelial BEAS-2B cells treated (24 h) with the same indicated stimuli as in **C** were quantified by ELISA and compared to that by adipose stem and progenitor cells (hASC). $n = 3$ independent experiments per group. Data analyzed by ANOVA with Tukey's multiple comparisons. $**P < 0.01$, $***P < 0.001$, $****P < 0.0001$. Figure from Ni et al. [56], open source.

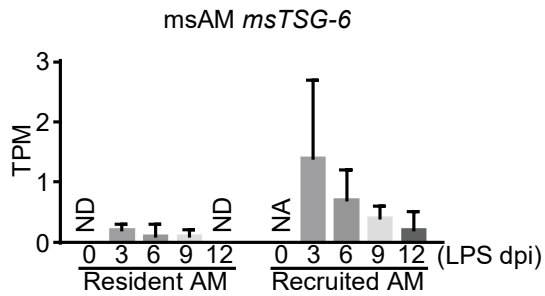


Figure 2.3. *TSG-6* expression in mouse AM during ALI

Resident and bone marrow-derived, recruited AM were obtained by flow cytometry sorting of bronchoalveolar lavage of mice at multiple time points (0, 3, 6, 9, and 12 days post injury) during a time course of IT LPS-induced injury and resolution. In this previously published RNA-Seq dataset [145], *TSG-6* expression was analyzed and presented as transcripts per million (TPM). Mean expression ($n = 3$ independently pooled samples, $n = 4-7$ mice in each pool) and error (SD) plotted. dpi, days post injury. TPM, transcript per million. ND, not detected. NA, not applicable. SD, standard deviation. Figure from Ni et al. [56], open source.

2.3.2 Microvascular endothelial TSG-6 expression and secretion

In the vasculature, while the circulating myeloid cells neutrophils and monocytes have the capacity to secrete TSG-6 [68, 140], the ability of endothelial cells to secrete TSG-6 has not been investigated. In light of gene expression data from human umbilical vein endothelial cells suggesting that IL1 β may be a potential stimuli [140], we comprehensively measured human lung microvascular endothelial (HMVEC-L) secretion of hTSG-6 in response to TNF α , LPS, or IL1 β . In contrast to LPS, both TNF α and IL1 β (20 ng/mL, 24 h) were able to stimulate hTSG-6 secretion with IL1 β more substantially inducing both hTSG-6 (38 kDa) and hTSG-6-HC intermediate bands as assessed by western blot (**Figure 2.4A**). These differences were consistent with the trends of hTSG-6 secretion (TNF α ~3 ng/mL vs. LPS ~7 ng/mL) assessed by ELISA (**Figure 2.4B**) and TSG-6 transcript (TNF α ~391 vs. LPS ~1459 relative fold induction) assessed by qPCR (**Figure 2.4D**) and compared to that of hAM (**Figure 2.4C-D**).

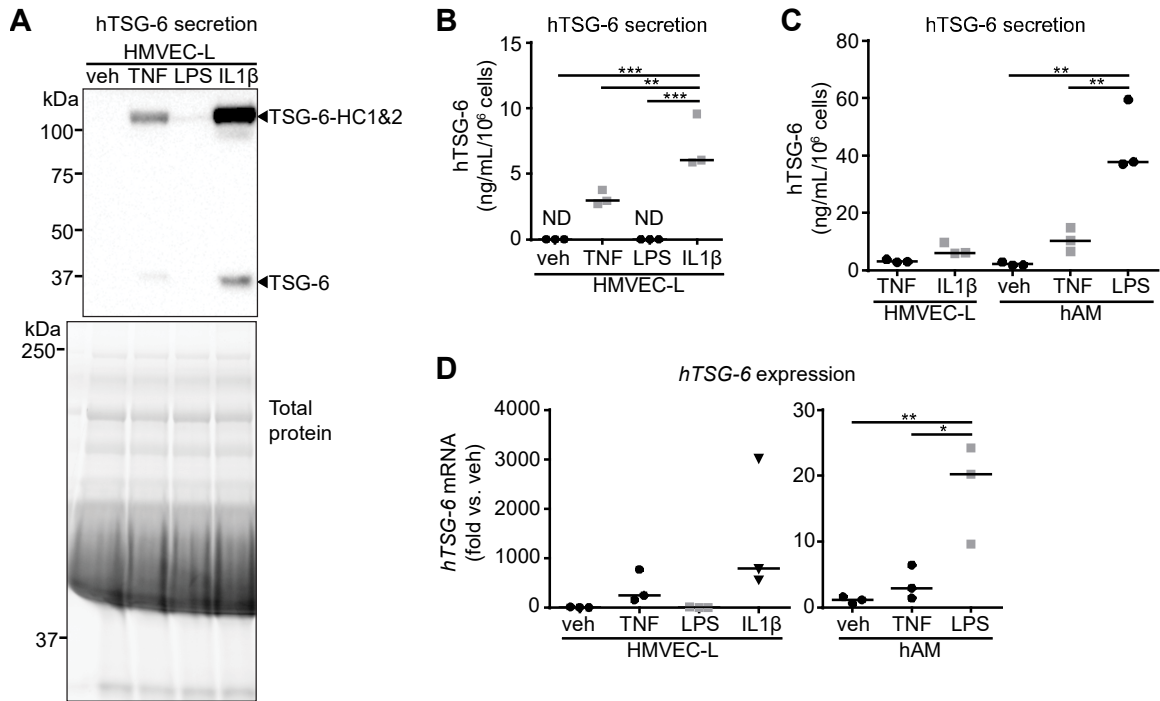


Figure 2.4. Inflammatory induction of HMVEC-L TSG-6 secretion and expression

A-B. Stimulation of hTSG-6 secretion into HMVEC-L conditioned media by vehicle, TNF α , LPS, or IL1 β (20 ng/mL, 24 h) was assessed by hTSG-6 western blot (**A**) and ELISA (**B**). Full growth media (EGM-2-MV) containing FBS, an Ial source, was used for the conditioned media, which allowed the formation of TSG-6-HC covalent intermediate (120 kDa). Total protein was imaged using Stain-Free technology. **C-D** The induction of hTSG-6 secretion (**C**, ELISA) and *hTSG-6* gene expression (**D**, qPCR) by HMVEC-L was compared to myeloid hAM. ND, not detected. $n = 3$ independent experiments per group. Data analyzed by ANOVA with Tukey's multiple comparisons. * $P < 0.01$, ** $P < 0.01$, *** $P < 0.001$. Ni et al., manuscript submitted.

2.4 Discussion

To assess which cells contribute to TSG-6 production during ALI and endotoxic shock, we compared TSG-6 secretion across different cell types using quantitative ELISA. Based on the findings that stromal cells prolifically secrete TSG-6, we were not surprised to see that cultured lung fibroblasts would be able to respond to TNF α by secreting TSG-6. But it was unclear whether the other cells would also induce secretion of TSG-6 in response to TNF α . Our findings that bronchoepithelial BEAS-2B and lung fibroblast Wi38 cells produced more TSG-6 in response to TNF α and that alveolar macrophage produced more TSG-6 in response to LPS are consistent with previous observations that TNF α elicits a stronger TSG-6 response in non-hematopoietic cells and LPS elicits a stronger response in myeloid-derived cells [68]. This myeloid-specific response to LPS is likely due to the high expression of the LPS receptor TLR4 in myeloid cells [146] and would suggest that TSG-6 may be a paracrine effector in the myeloid innate immune response to gram negative bacterial respiratory infection.

As airway epithelial cells and terminally differentiated alveolar macrophages are situated in the respiratory tract, they would be directly exposed to LPS or gram negative bacteria and TNF α secreted by activated AM and recruited neutrophils. Thus, the acute inflammatory environment of respiratory infection would be expected to provide optimal signaling for TSG-6 secretion throughout the respiratory tract. Similarly, TNF α upregulated throughout the lung interstitium during ALI would stimulate parenchymal TSG-6 secretion by stromal cells, infiltrated neutrophils, and both interstitial and recruited macrophages. Since IT LPS and IP LPS also induce microvascular permeability, this would allow the leak of serum I α I into lung interstitium and alveoli that will serve as HC substrate. Thus, ALI may potentially induce HC-HA formation, and HC-HA formation in both the lung parenchyma and respiratory tract may be part of a protective

innate immune response to gram negative bacterial respiratory infection, a hypothesis addressed in Chapter 3.

Sepsis is characterized by a cytokine storm that precipitates microvascular permeability, which can lead to life-threatening septic shock. Since microvascular endothelial cells are particularly affected by the cytokine storm, our finding that HMVEC-L secreted TSG-6 in response to two key proinflammatory cytokines (TNF α and IL1 β) increased systemically during sepsis [147] temporally places TSG-6 secretion during conditions of vascular barrier instability. Considering the number of microvascular endothelial cells lining the vascular beds and that myeloid cells (neutrophils and monocytes) make up 30-50% of circulating hematopoietic cells in plasma [148], endothelial cells likely work together with myeloid cells to make sizeable contributions to intravascular TSG-6 production. Given the enzymatic availability of HA-modifying TSG-6 and the immediate availability of I α I, extensive and repeated HC-modification of HA can potentially occur during endotoxic shock, which is discussed in Chapter 4. Since TNF α and especially IL1 β induce both HA synthesis and HA-dependent monocyte adhesion in endothelial cells [149], the concurrent TSG-6 and HA secretion may direct hematopoietic trafficking during systemic inflammation.

Most studies of stromal progenitor cells (MSC and ASC), which highly express and secrete TSG-6, have been completed with the assumption that the other non-stromal cells (i.e. macrophage) are not a major source of TSG-6 [150, 151]. Our finding that TNF α and LPS can upregulate TSG-6 secretion in terminally differentiated hAM and that LPS treated hAM secrete considerable amounts of TSG-6 adds these non-stromal cells to peripheral blood monocytes and monocyte-derived cells as sources of TSG-6 [68, 140]. Therefore, MSC and ASC are not an exclusive source of TSG-6, and the potential myeloid contribution of TSG-6 should be considered during inflammation.

Chapter 3. Rapid clearance of HC-HA during resolving ALI

3.1 Introduction

With the discoveries that HC-HA regulates neutrophil trafficking in liver sinusoids during systemic LPS exposure [133, 134], and that HC-HA deficient mice were more susceptible to IP LPS-induced endotoxic shock [135, 136], one key question that remained unanswered was whether HC-HA also exerted a protective role during localized acute lung injury, where the inciting injurious agent would be in the respiratory tract instead of the vasculature. The discovery that TSG-6 secretion can be induced in LPS-treated hAM and TNF α -treated bronchoepithelial cells and lung fibroblasts (Chapter 2.3 Results) suggested that TSG-6 induction in the lung may be part of the innate immune response to gram negative bacterial respiratory infection. This observation, together with the fact that both IP and IT LPS causes ALI, suggested that TSG-6 and HC-HA may also play a protective role during respiratory infection models of ALI.

A second key unanswered question was whether TSG-6 catalyzed formation of lung HC-HA during ALI. In contrast to the numerable reports that HC-HA accumulates in pathological lesions of chronic lung diseases, the induction and kinetics of HC-HA formation during ALI had not been reported. To better understand lung HC-HA induction and kinetics, we performed a time course of ALI injury and resolution *in vivo*. To model gram negative bacterial respiratory infection, we administered either LPS or live gram negative bacteria *PA*. In this context, we investigated whether HC-HA plays a protective role during IT LPS-induced ALI using *TSG-6* KO mice and littermate controls.

3.2 Methods

3.2.1 Animal husbandry

All animal experiments were approved by the IACUC at National Jewish Health. *TSG-6* HT mice (BALB/c background) were obtained from Stavros Garantziotis and were originally constructed by Dr. Katalin Mikecz [77]. *TSG-6* KO was confirmed by

genotyping (**Table 3-1**) and demonstrated inability to form HC-HA, as originally and repeatedly described for these mice [56, 77, 126]. All studies were conducted using sex (both male and female)- and age (8-12 week old)- matched *TSG-6* KO mice and wild type (WT) and heterozygous (HT) littermate controls. Mice were kept in standard cages with *ad libitum* access to regular chow and water in regular mouse housing sectors with sentinel monitoring of murine pathogens and 12:12 light darkness cycling. Mice used for *PA* experiments were transferred and treated in biosafety level 2 (BSL2) housing sectors.

Primers	Sequence
10840	5'-CAA TGT TAG CAC ATC TTA ACC TCT TT-3'
10839	5'-TTT GCT TAT GCG TCT TGC TG-3'
oIMR7415	5'-GCC AGA GGC CAC TTG TGT AG-3'

Primer sets	Expected size
10840 and 10839	Wild type = 327 bp. Mutant = no band
oIMR7415 and 10839	Wild type = no band. Mutant = 215 bp.

Expected results

WT (only 327bp). HT (327, 215bp), and KO (only 215bp)

PCR Reaction mix	uL
KAPA 2G HS Buffer	10
Water	5.8
Primer #1 (20uM each)	0.6
Primer #2 (20uM each)	0.6
1:10 diluted template	3

PCR cycling

Step #	Temp	Time	Note
1	94	2 min	
2	94	20 sec	
3	65	15sec	-0.5 C per cycle decrease
4	68	10sec	
5			repeat steps 2-4 for 10 cycles
6	94	15sec	
7	60	15sec	
8	72	10sec	
9			repeat steps 6-8 for 28 cycles
10	72	2 min	
11	10	hold	

Table 3-1. Genotyping of *TSG-6* mice

Jackson Laboratory's *TSG-6* mice genotyping strategy was followed. Two PCR reactions, one to identify WT allele presence and a second to identify KO allele presence, were utilized to assign a genotype for each mouse.

3.2.2 Mouse IT LPS- and PA- induced ALI

E. coli O55:B5 LPS (20 µg, L2880) or live gram negative *PA* bacteria (2×10^6 CFU, colony forming unit, PA01 strain) was administered in a 50 µL PBS vehicle that was intratracheally instilled in the morning. Instillates were given directly into the tracheas *via* a 22-gauge oral gavage needle (7920, Cadence Science, Cranston, RI, USA) with its distal 0.5 cm end bent 40° to expedite tracheal insertion. Palpation of the needle over the tracheal rings was used to confirm position inside trachea. *PA* was obtained from Dr. Fabienne Gally (National Jewish Health) who used stocks from Dr. Kenneth Malcolm (National Jewish Health) that were from *Pseudomonas* Genetic Stock Center (East Carolina University) [77]. *PA* was grown in Luria-Bertani broth (LB). A new *PA* culture was freshly inoculated in the morning from an overnight starter culture to obtain bacteria in the exponential phase of growth with minimal dead bacteria. *PA* was centrifuged and resuspended at the appropriate CFU dilution for instillation. CFU was confirmed by plating dilutions of *PA* on LB agar. Mice were weighed every day, for up to 6 days post-instillation. Mice welfare were monitored twice daily per IACUC protocol.

3.2.3 Lung parenchymal HC-HA formation

Mice were euthanized by isoflurane overdose and then lavaged by bronchoalveolar route. Bilateral thoracotomy was next performed as secondary euthanasia. Lungs were then perfused *via* the right ventricle using 10 mL of blood bank saline. HC-HA was measured in these lavaged and perfused lungs as previously described [152] with minor modifications to increase throughput. Rather than individually mincing each lung, equal mass (50 mg) of flash frozen mouse lung tissue was homogenized in PBS for 3 min using Mini-Beadbeater-16 (Biospec, Bartlesville, OK, USA). Lung homogenates were treated with either 1 U of *Streptomyces hyaluronolyticus* (*S. hyaluronolyticus*) hyaluronidase (389561, MilliporeSigma) or PBS control (45 min, 4 °C) with mechanical agitation. Treated homogenates were then centrifuged (13,000 *g*,

5 min, 4 °C) and cleared supernatants were then incubated (45 min, 37 °C) with mechanical agitation. Laemmli Buffer was then added to stop the digestion. The samples were separated by SDS-PAGE (Stain-free Criterion TGX 7.5% gels, Biorad) and transferred to Immobilon-P PVDF membrane (MilliporeSigma) using TransBlot Semi-Dry apparatus (Biorad) and 1X Towbin buffer (Biorad). All western blot wash steps were completed using Tris-buffered saline with 0.1% TWEEN-20. Blocking was completed in 5% nonfat dried milk (1 h) and blot was probed using rabbit-anti-hIal antibody (A0301, DAKO, Agilent, Santa Clara, CA, USA), which was validated for detecting mouse Ial and HC-HA formation in various tissues [77, 126]. Donkey anti-rabbit IgG-HRP (NA9340, GE Healthcare) secondary was used at 1:20,000 in TBS with 5% milk and 0.1% TWEEN-20. Stain-free total protein images were obtained and densitometry performed as described previously (Chapter 2.2 Methods).

3.2.4 Measurements of whole lung messenger RNA (mRNA)

Total RNA was extracted from whole lung using Trizol Plus RNA Purification Kit with on-column deoxyribonuclease (DNase) digest (PureLink DNase). Lungs were homogenized in 1 mL Trizol using a Mini-Beadbeater-16 (Biospec). cDNA reverse transcription and qPCR were performed as described previously (Chapter 2.2 Methods). The following Taqman probes were used: *msTNF α* (Mm00443258_m1), *msTSG-6* (Mm00493736_m1) [153, 154], *msHAS1* (Mm03048195_m1), *msHAS2* (Mm00515089_m1), *msHAS3* (Mm00515092_m1), *msHYAL1* (Mm00476206_m1), *msHYAL2* (Mm01230688_g1), *msTMEM2* (Mm00459599_m1), and *msCEMIP* (Mm00472921_m1). Relative mRNA expression was determined using the double delta comparative ($\Delta\Delta C_t$) method with *18s* RNA as the endogenous loading control (Taqman Hs99999901_s1).

3.2.5 HA histology

Mice were euthanized by isoflurane overdose and bilateral thoracotomy. Lungs were perfused *via* puncture of right ventricle using 10 mL of blood bank saline. 18-gauge stainless steel cannulas were inserted into trachea to inflate the lungs with a PBS solution containing 4% paraformaldehyde (PFA) (15710, Electron Microscopy Sciences, Hatfield, PA, USA) and 0.33% low melting point agarose. Inflated lungs were then tied and immersion-fixed overnight in 4% PFA (1 d, 4 °C) with gentle rocking and then washed with PBS (4 x 30 min) and incubated in PBS containing 25% sucrose and 25% optimal cutting temperature (OCT) compound (6 h). Lungs were then embedded in OCT compound and then sliced at 10 µm thickness. Sections were allowed to air dry before rinsing in PBS to remove OCT compound.

Lungs from *PA*-treated mice were inflated with 10% neutral buffered formalin containing 0.25% low melting point agarose and fixed by full submersion in 10% neutral buffered formalin (overnight, room temperature). Fixed lung was paraffin embedded, cut at 3 µm thickness, and mounted on slides. Slides then underwent the following processing: deparaffination and rehydration using successive incubations in xylene (3 x 5 min), 100% ethanol (2 x 5 min), 95% ethanol (2 x 5 min) and equilibration in PBS followed by water. Antigen retrieval was performed by placing slides in a pressure cooker containing citric acid based antigen unmasking solution (Vector Labs, Burlingame, CA, USA) and microwaved.

Staining was accomplished through the following steps. Sections were blocked in PBS with 3% BSA and 0.1% Triton X-100 (MilliporeSigma) and primary probes added. Biotinylated hyaluronan binding protein (50 µg/100 µl stock, 385911, MilliporeSigma), rabbit anti-human HC2 (NBP2-31750, Novus, Littleton, CO, USA), and rat anti-mouse CD68 (FA-11, Biolegend, San Diego, CA) were added at 1:100 and incubated (overnight, 4 °C). On the next day, washes were performed with PBS in Coplin jar with

rocking (3 x 10 min) and secondary antibody was added for 1 h at room temperature. Streptavidin Alexa Flour 488 (S-11223) was used at 1:1000. Cy3 donkey anti-rabbit (711-165-152, Jackson ImmunoResearch, West Grove, PA, USA) and Cy5 donkey anti-rat (712-175-153, Jackson ImmunoResearch) were used at 1:2000. Slides were mounted using ProLong Gold AntiFade with 4',6-diamidino-2-phenylindole (DAPI) and imaged using laser scanning confocal LSM 700 (Zeiss, Jena, Germany).

3.2.6 Histologic ALI scoring

Unlabeled mice lungs were perfused with 10 mL of blood bank saline. Left lung was inflated with 0.25% agarose in 10% neutral buffered formalin to 20 cm H₂O and immersion-fixed in neutral buffered formalin (overnight, room temperature) [94]. To ensure representative sampling of the entire lung, the fixed lung was placed in a molding box, encased in agarose, and sliced transversely (lung apex to base, 3 mm thick). Transverse lung pieces were embedded together in paraffin, sectioned at 3 µm, mounted on slides, deparaffinized, and rehydrated as described above. Slides were then stained with Harris Hematoxylin (2 min), Clarifier 1 (1 min), Bluing reagent (1 min), Eosin Y (30 sec), dehydrated, and mounted. Lung processing and staining were performed by Erica Beatman in the Petrache lab. Paraffin embedding, block sectioning and slide mounting was performed by the pathology core (National Jewish Health).

Slides were blindly scored by a pathologist (Cassie Xu, University of Colorado School of Medicine) following an American Thoracic Society ALI scoring system [94]. 4-5 fields (400X total magnification) of each transverse lung piece (4-5 pieces total) were assessed for five weighted parameters of ALI injury and a final averaged score between 0 (no injury) and 1 (most severe) was calculated for each mouse.

3.2.7 Expression time-course of genes implicated in HA breakdown in LPS-challenged mice

Gene expression of *msHYAL1-2*, *msTMEM2*, *msCEMIP*, and *msCD44* in mouse resident and recruited alveolar macrophages was identified using Ensembl gene annotation of the previously described RNA-seq dataset (Chapter 2.2 Methods) [145].

3.2.8 HA fragmentation assessment in whole lung

HA fragmentation in perfused lung tissue was assessed using the protocol developed by Cleveland Clinic Program of Excellence in Glycoscience and previously described [155]. Non-lavaged lungs were perfused with 10 mL blood bank saline and flash frozen. 50 mg of lung tissue was proteolytically digested using Proteinase K (1 mg/mL) resuspended in 100 mM ammonium acetate (pH 7.0) with 0.01% sodium dodecyl sulfate (24 h, 60 °C). GAG were precipitated using 100% ethanol and washed using 75% ethanol. GAG pellets were resuspended in 100 mM ammonium acetate and heated at 100 °C to inactivate Proteinase K. Nucleic acids were degraded with an overnight benzonase incubation (MilliporeSigma) and then warmed to 100 °C to denature benzonase. GAG was then precipitated with 100% ethanol and washed in 75% ethanol. GAG pellet was resuspended in 100 mM ammonium acetate and equally divided, with half left untreated and half treated with 0.2 turbidity reducing units (TRU) of *S. hyaluronolyticus* hyaluronidase (Seikagaku, amsbio, Cambridge, MA), which allows for confirmation that the GAG present is specifically HA.

All samples were lyophilized using a rotovap and resuspended in formamide (MilliporeSigma) and then loaded on 1% agarose gel (SeaKem HGT Agarose, Lonza). Stains-All (MilliporeSigma) was used to stain the gel overnight (1.25 mg/200 mL in 30% ethanol). On the next day, the gel was equilibrated in water and destained using brief exposure to ambient light. Gels were imaged on ChemiDoc MP (Biorad) using the Cy5 695/55 epi-fluorescence filter, which detects HA stained with Stains-All [156]. HA

fragments were sized using a ladder consisting of Select-HA (Hyalose, Oklahoma City, Oklahoma, USA) of predetermined sizes (2500, 1000, 500, and 250 kDa HA) as well as the Select-HA HiLadder (Hyalose). ImageJ was used to analyze the distribution of HA staining and perform densitometry calculations as described before [157]. Due to the large pore size, agarose gel electrophoresis is optimally suited for resolving high and medium molecular weight HA (>200 kDa). Alternative methods such as chromatography and polyacrylamide gel electrophoresis can provide better resolution and quantification of LMW HA [158, 159].

3.2.9 Lung tissue HA staining and discontinuity quantification

Confocal Z-stacks of HA-stained lung sections were de-identified for the treatment received and blindly scored by a pulmonologist (Victor Tseng, University of Colorado School of Medicine). 3-5 representative images (320 x 320 μm) of the left lung were taken from each mouse. For each image, the HA staining in the peri-broncho-vascular interstitial area was sampled with five representative snapshots (9.4 x 9.4 μm). Max intensity Z projections were prepared within the Fiji distribution of ImageJ [160]. Roughness was derived from the surface area [161] of the plotted intensity of HA staining, which was calculated using the SurfCharJ plugin [162]. Normalized roughness was calculated by dividing the surface area by average staining intensity of the snapshot. Normalized roughness values across the representative snapshots were averaged to assign a score for each individual mouse.

3.2.10 Bronchoalveolar lavage fluid (BALF) collection and flow cytometry

Mice underwent tracheotomy with the insertion of an 18-gauge angiocatheter (4075, JELCO-W, Smiths-Medical, Minneapolis, MN). BALF was collected by five serial instillations (1 x 1 mL and 4 x 0.9 mL) of PBS containing 2 mM EDTA (a return of 4 mL of total BALF was consistently obtained). For calculating the total CD45⁺ count, representative aliquots of the five lavages were combined, blocked with CD16/CD32

(clone 93, eBioscience), and stained with CD45 (30-F11, Becton Dickinson or BD Biosciences, Franklin Lakes, NJ, USA). 100 μ L of 1:10 diluted 123count eBeads (eBioscience) were added to stained cells. For the total cell count, centrifugation was avoided to minimize variability introduced by spinning and aspiration. With the known concentration of the added counting beads and the ratio of CD45⁺ events to counting bead events given by the flow cytometer, the concentration of CD45⁺ cells was calculated and multiplied by 4 mL to get the total CD45⁺ cell counts.

For the BALF differential, the five lavages were centrifuged and cell pellets combined. Flow wash buffer consisting of PBS with 9% FBS and 0.5 mM EDTA was used to resuspend and wash cells. Cell pellet was resuspended in flow wash buffer containing CD16/CD32 (eBioscience) and the fluorescently-conjugated antibodies: CD45 (30-F11, BD Biosciences), Ly6G (1A8, Biolegend), CD64 (X54-5/7.1, BD Biosciences), CD11c (N418, eBioscience), F4/80 (BM8, eBioscience), CD11b (M1/70, eBioscience), Siglec-F (E50-2440, BD Biosciences), CD4 (RM4-5, Biolegend), and CD8a (53-6.7, Biolegend). On the LSR II cytometer (BD Biosciences), a minimum of 20,000 (PBS group) and 100,000 (LPS group) CD45⁺ leukocyte events were collected for each sample. Raw flow cytometry data was exported and analyzed in FlowJo software (FlowJo, Ashland, Oregon, USA). Schematic of gating used for BALF differential and CD45⁺ total cell counts is depicted (**Figure 3.1**).

3.2.11 ELISA

To measure albumin-, receptor for advanced glycation end products (RAGE)-, and HA, ELISAs were performed following manufacturer's protocols: mouse albumin ELISA quantitation set (Bethyl Labs, Montgomery, TX); RAGE DuoSet ELISA (R&D Systems); HA DuoSet ELISA (R&D Systems). Combined supernatant obtained by pelleting (600 g, 8 min) the first three BALF aliquots (total 2.6 mL volume) was assayed using sample dilutions of 1:3000; 1:6; and 1:4 (control group) or 1:12 (LPS group),

respectively. 96-well plates (Nunc MaxiSorp) were coated and were read as previously described for TSG-6 ELISA (Chapter 2.2 Methods).

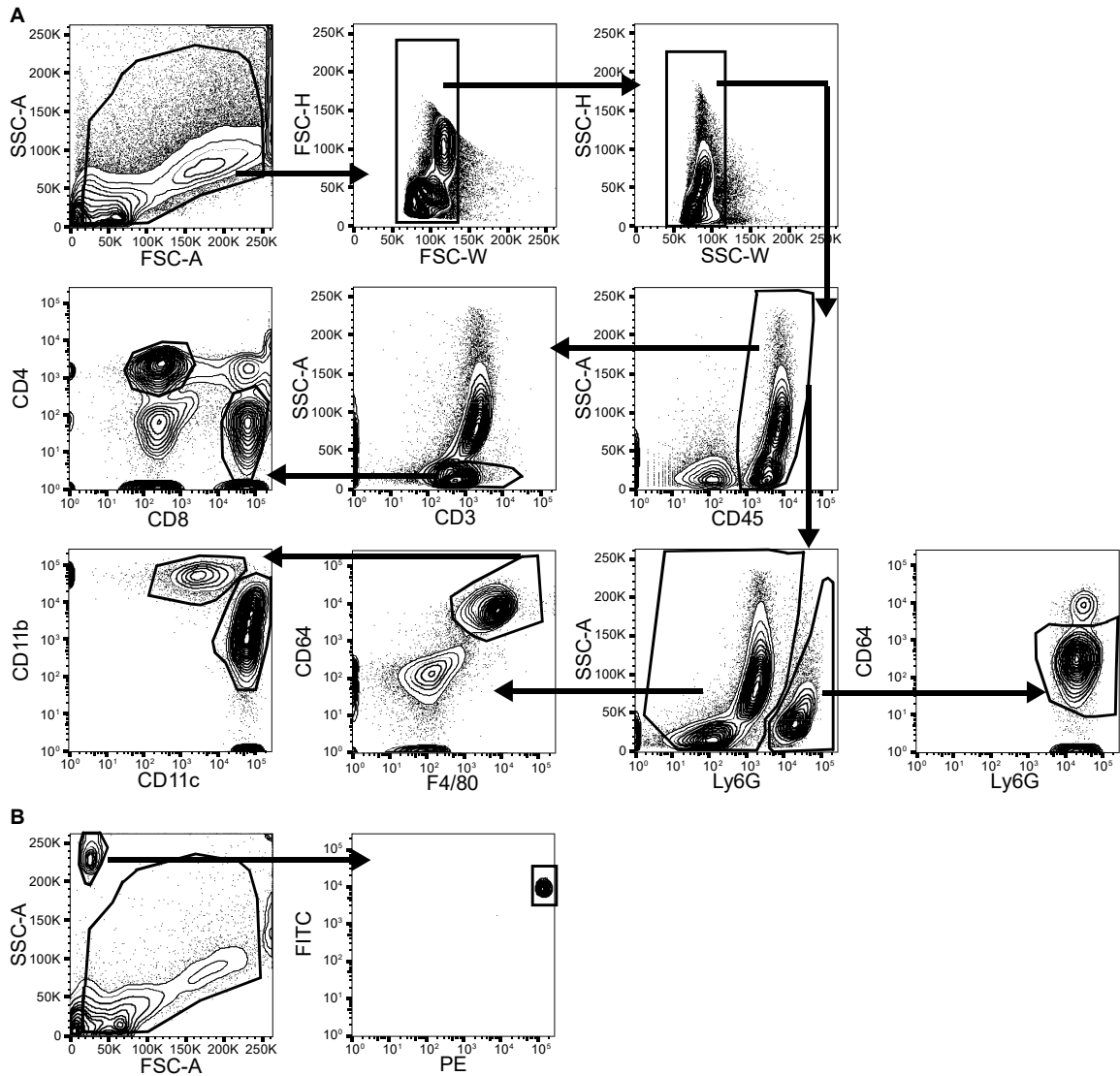


Figure 3.1. Flow cytometry analysis of bronchialveolar lavaged leukocytes

Bronchoalveolar lavage fluid (BALF) collected from a mouse (4 days post LPS instillation) is depicted to show all the recruited cells analyzed. **A.** Hematopoietic cells were identified by excluding debris and doublets and CD45⁺ staining. T cells were gated on CD3⁺ staining and distinguished by CD4⁺ CD8⁻ and CD8⁺ CD4⁻ staining. Neutrophils were gated as Ly6G⁺CD64⁻ cells. Macrophages were gated as CD64⁺F4/80⁺ cells and differentiated as resident (CD11b^{low}CD11c⁺SiglecF⁺) or recruited (CD11b⁺CD11c^{low}). **B.** Counting beads were gated using their unique light scatter profile (SSC^{hi}FSC^{lo}) and fluorescently embedded dyes (FITC⁺PE⁺). Figure from Ni et al. [56], open source.

3.3 Results

3.3.1 Lung parenchymal HC-HA induction and clearance

To ascertain the kinetics of HC-HA induction during respiratory infection-induced ALI, we intratracheally administered either LPS (20 μ g) or *PA* (2×10^6 CFU) and collected lavaged and perfused lungs from two timepoints, initial injury (1 day post LPS or 2 day post *PA*) and resolution phase (4 days post injury), for measuring HC-HA content. We treated homogenized lung with hyaluronidase (1U, HAse), which would release any HC linked to HA by degrading all HA into disaccharides. Using an I α I western blot, we were able to detect and quantify the robust release of HC initially after LPS (1 day post injury, **Figure 3.2A**) or *PA* (2 days post injury, **Figure 3.2B**) challenge, which suggest rapid and extensive lung parenchymal HC-HA formation. But by resolution phase (4 days post injury) after either LPS or *PA* challenge, released HC was largely absent, which suggests rapid clearance of HC-HA during resolving ALI. To confirm the role of TSG-6 as the exclusive mediator of HC-HA formation, lungs from *TSG-6* KO and littermate controls (WT and HT) exposed to IT LPS and collected 1 day post injury were assessed for their HC-HA content (**Figure 3.2C**). As expected, released HC was notably absent in *TSG-6* KO mice lungs when compared to control lungs, which confirmed TSG-6's exclusive enzymatic function and validated the *TSG-6* KO mice.

After demonstrating rapid HC-HA induction, we investigated whether the whole lung transcript levels of *TNF α* , the eponymous TSG-6 stimulus, and *TSG-6* were temporally associated with HC-HA induction during ALI. Both whole lung *msTNF α* (**Figure 3.2D**) and *msTSG-6* (**Figure 3.2E**) were upregulated at 1 day post injury and returned to baseline levels at 4 days post injury in a manner that paralleled the induction of HC-HA: ~ 99 (1 day) vs. ~ 2 (4 day) relative fold *msTNF α* induction and ~ 3 (1 day) vs. ~ 1 (4 day) relative fold *msTSG-6* induction. While HC-HA accumulates in established interstitial lesions of chronic lung diseases, the location of HC-HA induced during

resolving ALI is unknown. To determine the localization of HC-HA, we co-stained sections of *PA*-challenged lung with probes for HC and HA (**Figure 3.3**). We found that HC appeared in peri-broncho-vascular regions and co-localized with HA at both 1 and 2 days following IT *PA* injury, which was in agreement with the HC-HA induction noted in the homogenized lung.

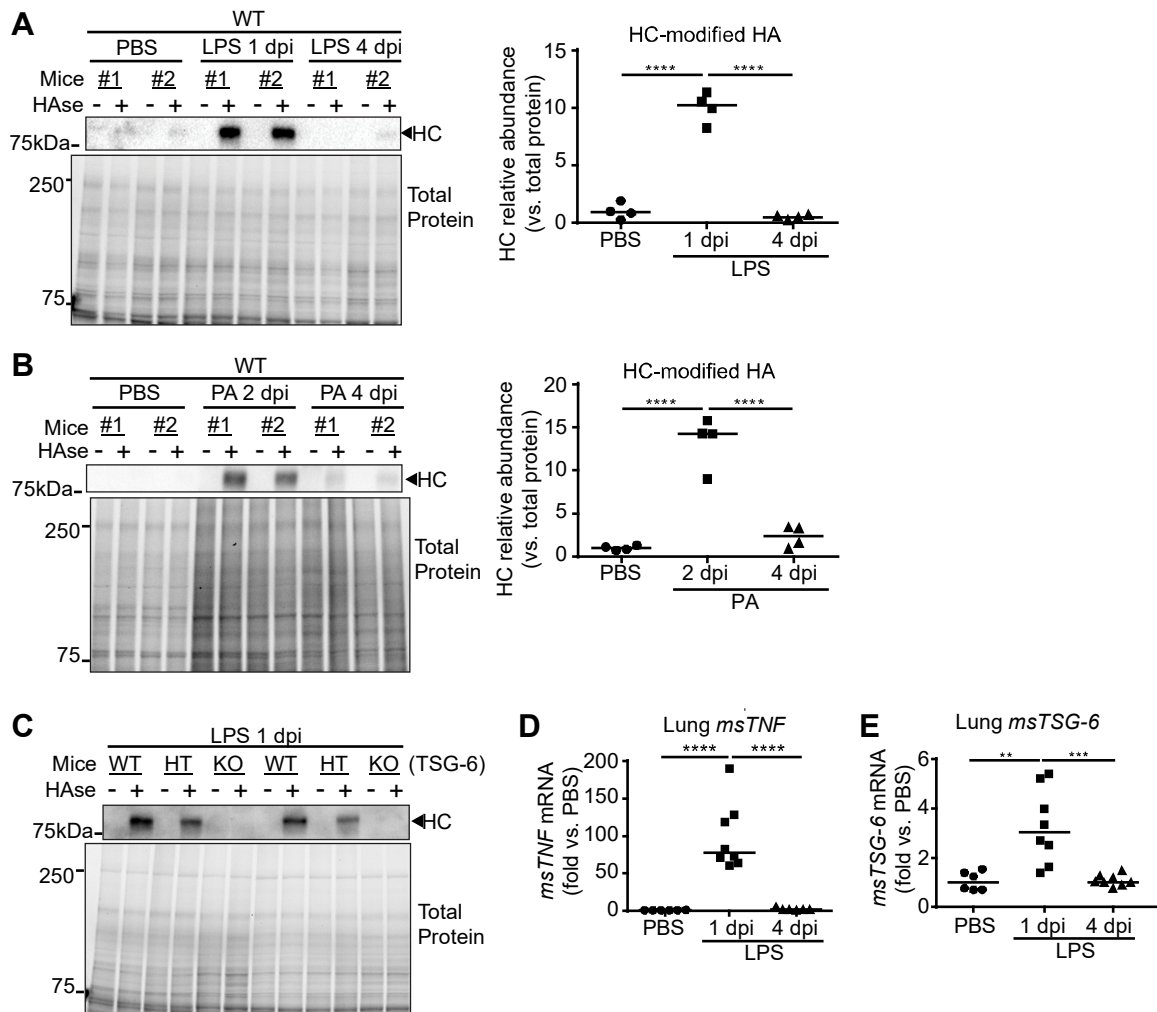


Figure 3.2. Lung parenchymal HC-HA formation after LPS or PA injury

A-C. Lung parenchymal HC-HA content was assessed by homogenizing bronchoalveolar lavaged and perfused lung tissue and treating with PBS (-) or hyaluronidase (+) to liberate any HC linked to HA, which can be detected by Ial western blot. Each mouse lung (pair of + and – HAse lanes) was isolated following exposure to IT LPS (20 μ g, **A**) or PA (2 x 10⁶ CFU, **B**) at an acute and a resolution time point and compared to PBS control. **C.** The role of TSG-6 as the exclusive mediator of HC-HA formation was confirmed by assessing the absence of HC-HA content in TSG-6 KO mice tissue collected 1 day post injury after IT LPS and comparing to littermate controls (WT and HT). **D-E.** Whole lung *msTNF* (**D**) and *msTSG-6* (**E**) transcript levels from mice

exposed to indicated treatments were measured by qPCR. WT, wildtype. HT, heterozygous. KO, knockout. dpi, days post injury. $n = 4-8$ mice per group. Data analyzed by ANOVA with Tukey's multiple comparisons. $**P < 0.01$, $***P < 0.001$, $****P < .0001$. Figure from Ni et al. [56], open source.

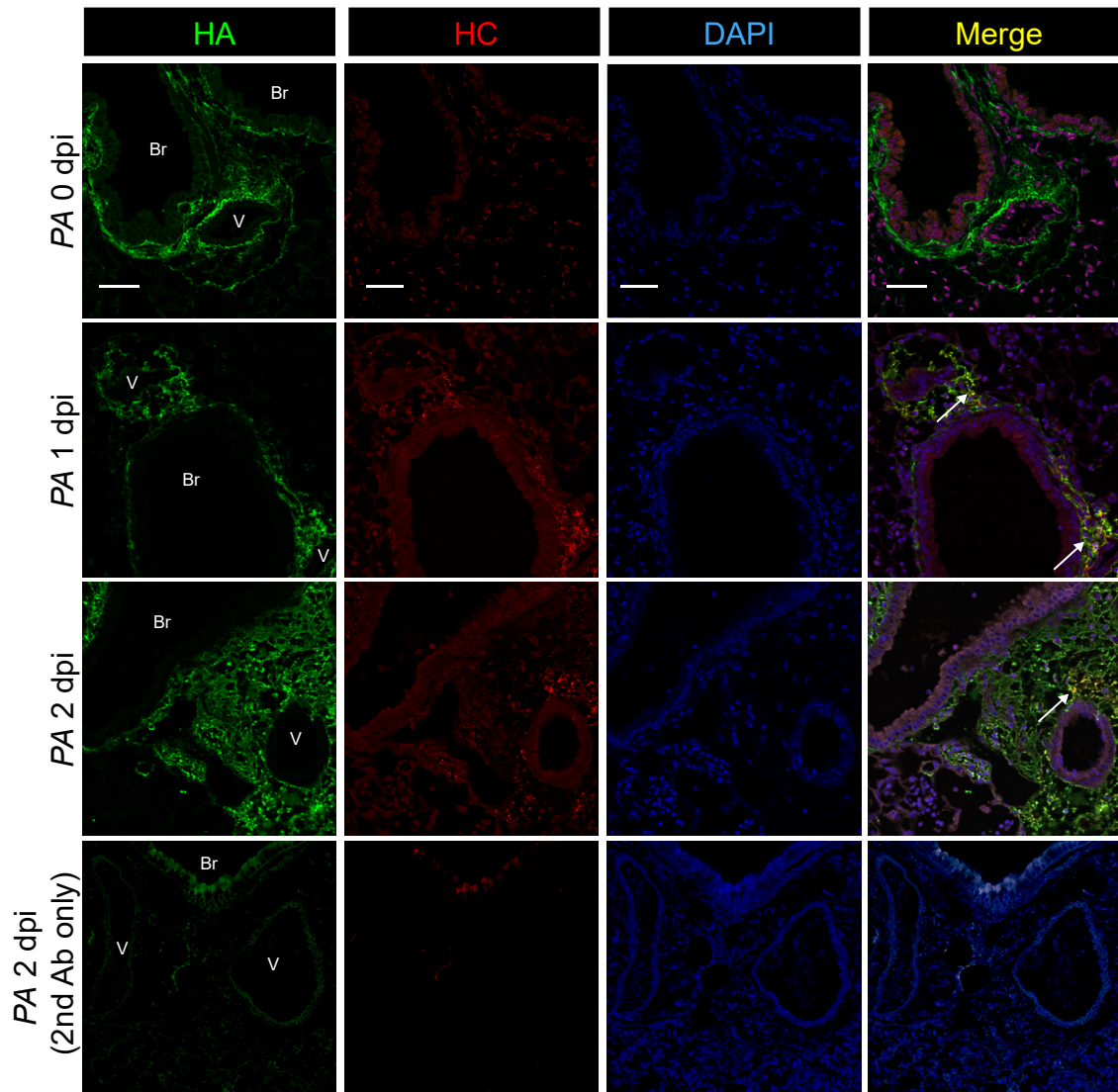


Figure 3.3. Distribution of HC and HA staining after *PA* injury

Sections of lung isolated from mice after exposure to IT *PA* (1 or 2 days post injury) or uninjured control (0 days post injury) were stained with HA binding protein (green) and HC2 antibody (red). Nuclei were stained by DAPI (blue). White arrows denote colocalization of HC and HA staining (yellow) in the peri-broncho-vascular interstitium. 2nd antibody only staining (bottom row) was performed as a control. Br, large airway bronchus. V, vessel. Scale bar, 50 μ m. Figure from Ni et al. [56], open source.

3.3.2 HA turnover and remodeling during ALI

Since HC-HA was rapidly induced after injury and then absent by the onset of resolution of ALI (4 days post injury), we investigated whether active HA breakdown was induced during ALI. To investigate the molecular weight distribution of HA, we extracted glycosaminoglycans (GAG) from lung tissue taken from mice at two time points (1 or 2 days post injury) following IT LPS (20 µg) exposure or PBS control, separated the polysaccharides by size under agarose gel electrophoresis, stained the polysaccharides with Stains-all, and performed densitometry (**Figure 3.4**). Samples treated with hyaluronidase (0.2 TRU, HAse) were analyzed to confirm specific HA staining. Additionally, as the largest GAG, high and medium molecular weight HA (2500-250 kDa) have no overlap with other GAG, which are all smaller than 50 kDa. In contrast to the abundance of HMW HA fragments (1000-2500 kDa) in PBS control, immediately following LPS challenge (1 or 2 days post injury), a large amount of HMW HA was replaced with an increasing amount of medium molecular weight HA fragments (250-500 kDa).

No striking differences in HA fragment distribution between *TSG-6* KO and HT mice were observed, which would suggest that the increase in medium molecular weight fragments appeared independently of HC-HA formation (**Figure 3.5A**). Additionally, total HA content in the BALF measured by ELISA (which detects HA fragments of all sizes with a minimum limit of detection between 6 kDa and 15kDa [163]) was upregulated initially after injury (1 day post injury) and largely returned to baseline during the two resolution time points (4 and 6 days post injury). This finding suggests active HA clearance in the respiratory tract (**Figure 3.5B**). No difference in the levels of HA content was noted between *TSG-6* KO and control (WT and HT) to suggest that HC-HA formation had any effect on HA turnover. Together, these results suggested that HA fragmentation and clearance occurred independently of HC modification.

Having demonstrated induction of HA breakdown and turnover during ALI, we investigated whether interstitial HA staining in lung sections underwent morphologic changes after LPS exposure. Lungs from mice exposed to LPS (20 µg, 4 days post injury) were stained with HA binding protein and compared to PBS control (**Figure 3.6A-B, Figure 3.7**). While the pattern of HA staining appeared lamellar in texture in uninjured lungs, LPS injury induced a switch to more punctate and granular HA staining. To quantify the morphologic changes that are thought to represent HA remodeling driven by HA synthesis and fragmentation, we generated surface intensity plots of HA staining and measured the surface roughness. LPS injury significantly ($P<0.05$) increased the roughness of HA staining (**Figure 3.6C**).

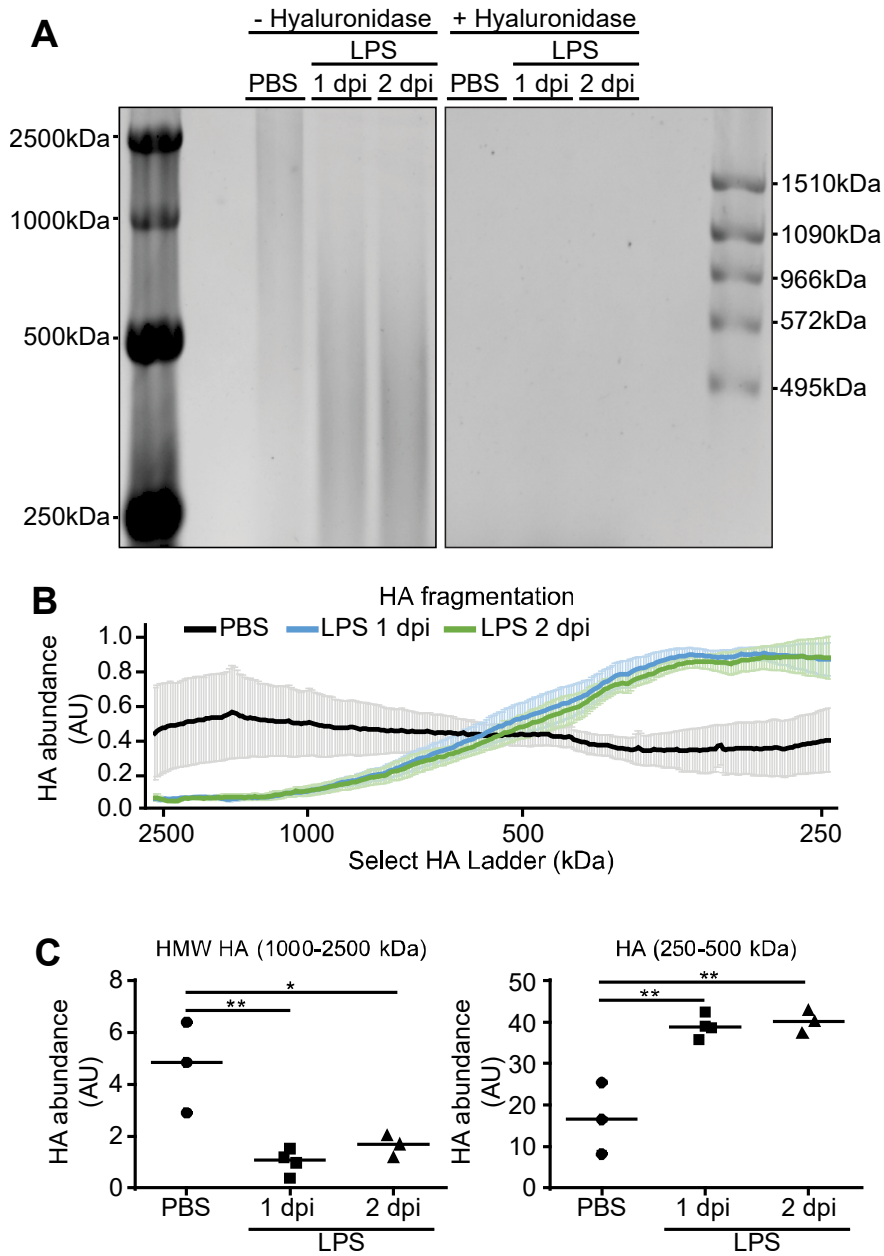


Figure 3.4. Lung HA molecular weight distribution after LPS injury

A. Stains-All detection of HA extracted from lung tissue of mice exposed to LPS (1 or 2 days post injury) or PBS control and resolved by agarose gel electrophoresis. Samples were divided in half and treated in parallel with hyaluronidase to confirm that HA was specifically stained. Select-HA of the following sizes (2500, 100, 500, 250 kDa) and Select-HA HiLadder were used to size HA. **B.** Distribution of HA staining (mean +/- SEM)

by molecular weight was quantified by densitometry in ImageJ and plotted. **C**.
Abundance of high and medium molecular HA staining was determined by integrating the area of HA abundance over specified size ranges. Data analyzed by ANOVA with Tukey's multiple comparisons. * $P < 0.01$, ** $P < 0.01$. Figure from Ni et al. [56], open source.

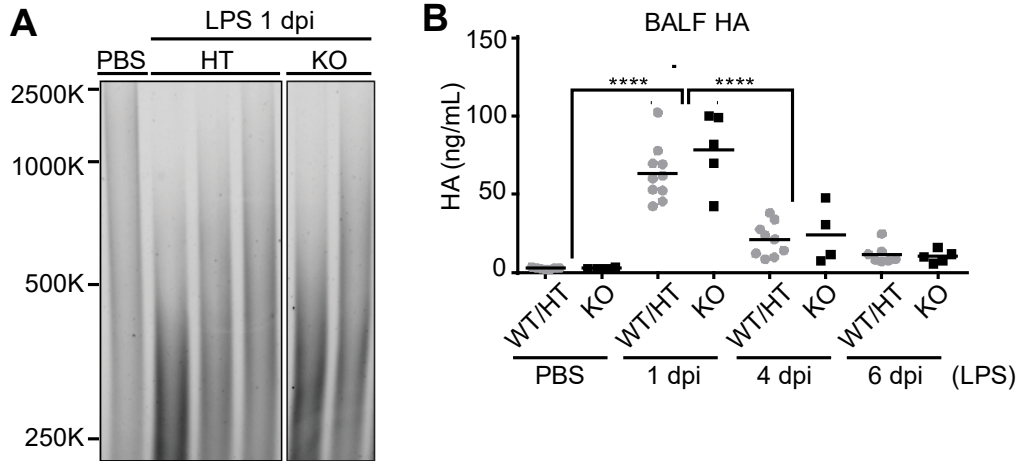


Figure 3.5. Effect of TSG-6 on lung HA molecular weight and lavage levels

A. Stains-All detection of HA isolated from lung tissue of *TSG-6* HT and KO mice exposed to LPS (1 day post injury) or PBS control and resolved by agarose gel electrophoresis. **B.** Total HA content in BALF was analyzed by ELISA during a time course of LPS injury and resolution (1, 4, or 6 days post injury) and compared to PBS control. $n = 4-10$ mice per group. Data analyzed by ANOVA with Tukey's multiple comparisons. **** $P < .0001$. Figure from Ni et al. [56], open source.

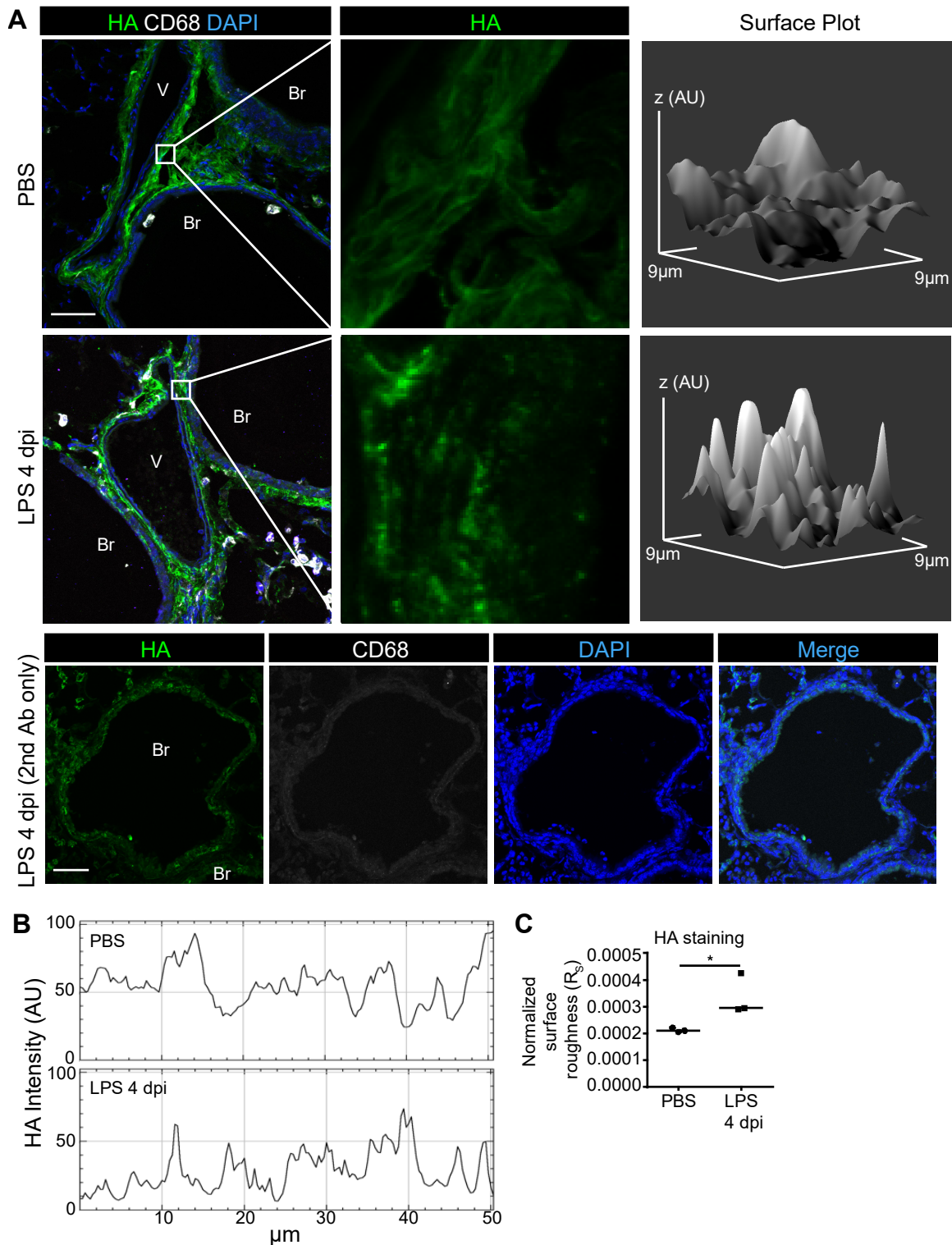


Figure 3.6. Morphological changes in interstitial HA staining after LPS injury

A. Identification of prominent HA staining in peri-broncho-vascular interstitium bordered by bronchi (Br) and blood vessels (V) in paraformaldehyde-fixed, frozen lung sections of

mice exposed to LPS 4 days post injury or PBS control that were stained with HA-binding protein (green), macrophage marker CD68 (white), and nuclear stain DAPI (blue). A section stained with only the secondary probes is shown in the bottom row as control. Surface plots of the maximum intensity Z-projections of 9.4 x 9.4 μm interstitial areas were graphed and depicted on the right, measured in arbitrary units (AU). Scale bar, 50 μm . **B.** Line profile of HA staining in a max intensity Z-projection of a representative 50 x 50 μm area from the two treatments groups. **C.** Normalized surface roughness of HA staining was determined by dividing the surface area of staining by average staining intensity and compared between the indicated treatment groups. $n = 3$ mice per group. Data analyzed by Student's T-test. $*P < 0.01$. Figure from Ni et al. [56], open source.

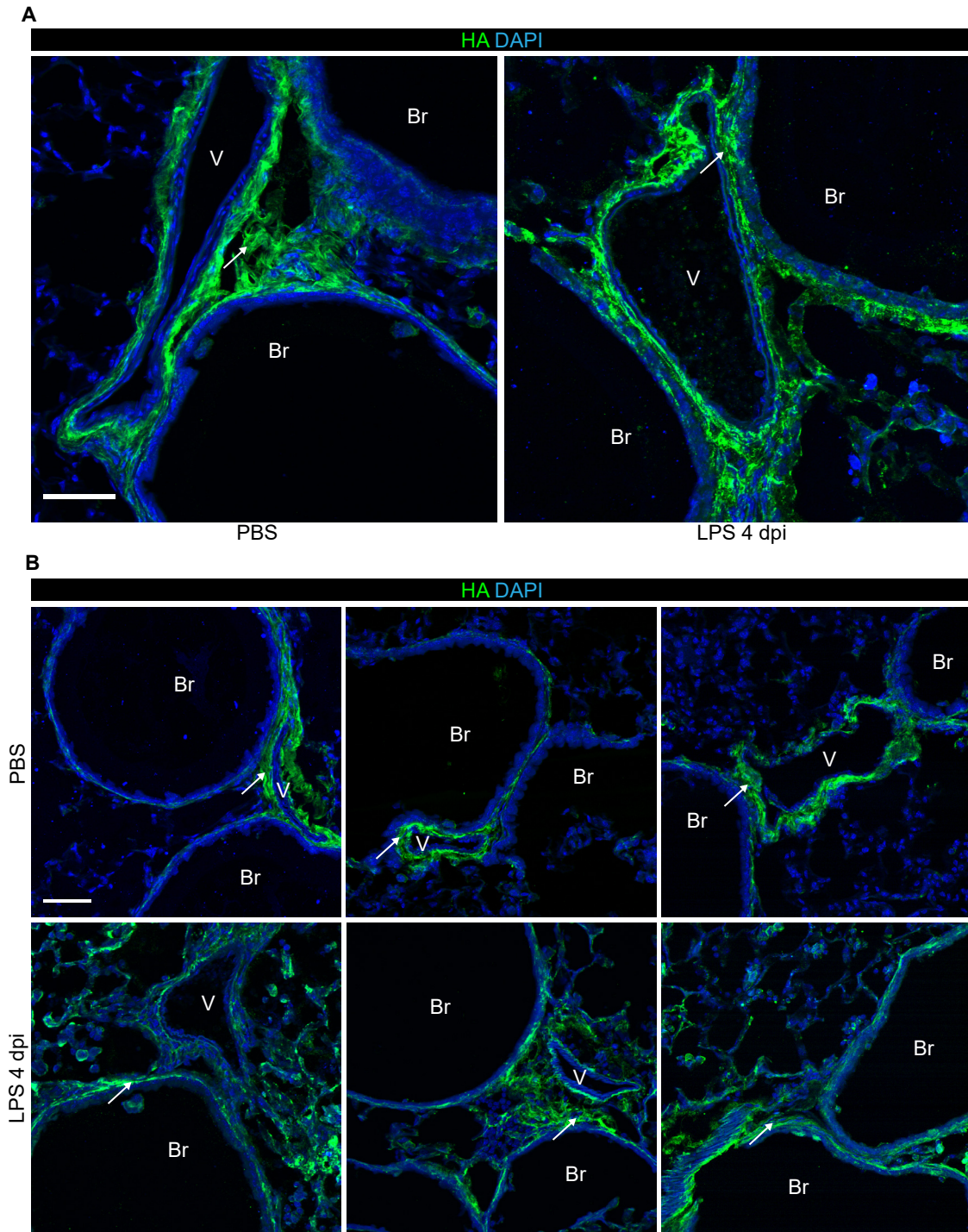


Figure 3.7. HA staining after LPS injury

A. Images of the paraformaldehyde-fixed, frozen lung sections stained with HA-binding protein (depicted in **Figure 3.6**) shown in more detail. Morphological changes were observed for HA staining in the peri-broncho-vascular interstitium (white arrow).

Bronchus (Br) and large vessel (V) depicted. **B.** Representative sections from independent mice ($n = 3$ mice per group). Scale bar 50 μm . Figure from Ni et al. [56], open source.

To better understand the active HA turnover and morphological changes in HA staining suggestive of HA remodeling, we investigated the transcript levels of genes encoding key enzymes responsible for synthesizing and breaking down HA. In whole lung tissue, expression of all three HA synthases (*HAS1-3*) were initially upregulated at 1 day post LPS (*msHAS1* ~2, *msHAS2* ~5, and *msHAS3* ~3 relative fold induction, respectively) and returned to baseline (*msHAS1* ~0.3, *msHAS2* ~1, and *msHAS3* ~1 relative fold induction, respectively) by 4 days post injury (**Figure 3.8A**). In contrast, the two key somatic hyaluronidases (*HYAL1-2*) were downregulated initially and during resolution (**Figure 3.8B**). Two genes, *TMEM2* and *CEMIP*, encoding a HA degrading enzyme and a HA-binding protein recently implicated in HA endocytosis and degradation, respectively, were also assessed (**Figure 3.8C**). While *msTMEM2* was consistently suppressed (1 day ~0.7 vs. 4 days ~0.7 relative fold induction), *msCEMIP* was upregulated initially and returned to baseline (1 day ~4 vs. 4 days ~1 relative fold induction).

The steady clearance of HA in BALF with the resolution of inflammation (**Figure 3.5B**) suggested the presence of cells in the respiratory tract that actively cleared HA. Since alveolar macrophages (AM) can bind and degrade HA [164], we analyzed the previously described RNA-seq dataset (Chapter 2.2 Methods) to assess the transcript abundance of genes implicated in HA breakdown in resident vs. recruited AM over the time course of IT LPS-induced ALI and resolution. In contrast to whole lung, we found stable expression of *msHYAL1-2* and early induction of *msTMEM2* in both types of AM that peaked at 3 days post injury and fell to baseline with resolution of inflammation (**Figure 3.5D**). Unlike the abundant levels of *msHYAL2* and *msTMEM2*, *msHYAL1* was minimally expressed and *msCEMIP* levels were below the one transcript per million threshold cut-off. Since *HYAL2*'s ability to degrade HA requires *CD44* to first bind HA at the cell surface [33, 34], *CD44* expression was analyzed and found to be very highly

expressed (**Figure 3.5E**). In contrast to *msTMEM2*, *msCD44* expression in both resident and recruited AM steadily increased during resolution to reach peak levels on day 12 post injury.

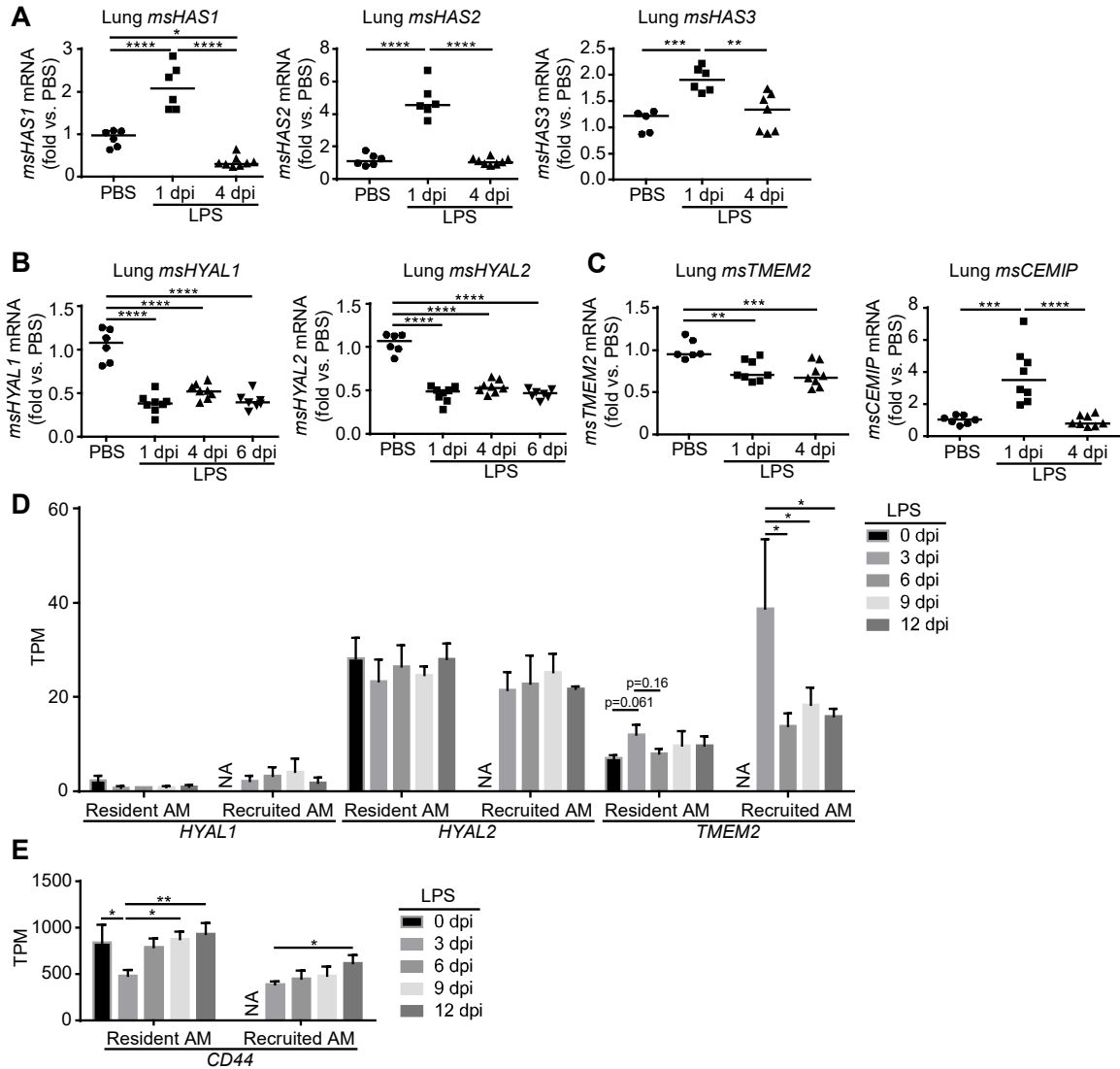


Figure 3.8. Effect of ALI on genes implicated in HA synthesis and breakdown

A-C. Whole lung transcript levels of genes implicated in HA synthesis (*HAS1-3*) and HA breakdown (*HYAL1-2*, *TMEM2*, and *CEMIP*) during a time course of LPS-induced ALI and resolution, assessed by qPCR. $n = 5-8$ mice per group. **D-E.** Resident and recruited AM expression of genes implicated in HA degradation (*HYAL1-2*, *TMEM2*, *CD44*), assessed by RNA-seq. TPM, transcript per million. Data analyzed by ANOVA with Tukey's multiple comparisons. * $P < 0.01$, ** $P < 0.01$, *** $P < 0.001$, **** $P < 0.0001$. Figure from Ni et al. [56], open source.

3.3.3 Effect of HC-HA on ALI outcomes

Since HC-HA is implicated in neutrophil trafficking and survival outcomes during systemic LPS exposure and its associated ALI, we utilized *TSG-6* KO mice to investigate the effect of HC-HA during localized IT LPS-induced ALI. We first examined the effect of HC-HA on weight loss severity and rate of recovery and noted no difference between *TSG-6* KO mice and HT control (**Figure 3.9A**). To assess the impact of HC-HA on lung inflammation, we then assessed the abundance of lavaged inflammatory cells in the respiratory tracts by flow cytometry. In response to IT LPS (20 μ g) challenge, absolute BALF counts of total hematopoietic (CD45⁺), neutrophils (Ly6G⁺), recruited macrophages (F4/80⁺CD64⁺CD11b⁺), CD4⁺ T cells, and CD8⁺ T cells were largely similar between *TSG-6* KO and control (WT and HT) (**Figure 3.9B-F**). Total CD45⁺ hematopoietic cells and Ly6G⁺ neutrophils peaked at day 1 post LPS: uninjured $\sim 2.2 \times 10^5$ vs. 1 day $\sim 1.4 \times 10^6$ CD45⁺ cells; uninjured $\sim 2 \times 10^3$ vs. 1 day $\sim 1.2 \times 10^6$ Ly6G⁺ neutrophils. As their numbers were dropping by day 4 of resolution, greater CD45⁺ (KO 1.3×10^6 vs. WT 1.0×10^6 , $p=0.013$) and Ly6G⁺ (KO 13×10^4 vs. WT 5.1×10^4 , $p=0.13$) counts were noted in *TSG-6* KO mice compared to control, which can result from a delayed onset in resolution. To confirm the BALF cellularity data findings, we measured in BALF the levels of albumin, a marker of microvascular endothelial damage (**Figure 3.9G**), and RAGE, a marker of airway epithelial damage (**Figure 3.9H**), by ELISA. No differences in albumin or RAGE levels were noted between *TSG-6* KO and control (WT and HT). Histologic evaluation of the extent of ALI resolution by 4 days following LPS was performed by hematoxylin and eosin staining of paraffin-embedded, formalin-fixed lung sections and blinded scoring for lung injury severity by a pathologist familiar with current recommendations [94] (**Figure 3.10**). We saw no evidence that lung injury scores were significantly different between *TSG-6* KO and WT mice (**Figure 3.10A**).

Finally, we examined the effect of HC-HA during a time course of *PA* infection (2×10^6 CFU, IT) in order to validate our findings in a live gram negative bacterial infection model. Similar to our findings with IT LPS challenge, there were minimal differences in absolute neutrophil counts (**Figure 3.11A**) or albumin levels (**Figure 3.11B**) in BALF collected from *TSG-6* KO vs. HT harvested at the following time points (2, 4, and/or 6 days) following IT *PA* challenge compared to IT PBS control. There was a trend toward increased BALF neutrophil count (KO $\sim 11 \times 10^6$ vs. HT $\sim 7 \times 10^6$ Ly6G⁺, $p=0.049$) and albumin levels (KO ~ 1000 ng/mL vs. HT ~ 600 ng/mL, $p=0.086$) in *TSG-6* KO 2 days after *PA* challenge. Together with the finding above that CD45⁺ and Ly6G⁺ counts were greater (15% more CD45⁺ in KO vs. HT, $p=0.096$; 13% more Ly6G⁺ in KO vs. HT, $p=0.34$) in *TSG-6* KO 4 days after LPS, our results suggest that *TSG-6* and HC-HA plays a modest protective role during IT LPS and *PA* challenge.

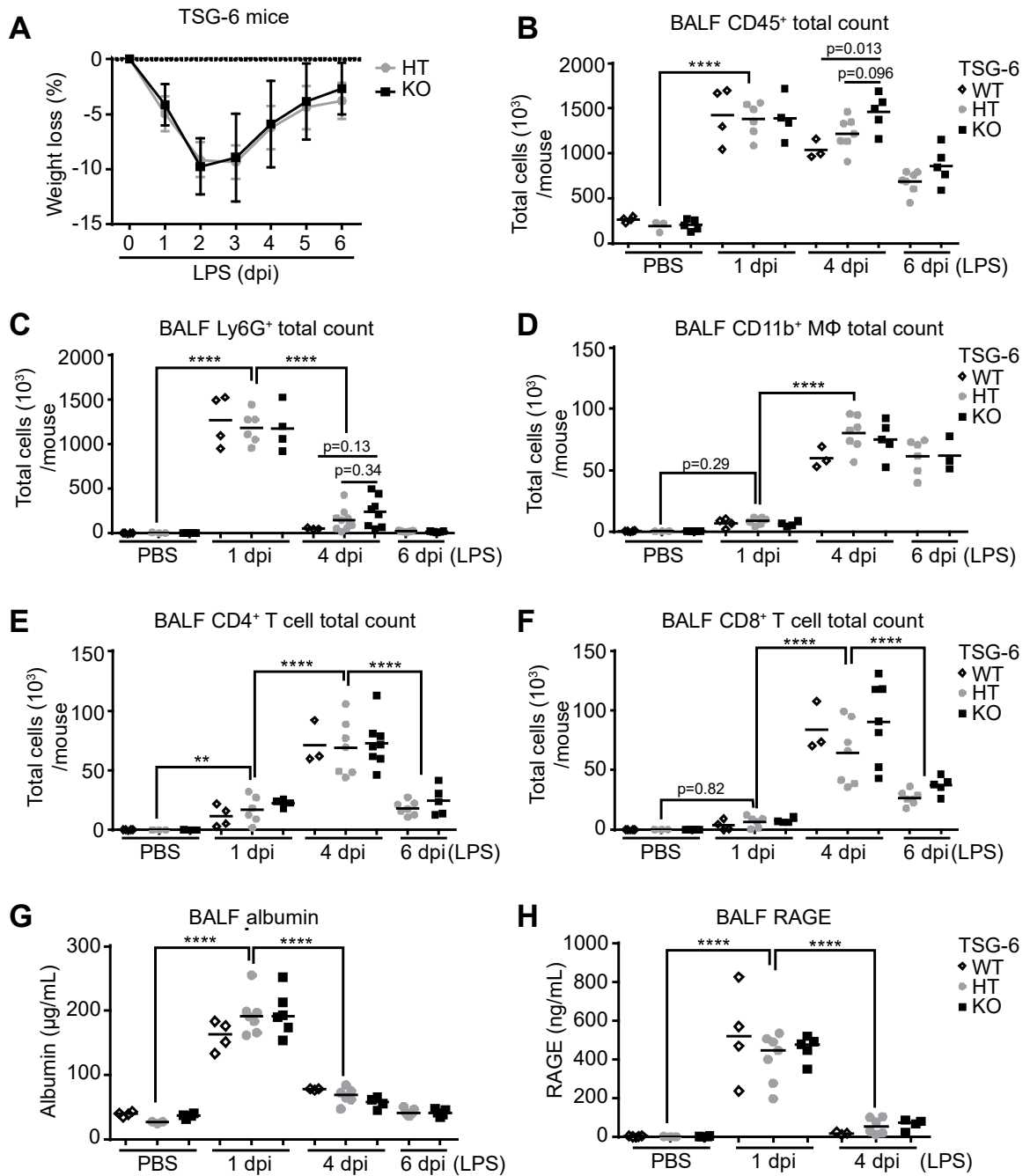


Figure 3.9. Effect of TSG-6 on severity and resolution of LPS-induced ALI

A. Rate of weight loss and recovery in *TSG-6* KO and HT during time course of IT LPS-induced ALI. **B-F.** Total counts of inflammatory cells in BALF of *TSG-6* KO mice and control littermates (WT and HT) during time course of LPS injury determined by flow cytometry. Total hematopoietic cells were gated by CD45⁺ staining. Neutrophils were

gated by CD45⁺Ly6G⁺ staining. Recruited CD11b⁺ macrophages were gated by CD45⁺F4/80⁺CD64⁺CD11b⁺ staining. CD4⁺ T cells were gated by CD45⁺CD3⁺CD4⁺ staining. CD8⁺ T cells were gated by CD45⁺CD3⁺CD8⁺ staining. **G-H.** Levels of albumin and RAGE in BALF of *TSG-6* KO mice and control littermates (WT and HT) during time course of LPS injury, as assessed by ELISA. $n = 3-8$ mice per group. Data analyzed by ANOVA with Tukey's multiple comparisons. $**P < 0.01$, $****P < 0.0001$. Figure from Ni et al. [56], open source.

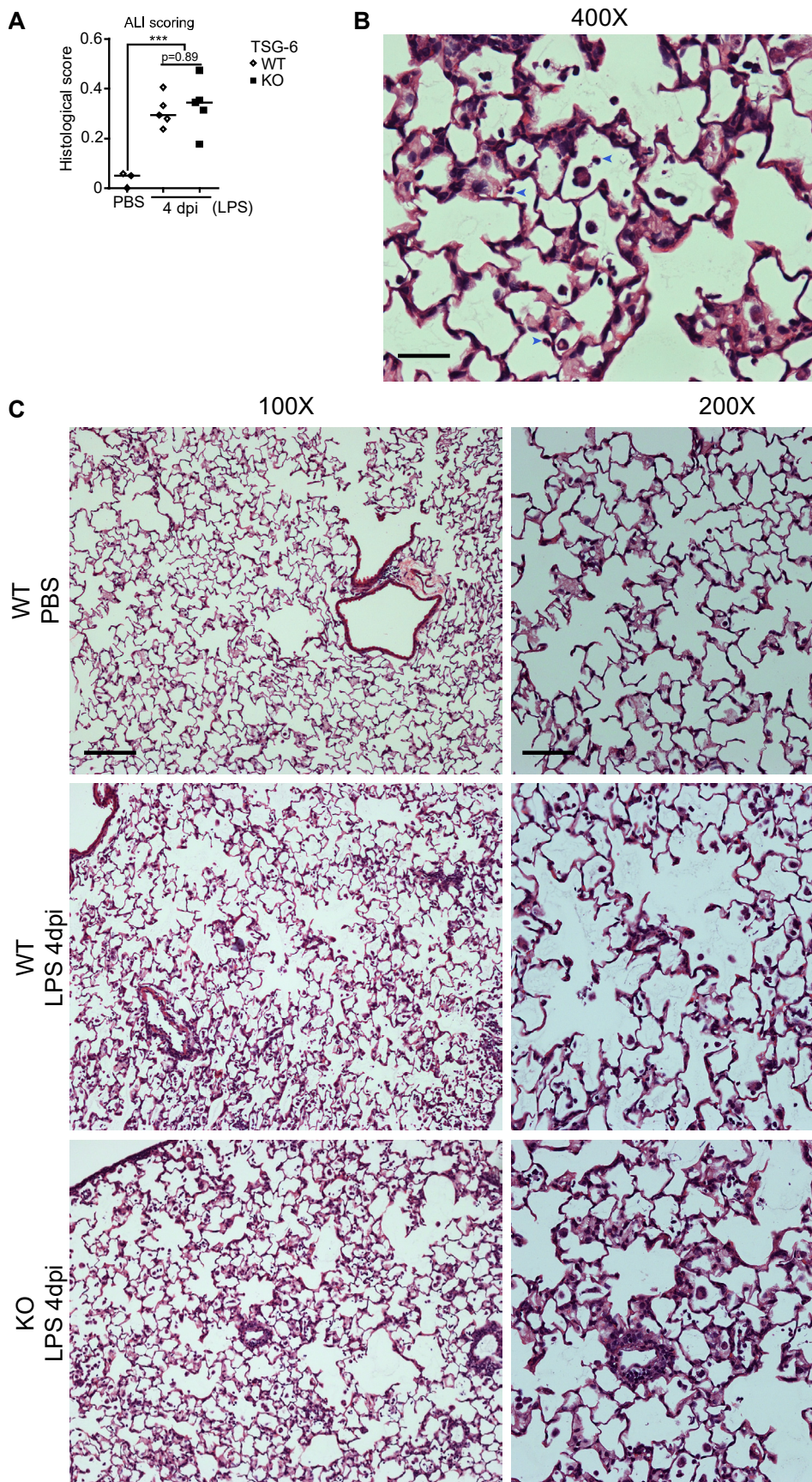


Figure 3.10. Effect of TSG-6 on histological injury scores of LPS-induced ALI

A. Histological ALI scoring of *TSG-6* KO and WT mice challenged with LPS (4 days post injury) compared to PBS control. $n = 3-5$ mice. **B.** Formalin-fixed, paraffin-embedded mice lungs were sectioned and stained with hematoxylin and eosin and scored at high power fields (400X). Blue arrowhead denotes neutrophils (4 days after IT LPS). **C.** Representative images taken at low power fields (100X and 200X) of lung sections from the following mice: *TSG-6* KO or WT 4 days after IT LPS compared to IT PBS control. Scale bars: 25 μm (400X), 50 μm (200X), and 100 μm (100X). Data analyzed by ANOVA with Tukey's multiple comparisons. *** $P < 0.001$. Figure from Ni et al. [56], open source.

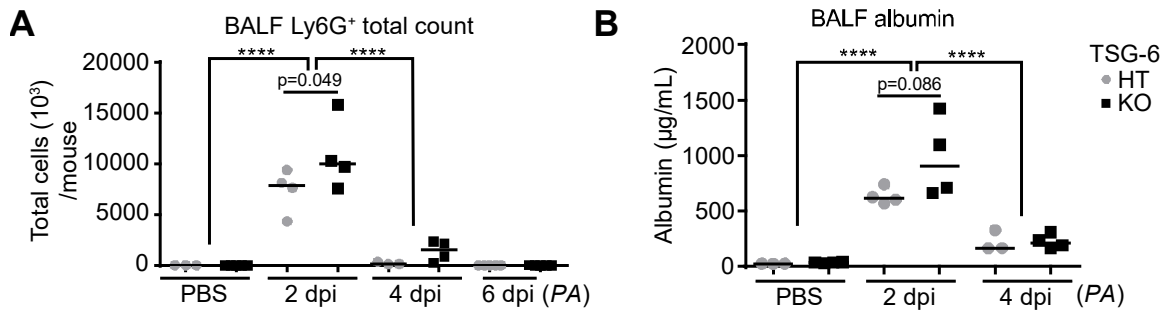


Figure 3.11. Effect of TSG-6 on severity and resolution of PA induced ALI

A. Absolute count of neutrophils ($\text{CD45}^+\text{Ly6G}^+$) in BALF, following 2, 4, 6 days post PA injury (2×10^6 CFU, IT), assessed by flow cytometry. **B.** Levels of albumin in BALF following 2 or 4 days post PA injury, assessed by ELISA. $n = 3\text{--}4$ mice per group. Data analyzed by ANOVA with Tukey's multiple comparisons. **** $P < 0.0001$. Figure from Ni et al. [56], open source.

3.4 Discussion

This study is the first to characterize the remarkable kinetics of lung parenchymal HC-HA induction and clearance during two resolving models of respiratory infection-induced ALI. We found that the rapid clearance of HC-HA was associated with induction of active HMW HA fragmentation, turnover, and histological changes suggestive of HA remodeling. We found that the rapid breakdown and clearance of HA occurred independently of HC-modification. Our reports are consistent with previous observations that lung HA undergoes a high rate of turnover during both homeostasis and inflammation [25, 26].

Our results are in striking contrast to the histopathological accumulation of HC-HA in lesions of various chronic lung diseases. This difference may be due to our models of IT LPS and *PA*-induced ALI are fully reversible and do not lead to fibroproliferative lesions as seen in ARDS patients. A key difference between ARDS and our resolving models of ALI is the repeated and continuous mechanical ventilation-induced epithelial insult that can trigger the fibroproliferative response in ARDS. A hallmark of chronic lung disease lesions is the deposition of collagen, which can envelop HA and HC-HA. It is conceivable that this collagen deposition may hinder access to hyaluronidase and ROS, which would allow HC-HA to accumulate instead of its clearance.

Using *TSG-6* KO mice deficient for HC-HA formation, we found that HC-HA only plays a modest protective role during both IT LPS- and *PA*-induced ALI. These results were surprising considering the key protective role of HC-HA in promoting survival during systemic IP LPS-induced endotoxic shock that has been demonstrated in both *TSG-6* [135] and *Iα1* [136] KO mice. But the discovery that HC-HA in the liver sinusoids can promote neutrophil adhesion during systemic LPS exposure suggests that HC-HA may be acting specifically in the vasculature during endotoxic shock. We address this

hypothesis in Chapter 4. Additionally, the lung compartmental localization of TSG-6 and levels of TSG-6 may be important. Using *TSG-6* KO and littermate controls, we focused on the physiological role of endogenous TSG-6, which catalyzes the formation of lung parenchymal HC-HA. In contrast, exogenous TSG-6 given intratracheally has been associated with anti-inflammatory effects, which may be due to the ability of TSG-6 to bind neutrophilic chemokines [165, 166] or its potential ability to modify macrophage polarization [135, 151] *via* HA interactions with its CD44 receptor. However, the differences in lung macrophage polarization in *TSG-6* KO vs. WT mice may be the result of markedly different inflammatory environments that can direct macrophage programming and functionality [135].

Our study is the first to investigate the role of TSG-6 and HC-HA during bacterial respiratory infection-induced ALI. TSG-6 deficiency was associated with greater neutrophilic inflammation in both IT LPS and *PA* models. These differences in BALF neutrophil counts were noted either directly following (LPS, 4 days post injury) or during (*PA*, 2 days post injury) peak inflammation, which was characterized by extensive HC-HA formation. Therefore, our results suggest that TSG-6 mediated HC-HA induction may have contributed to the protective effect seen with neutrophils. Considering the magnitude of the effect on BALF neutrophil counts and albumin levels, the protective effect of TSG-6 during ALI was modest. Given the importance of neutrophils in antibacterial defense [167-169], careful studies are needed with higher doses of *PA* to dissect whether TSG-6 and HC-HA are protective or harmful during gram negative bacterial ALI. While TSG-6 and HC-HA did not have huge effects on the outcomes of ALI, it is possible that they may be necessary for other injury and repair processes that require HA input including airway epithelial cell survival and homeostasis [170, 171]. Additionally, the rapid clearance of HC-HA during resolving ALI may have minimized the potential effects of HC-HA on lung injury and repair. Therefore, investigations with

experimental models that cause a more prolonged time course of inflammation and persistent HC-HA production are warranted to better understand HC-HA's potential roles, which will be proposed in Chapter 5.2 Future directions.

After our publication [56], similar results regarding kinetics of HC-formation and clearance during ALI have been reported with an IT influenza A (PR8 strain)-induced self-resolving respiratory infection model [172]: the highest HC-HA levels coincided with peak influenza inflammation (8 day post injury) and HC-HA was largely cleared by early resolution (14 days post injury) and absent at later time-points. In our IT LPS- and PA-induced ALI models, the rise and clearance of HC-HA paralleled the trends in whole lung *TNF α* and *TSG-6* transcript levels and alveolar barrier permeability as indicated by markers of epithelial and endothelial damage (RAGE and albumin). These results suggest that both the induction of *TSG-6* and microvascular leak of serum Ial substrate contribute to rapid HC-HA formation. During resolution, the downregulation of *TSG-6* expression and the restoration of alveolar epithelial/endothelial barrier, which would prevent any further extravasation of serum Ial, would critically limit the formation of any additional HC-HA.

While our results suggest that HC-HA has a minimal effect during resolving ALI, much work remains to fully understand the role of HA fragmentation and remodeling on lung injury outcomes and repair. Rapid clearance of HA and HC-HA may contribute to proper resolution of acute lung inflammation. Evidence for this idea comes from research using mice that found that IT administration of hyaluronidase accelerated recovery from influenza A infection [172] and hyaluronidase deficiency is associated with failure to clear HA and development of lung fibrosis [38].

The rapid clearance of HC-HA was associated with breakdown of HMW HA and/or *de novo* production of medium molecular weight HA. While we did not distinguish between these two processes, the upregulation of whole lung *HAS1-3* transcripts and

increase in BALF HA levels at 1 day post LPS instillation suggest that *de novo* HA production did take place. In contrast, levels of whole lung *HYAL1-2* transcripts were consistently downregulated. These results did not agree with the induction of HMW HA fragmentation and clearance of HA in the BALF. However, our results are consistent with previous reports that whole lung *HYAL1-2* expression may not accurately reflect actual HA turnover during inflammation [172, 173]. Instead, non-enzymatic ROS-mediated degradation of HA may play an important role in HA fragmentation during inflammation. While the precise *in vivo* contributions are unclear, the release of ROS by inflammatory cells can effectively degrade HA. Fragmentation of HA *in vitro* by activated neutrophils is almost completely inhibited by the addition of ROS scavengers [174]. Since ALI is characterized by significant neutrophil recruitment to lung tissue and alveoli, ROS would be expected to significantly contribute to HA degradation.

HA-degrading membrane protein TMEM2 and the HA-binding CEMIP that promotes HA degradation *via* clathrin-mediated endocytosis have also been recently implicated in promoting HA turnover [48]. The two proteins, which are unrelated to *HYAL1-2*, are abundantly expressed in the lung [47, 48, 175] and thus may contribute to lung HA turnover. Whereas levels of whole lung *TMEM2* transcript were suppressed following LPS challenge, expression of *CEMIP* mRNA paralleled the kinetics of HA fragmentation with highest expression at 1 day post injury, suggesting a potential role in HA turnover during peak neutrophilic inflammation.

HA turnover during inflammation may be finely regulated by factors besides gene expression of *HYAL1-2*. For example, *HYAL2* breakdown of HA requires CD44 binding of HA. CD44 can undergo a multitude of pre-mRNA splice variations, as well as post-translational modifications that are differentially regulated in response to inflammatory stimuli, such as TNF α and LPS, which may in turn regulate its HA binding ability [176-178].

Our analysis of resident and recruited AM transcripts revealed abundant expression of *HYAL2*, *CD44*, and *TMEM2*, which suggests a potential role for not only *CD44* and *HYAL2* working in concert to degrade HMW HA, but also *TMEM2*. *TMEM2* is a recently discovered membrane protein with an ability to degrade HMW HA: of importance, *TMEM2* features domains similar to bacterial polysaccharide lyases instead of *HYAL1-2*. Expression of *TMEM2* in both resident and recruited AM was highest during the acute neutrophilic phase of inflammation (3 days post injury), which suggests a potential role in HA turnover during initial induction of HA fragmentation. In contrast, *CD44* transcript in both resident and recruited AM steadily increased throughout the resolution phase and peaked at 12 days post injury following IT LPS challenge, which suggests a potential role of *CD44* in HA clearance during resolution.

Our results of upregulation of *HAS1-3* in whole lung and downregulation of *HYAL1-2* are consistent with the findings reported following influenza A infection [172]. In response to influenza A, peak lung inflammation is reached roughly one week after infection (8 days post injury). At this 8 days time point, exogenously instilled tagged HA was found to be cleared as rapidly as HA instilled into uninjured mice despite the whole lung downregulation of *HYAL1-2*. These findings support a model of additional HA degradation by ROS and other factors discussed above. Interestingly, during the later resolution phase (14 days post injury), exogenously instilled HA was found to be more rapidly cleared than during 0 or 8 days post injury. In the respiratory tract, enhanced clearance of HA during resolution may be attributed to increased tissue reparative programming of alveolar macrophages that can clear HA in contrast to a potential deficiency in HA binding and turnover during peak inflammation, which was noted during the time course of bleomycin injury [179]. This macrophage model is supported by the finding that HA clearance is impaired in *CD44* KO mice following bleomycin challenge,

but can be rescued with WT bone marrow transplant and reconstitution with WT myeloid cells [180].

Chapter 4. Intravascular HC-modification of HA during endotoxic shock

4.1 Introduction

As both systemic and localized IT LPS exposure lead to lung microvascular permeability and ALI, we hypothesized in the previous chapter that HC-HA would also be protective during respiratory infection-induced ALI. Our finding that HC-HA plays only a minimally protective role during respiratory infection-induced ALI was surprising and in striking contrast to HC-HA being critically implicated in promoting survival and regulating neutrophil trafficking in the liver sinusoids during systemic LPS exposure [133, 134]. To address this discrepancy, we looked for differences in HC-HA induction between these two models focusing on the lung and plasma. Based on our experiments presented in Chapter 2.3 that suggested that microvascular endothelial cells are a potential vascular source of TSG-6 during septic cytokine storm, we hypothesized that systemic IP LPS-induced shock uniquely stimulates intravascular HC-HA formation. Using *TSG-6* KO mice, we determined that TSG-6 delayed the onset of mortality following systemic IP LPS-induced shock and investigated potential differences in markers of vascular inflammation.

4.2 Methods

4.2.1 Animal husbandry

All animal experiments were approved by IACUC at National Jewish Health. *TSG-KO* mice were previously described (Chapter 2.2 Methods).

4.2.2 Mouse endotoxic shock model

E. coli O111:B4 LPS (L2630, MilliporeSigma) was resuspended in PBS as a 1.7 mg/mL solution and administered as single IP bolus dose (20 mg / kg body weight [135]) injected in the right lower quadrant with a 26G x 3/8 needle, in the morning. Animal welfare and survival were evaluated every 6 h. Wet chow in petri dish was provided at 6

h post injury per IACUC approved protocol and veterinarian recommendations. Plasma and perfused lung were collected 8 or 12 h after IP LPS, as specified.

4.2.3 Mouse IT LPS-induced ALI model

E. coli O55:B5 LPS (L2880, MilliporeSigma) was resuspended in PBS and administered as single instillation of 20 µg LPS in 50 µL PBS given in the morning as previously described (Chapter 3.2 Methods). Animal welfare and survival were evaluated twice daily per IACUC approved protocol. Mice were weighed daily up to four days after LPS challenge.

4.2.4 Plasma collection and lung perfusion

Mice were euthanized by isoflurane overdose first and then bilateral thoracotomy. Whole blood was removed by puncture of the right ventricle with a 1 mL syringe and needle (23G x 1 IM TW) containing 100 µL concentrated sodium citrate (S5770-50mL, MilliporeSigma). Lungs were then perfused through the right ventricle with 10 mL of blood bank saline, dissected, and snap frozen in liquid nitrogen. Whole blood was spun down (2000 g, 10 min, 12 °C), and the plasma supernatant was removed and frozen.

4.2.5 Lung parenchymal and plasma HC-HA levels

Perfused lung tissue was homogenized and digested with 1 U of *S. hyaluronolyticus* hyaluronidase (MilliporeSigma) or PBS control as previously described (Chapter 3.2 Methods). Plasma (40 µL) was incubated with *S. hyaluronolyticus* hyaluronidase (1 U) or PBS control in warm water bath (2 h, 37 °C) and then with mechanical agitation (2 h, room temperature). Laemmli buffer was then added and equal volumes of plasma preparations were separated by SDS-PAGE, followed by western blot with the rabbit-anti-hIal antibody as previously described (Chapter 3.2 Methods).

4.2.6 Whole lung mRNA analysis

RNA extraction from whole lung, cDNA synthesis, and qPCR were performed as previously described (3.2 Methods). The Taqman probes msTNFα (Mm00443258_m1)

and msCXCL2 (Mm00436450_m1) were used to measure the indicated gene transcripts.

4.2.7 TSG-6 activity assay

Plasma was assayed for endogenous TSG-6 activity as described previously [152] with minor modifications. Plasma (40 μ L) was incubated with 3 μ g of 10-oligosaccharide HA (HYA-OLIGO10EF-1, Hyalose, amsbio) for 2 h at 37 °C and then with mechanical agitation for 2 h at room temperature. Recombinant human TSG-6 (20 ng, R&D Systems) was used as positive control. Negative controls were generated by mixing plasma with EDTA at a final concentration of 0.1M before adding 10-oligosaccharide HA (HA₁₀): TSG-6 enzymatic activity requires divalent metal cations Ca²⁺ and Mg²⁺ [57-59]. Samples mixed with Laemmli buffer were resolved by SDS-PAGE, and western blot was performed using anti-IaI antibody, which can detect HC covalently linked to HA₁₀ [152].

4.2.8 Analysis of plasma by flow cytometry

Whole blood was similarly collected as above, but 0.5M EDTA (100 μ L) was used instead as an anticoagulant (~83 mM final EDTA when added to ~500 μ L blood draw). EDTA-treated whole blood (100 μ L) was diluted with flow wash buffer solution (900 μ L, PBS with 9% FBS and 0.5 mM EDTA) and spun (450 g, 4 °C) to pellet the cells. Packed cells were resuspended in 1 mL of red blood cell lysis buffer (Pharm Lyse, BD Biosciences) by pipetting up and down to lyse red blood cells. 1 mL of flow wash buffer and 5 mL of PBS was added to quench the lysis buffer and centrifuged. The cell pellet was resuspended in flow wash buffer solution containing CD16/CD32 (clone 93, eBioscience) and fluorescently conjugated antibodies: TER-119 (Biolegend), CD45 (30-F11, BD Biosciences), Ly6G (1A8, Biolegend), CD11b (M1/70, eBioscience), Siglec-F (E50-2440, BD Biosciences), CD115 (AFS98, eBioscience). LSR II cytometer (BD Biosciences) was used to collect a minimum of 20,000 CD45⁺ leukocyte events for each

sample and raw data was analyzed in FlowJo software (FlowJo). Gating strategy depicted (**Figure 4.4A**).

4.2.9 Mouse TNF α ELISA

Plasma TNF α levels were measured using mouse TNF α DuoSet ELISA kit (R&D Systems) according to manufacturer's instructions. Plasma from mice exposed to IP LPS were diluted with reagent diluent (1% BSA in PBS). 96-well plates (Nunc MaxiSorp) were coated and read as previously described (Chapter 2.2 Methods).

4.3 Results

4.3.1 Effect of TSG-6 on survival during endotoxic shock

To confirm previous observations [135, 136] that HC-HA promotes survival during endotoxic shock, we administered a high bolus dose of LPS (20 mg / kg total body weight) *via* IP route that induces severe endotoxic shock and mortality (**Figure 4.1A**). *TSG-6* KO mice unable to form HC-HA exhibited more rapid onset of mortality than WT control: median survival of 18 h in KO vs. 21 h in WT. In contrast, following localized IT LPS (20 μ g)-induced ALI, *TSG-6* KO and WT control mice exhibited similar survival outcomes and speed of total body weight loss and recovery (**Figure 4.1B**).

4.3.2 Lung parenchymal HC-HA formation after endotoxic shock

Since both IP and IT LPS administration cause ALI, we investigated HC-HA induction in both models. As previously described (Chapter 3.2 Methods), perfused lung tissue was homogenized and treated with hyaluronidase, which liberates any HC linked to HA for detection by Ial western blot. We found significant induction of HC-HA in lungs from mice collected 8 h after IP LPS (**Figure 4.2A**). To confirm that *TSG-6* is the exclusive mediator of HC-HA formation and that our *TSG-6* KO mice are valid, HC-HA content was assessed in *TSG-6* KO mice and found to be absent when compared to control (**Figure 4.2B**). To compare the two routes of exposure, lung HC-HA content was

assessed 12 h after either IP or IT injury (**Figure 4.2C**). Both IP and IT routes were found to induce HC-HA formation with no significant differences between the two.

To control for the effect of HC-HA on lung inflammation in the two models, we assessed lung inflammation by measuring levels of *TNF α* transcript during an IT LPS time course (**Figure 4.2D**) or 8 h after IP LPS (**Figure 4.2E**) in *TSG-6* KO vs. control (WT and HT) mice and compared to IP PBS. We additionally measured levels of neutrophilic chemokine *CXCL2* 8 h after IP LPS (**Figure 4.2E**). Neither marker of inflammation was statistically different in the two models, which suggests that lung parenchymal HC-HA, while significantly induced in both models, had a minimal effect on the outcomes of lung inflammation.

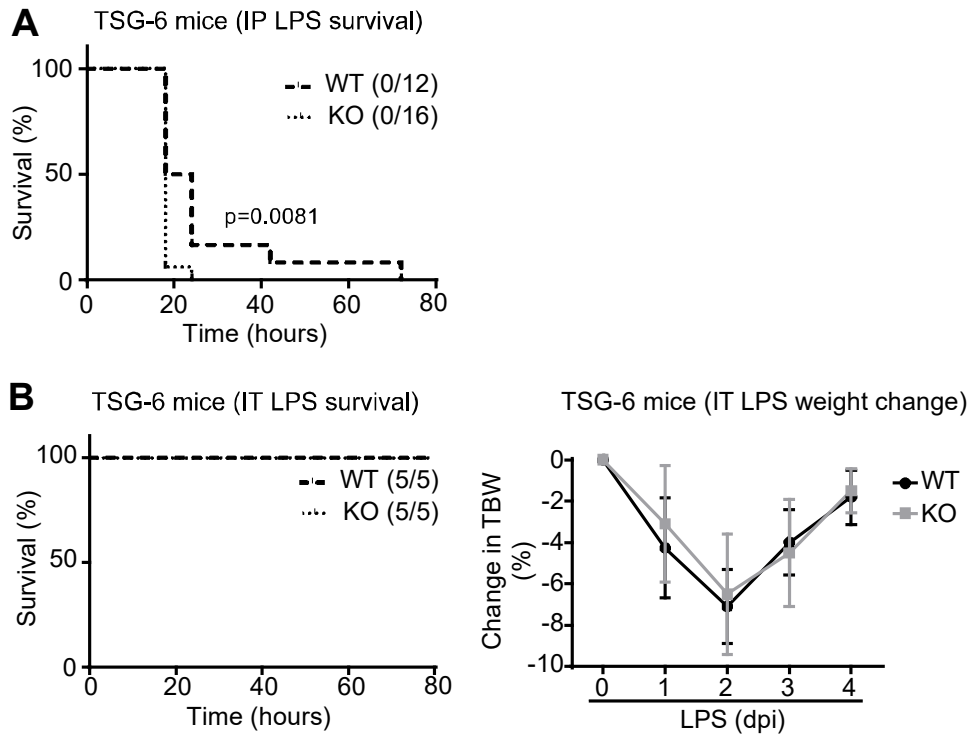


Figure 4.1. Effect of TSG-6 on survival during endotoxic shock

A. Survival following IP LPS-induced endotoxic shock (20 mg / kg total body weight or TBW) was assessed over three days in *TSG-6* KO and WT mice. $n = 12-16$ mice per group. Data analyzed with Log-rank (Mantel-Cox test). **B.** Survival and daily TBW change (mean \pm SD, % change from initial weight) following IT LPS challenge (20 μ g / mouse) were assessed for four days. WT, wildtype. KO, knockout. dpi, days post injury. $n = 5$ mice per group. Data analyzed by ANOVA with Tukey's multiple comparisons. Figure from Ni et al. [181], open source.

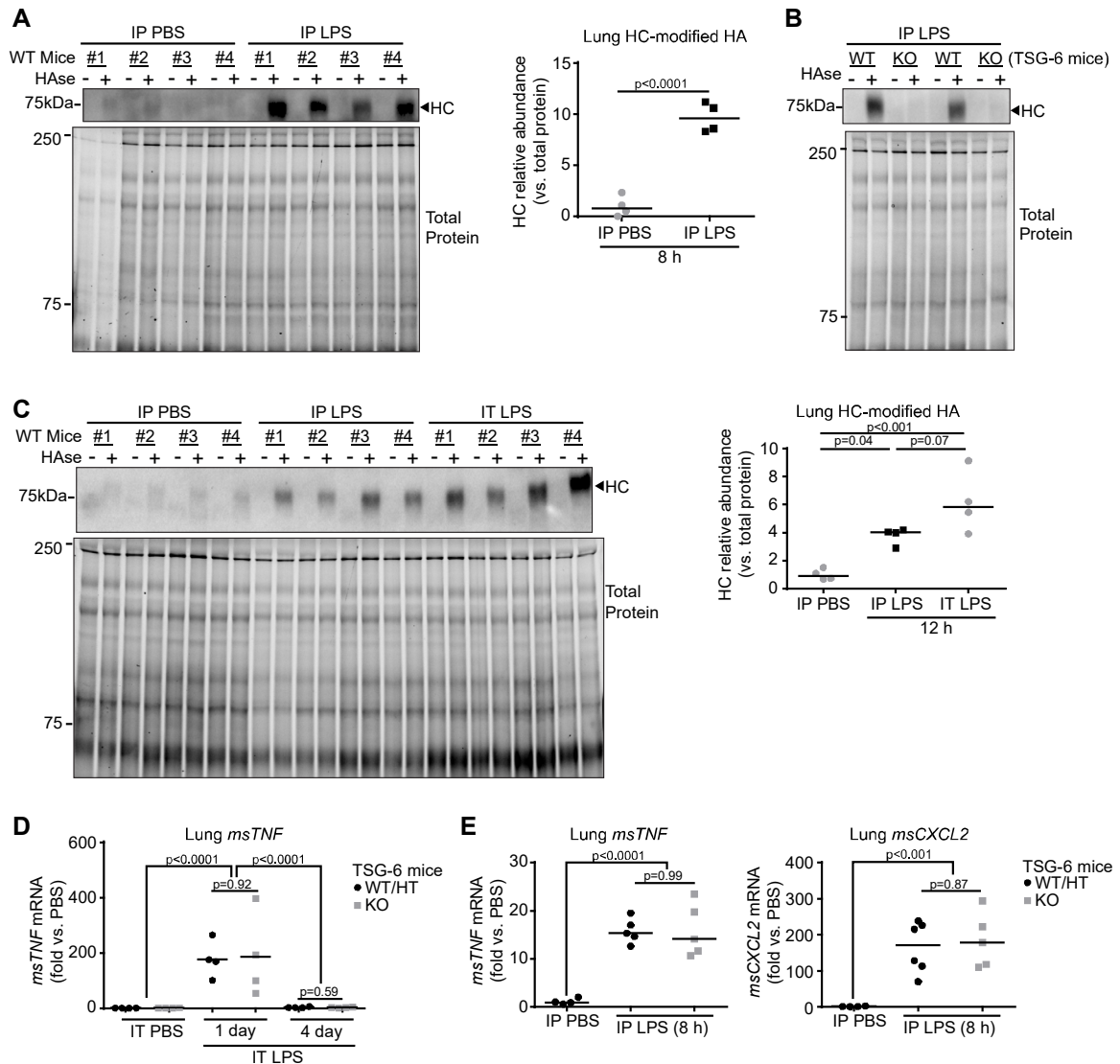


Figure 4.2. Lung parenchymal HC-HA after IP and IT LPS injury

A-C. HC-HA content in homogenized lung tissue was assessed by hyaluronidase (HAse) digest which releases any HC linked to HA that can then be detected by Ial western blot analysis. Lungs were obtained from mice harvested 8 h after exposure to IP LPS (20 mg / kg TBW) or IP PBS control, and released HC was quantified and normalized to total protein (**A**). HC-HA content was assessed in lungs from *TSG-6* KO and WT mice collected 8 h after IP LPS exposure to confirm that *TSG-6* is the exclusive mediator of HC-HA formation (**B**), as evidenced by the absence of released HC with *TSG-6* deficiency. HC-HA content was assessed in lungs obtained from mice harvested 12 h

after exposure to IP LPS, IT LPS (20 μ g), or IP PBS control (**C**). **D**. Whole lung expression of *msTNF α* was assessed in *TSG-6* KO and WT/HT mice during a time course of IT LPS-induced injury and resolution (LPS 1 or 4 days post injury) and compared to IT PBS control. **E**. Whole lung *msTNF α* and *msCXCL2* were assessed in *TSG-6* KO and control (WT and HT) mice 8 h after IP LPS exposure and compared to IP PBS control. $n = 4-6$ mice per group. Data analyzed by ANOVA with Tukey's multiple comparisons. Figure from Ni et al. [181], open source.

4.3.3 Intravascular HC-HA and TSG-6 induction after endotoxic shock

Since vascular endothelial cells can respond to cytokines upregulated during sepsis by secreting TSG-6 (Chapter 2.3 Results), we investigated whether HC-HA was systemically induced after IP LPS (20 mg / kg TBW)-induced endotoxic shock. The presence of HC-HA in plasma was similarly assessed as in lung tissue by treating with hyaluronidase, which released any HC linked to HA that can be detected by Ial western blot. While HC-HA was robustly induced 12 h after IP LPS compared to IP PBS control, HC-HA was absent after IT LPS (20 µg, **Figure 4.3A**). As HC-HA is continuously cleared by the liver, the presence of HC-HA suggested continuous production of TSG-6 to generate additional HC-HA. To determine the presence of endogenous TSG-6 in plasma, we measured TSG-6 activity by adding 10-oligosaccharide (HA₁₀) and assessing the formation of HC-HA₁₀, which can be detected by Ial western blot (**Figure 4.3B**). As a positive control, recombinant human TSG-6 (rhTSG-6) was tested to confirm that sodium citrate anticoagulant used to collect plasma did not inhibit TSG-6 activity (**Figure 4.3B**). The irreversible divalent metal chelator EDTA was used as negative control, because TSG-6 enzymatic activity requires the presence of divalent metal cations Mg²⁺ and Ca²⁺ [57-59]. When we assessed TSG-6 activity, HC-HA₁₀ was induced after IP LPS compared to IP PBS control and noticeably absent following IT LPS (**Figure 4.3C**: IP PBS ~1 vs. IP LPS ~5.6 vs. IT LPS ~1.7 normalized abundance, $p < 0.0001$), which was in agreement with our observation that HC-HA was only induced after IP LPS.

4.3.4 Vascular markers of inflammation in TSG-6 KO mice

While HC-HA promotes survival outcomes during IP LPS-induced systemic inflammation and regulates neutrophil trafficking locally in the liver sinusoids, the effect on neutrophils systemically had not been explored. Since we discovered that intravascular HC-HA is induced after IP LPS, we utilized TSG-6 KO mice to investigate whether HC-HA had any effect on circulating neutrophils numbers. Plasma was collected

8 h after IP LPS (20 mg / kg TBW) and flow cytometry was used to identify neutrophils and mononuclear cells (**Figure 4.4A**). IP LPS induced an increase in the percentage of circulating neutrophils (Ly6G⁺ / CD45⁺) after IP LPS (**Figure 4.4B**: IP LPS ~42% vs. IP PBS ~27%). Lack of HC-HA in *TSG-6* KO mice tended to further increase the percentage of circulating neutrophils (**Figure 4.4B**: KO 46% vs. WT/HT 39%, p=0.27) and lower the percentage of circulating mononuclear cells (**Figure 4.4C**: KO 42% vs. WT/HT 49%, p=0.13) when compared to control. HC-HA deficiency in *TSG-6* KO mice was additionally associated with a trend of greater circulating TNF α levels in plasma compared to control (**Figure 4.4D**: KO ~51 pg/mL vs. WT/HT 39 pg/mL, p=0.21). To ascertain potential effects of sex on circulating neutrophils during endotoxic shock, the results in **Figure 4.4B** were subdivided into male vs. female (**Figure 4.4E**). The tendency toward greater percentage of circulating neutrophils in *TSG-6* KO mice was more pronounced in female mice and largely absent in male mice. As expected, the dose of LPS administered by IP route was higher on average for male mice due to their heavier weights and the strategy of dosing proportionally to TBW (**Figure 4.4F**).

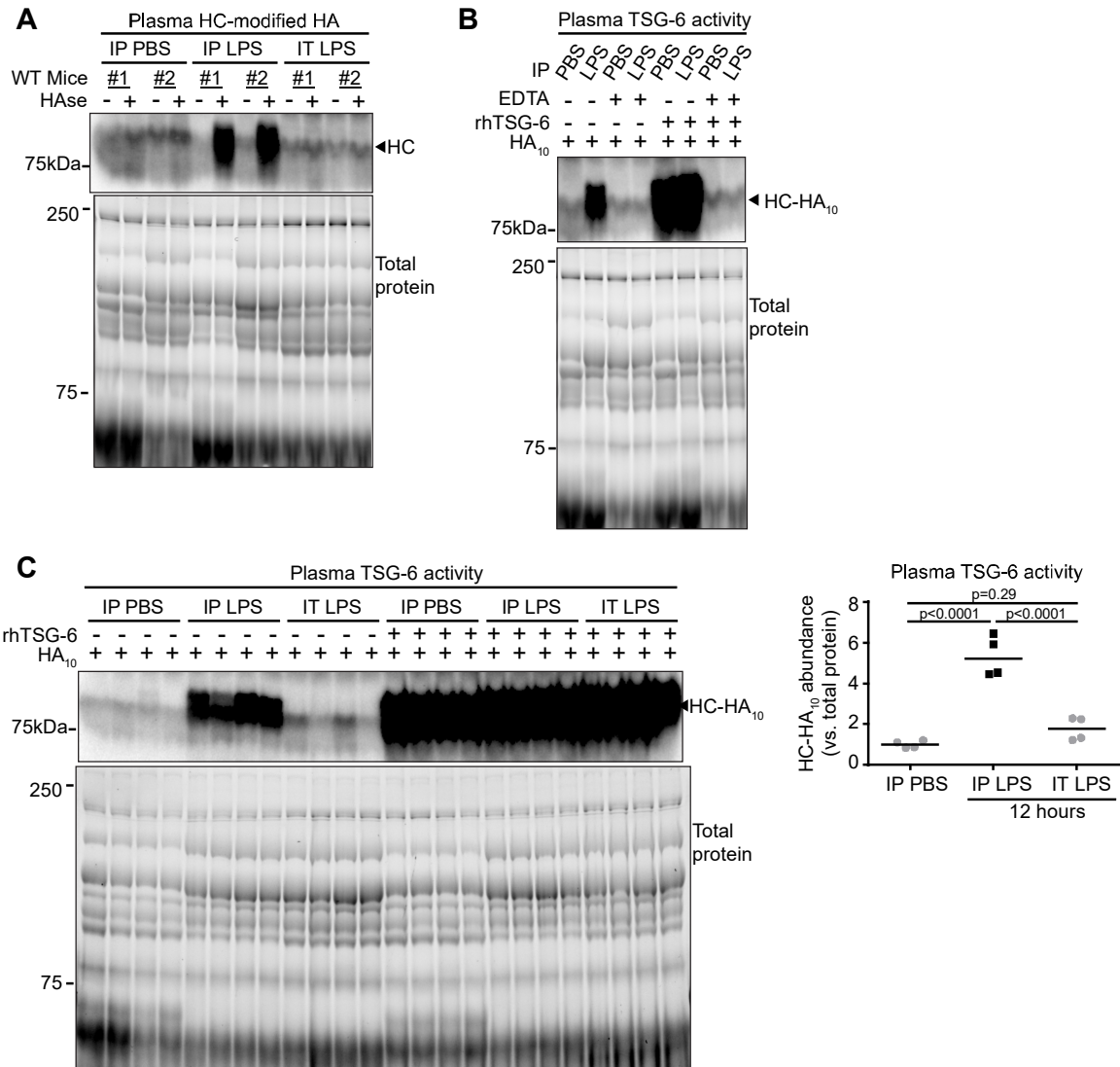


Figure 4.3. Plasma HC-HA and TSG-6 activity after IP and IT LPS injury

A. HC-HA content in plasma from mice 12 h after exposure to IP LPS (20 mg / kg TBW), IT LPS (20 μ g), or IP PBS control was similarly assessed by hyaluronidase digest and lal western blot. **B.** TSG-6 activity in plasma was measured by incubating with 10-oligosaccharide HA (HA₁₀) and assessing the formation of HC-HA₁₀ by lal western blot. Recombinant human TSG-6 (rhTSG-6) was used as positive control. Plasma pre-mixed with EDTA before adding HA₁₀ was used as a negative control. **C.** HC-HA₁₀ formation was assessed in plasma from mice exposed to the indicated treatments and quantified

by densitometry. $n = 4$ mice per group. Data analyzed by ANOVA with Tukey's multiple comparisons. Figure from Ni et al. [181], open source.

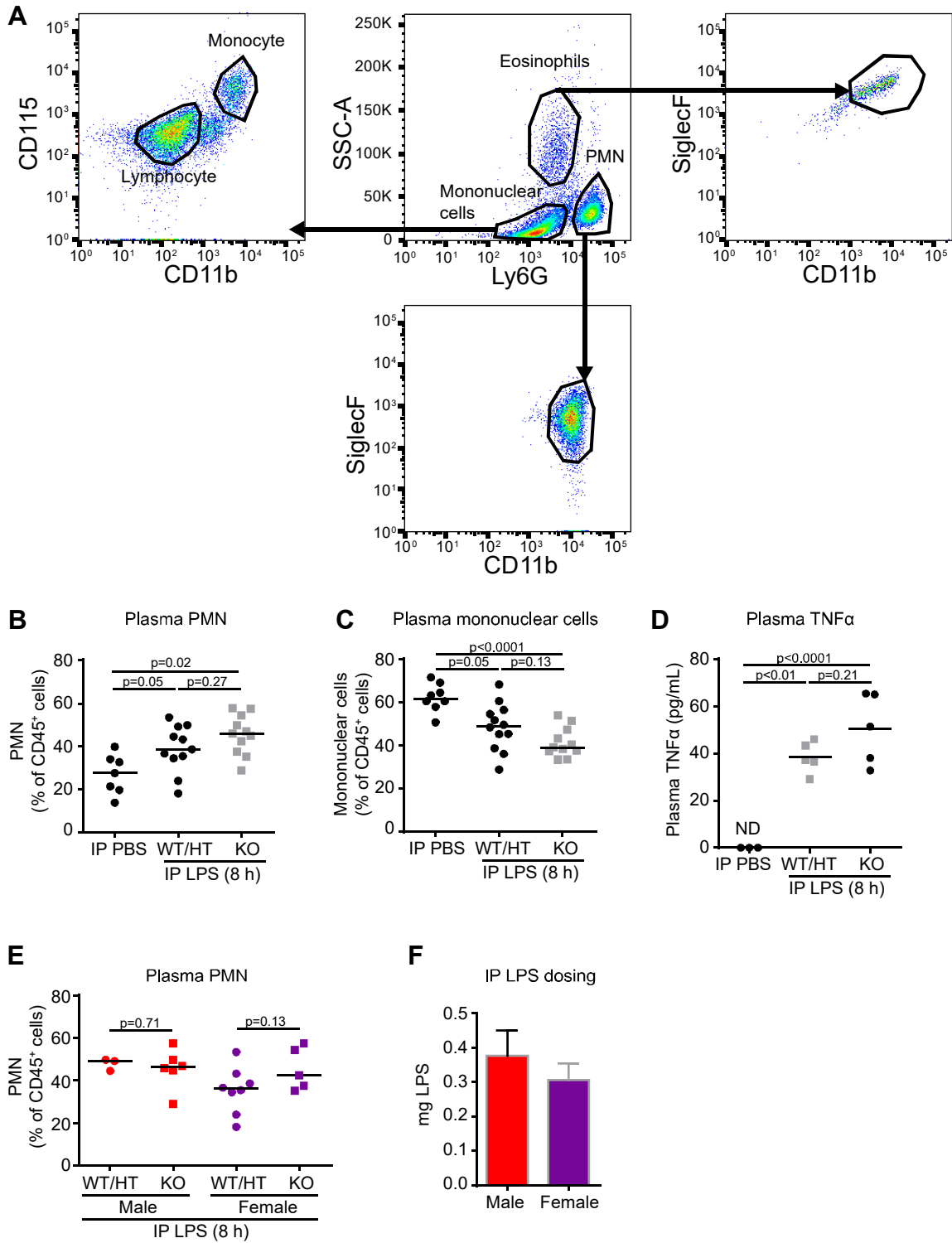


Figure 4.4. Effect of TSG-6 on circulating PMN and plasma TNF α

A. Flow cytometry gating strategy used to identify neutrophils (polymorphonuclear cells or PMN) and mononuclear cells in the plasma. In the center, hematopoietic cells were

gated by debris and doublet exclusion and CD45⁺ TER-119⁻ staining. Mononuclear cells including lymphocytes and monocytes were gated as SSC^{lo}Ly6G⁻. PMN was gated as Ly6G⁺CD11b⁺SiglecF⁻. Eosinophils were gated as SSC^{hi}Ly6G⁻CD11b⁺SiglecF⁺. **B-C**. Circulating abundance of PMN (**B**) and mononuclear cells (**C**) in plasma were expressed a percentage of CD45⁺ cells after indicated treatments. **D**. Plasma levels of TNF α cytokine after indicated treatments were measured by ELISA. $n = 4-12$ mice per group. **E**. Circulating PMN results of IP LPS plasma based on sex. **F**. Amount of LPS given by IP route (mean +/- SD) to male ($n = 9$) and female ($n = 13$) mice. LPS dose was calculated based on weight (20 mg / kg TBW). SD, standard deviation. Data analyzed by ANOVA with Tukey's multiple comparisons. Figure from Ni et al. [181], open source.

4.4 Discussion

Sepsis is a serious condition characterized by a systemic inflammatory response for defeating bacteremia that also causes life-threatening endotoxic shock. In this chapter, we investigated how HC-HA can have a distinctly protective role during endotoxic shock in contrast to a minimal role during localized IT LPS exposure (Chapter 3.3 Results). We showed for the first time that systemic IP LPS-induced endotoxic shock is characterized by the specific induction of intravascular TSG-6 and HC-HA, which were noticeably absent after localized IT LPS exposure. In contrast, both IP and IT LPS exposure non-specifically induced lung parenchymal HC-HA, which was expected because both models cause ALI. We noted that *TSG-6* KO mice were more susceptible to endotoxic shock-induced mortality. Lack of HC-HA formation in *TSG-6* KO mice was associated with tendency toward greater numbers of circulating neutrophils and plasma levels of TNF α , which suggest that greater systemic inflammation may have contributed to the increased susceptibility to mortality.

Our finding that TSG-6 promotes survival during endotoxic shock is consistent with previous reports that *TSG-6* and *Ial* KO mice exhibit greater mortality following systemic IP LPS administration [135, 136]. We followed the previously published endotoxic shock paper (same LPS preparation and 20 mg / kg TBW dosing strategy) [135] that had reported that *TSG-6* KO mice display 100% mortality and WT mice 0% mortality at 24 h post IP LPS [135]. However, for this key result, since survival was not reported past 24 h, it is not known whether the 0% mortality result would still hold if survival was assessed over a longer time frame. This is an important concern, because depending on the effective dose, IP LPS-induced mortality can still occur later, after the first 24 hours, but during the first 96 hours, as reported by other experiments in the same paper [135] and by us (**Figure. 4.1**). Therefore, our survival findings may have been much closer to what had been published with regards to promoting survival. Since

overall we observed a more rapid onset of mortality, our actual effective LPS dose may have been higher despite our efforts to follow the same LPS dosing strategy. Thus, titrating down the LPS dose may better accentuate the physiologic differences during endotoxic shock between *TSG-6* KO and WT control mice. This is especially relevant for male mice, who received a higher dose of LPS due to their reaching heavier body weights than female mice of the same age and may also respond differently due to sex differences [182]. In support of the premise that male mice did not receive an optimal LPS dose for discerning protective effects of HC-HA, the ability of HC-HA to decrease circulating percentage of neutrophils was limited to female mice. Other potential considerations include institutional differences in environmental and intestinal microbiota, which have been shown to influence the magnitude of inflammatory responses to IP LPS [167, 183].

Our results expand on a previous effort to understand *TSG-6* KO mice's susceptibility to endotoxic shock that focused exclusively on differences in lung inflammation and lung macrophage polarization [135]. Since the key pathologic development during endotoxic shock is vascular barrier dysfunction and microvascular endothelial cells can respond to the septic cytokine storm by secreting *TSG-6* (Chapter 2.3 Results), we instead focused on the vasculature. Specifically, we addressed whether *TSG-6* and HC-HA were specifically induced after systemic IP LPS, but not after localized IT LPS administration. The induction of *TSG-6* and HC-HA in the vasculature may serve as an evolutionarily conserved endogenous innate immune response to sepsis to regulate hematopoietic cell trafficking and clearing bacterial infection during systemic inflammation. This model is supported by the discovery that HC-HA interactions with CD44 receptor enhanced neutrophil adhesion in the liver sinusoids during endotoxic shock [133, 134]. Enhanced neutrophil adhesion in the liver sinusoids may be beneficial in sepsis in many ways. Firstly, neutrophil adhesion may enhance

Kupffer cell clearance of damaged and apoptotic neutrophils, which would minimize unnecessary neutrophilic damage in other organs [107]. Secondly, adhered neutrophils may more effectively trap and kill their bacterial targets *via* extrusion of neutrophil extracellular traps [102, 103, 184].

Robust intravascular HC-HA induction is likely specifically activated during sepsis and endotoxic shock. With the continuous clearance of circulating HA by the liver sinusoids (2.5-5 min half-life in plasma [27, 28]), the formation of small amounts of HC-HA would be expected to be rapidly cleared. However, during endotoxic shock, the septic cytokine storm would induce robust TSG-6 secretion that can sustain substantial catalysis of intravascular HC-HA formation. Additionally, any shock-induced end-organ damage to the liver would result in decreased turnover leading to HC-HA accumulation.

Evidence that robust HC-HA induction is a specific innate immune response of sepsis and endotoxic shock comes from the observation that either systemic LPS or live gram negative *E. coli* exposure induces HA/CD44-dependent neutrophil adhesion in the liver sinusoids and the specific retaining of adherent neutrophils in the liver sinusoids without emigrating out to liver tissue [109]. In contrast, during local injury to liver surface by the bacterial PAMP/DAMP N-formyl peptide, neutrophil adhesion in the liver sinusoids did not depend on HA/CD44 interactions and neutrophils emigrated into liver tissue [109]. These distinct results reveal how neutrophil trafficking and emigration into tissue are carefully regulated. When the site of liver injury is extravascular, adherent neutrophils emigrate into liver tissue. In contrast, during systemic LPS or *E. coli*-induced inflammation, adherent neutrophils stay in the liver sinusoids. This compartmentalization may be important, because if neutrophils emigrated into liver tissue during systemic inflammation in the absence of local injury, there could be unnecessary tissue damage. Additionally, these results highlight the involvement of other adhesion molecules (i.e. interactions between CD11b/CD18 integrin and ICAM-1 during localized liver injury) that

regulate neutrophil trafficking [109], which may help explain why HC-HA has a minimal role during localized IT LPS-induced ALI.

The finding of intravascular TSG-6 and HC-HA induction during murine endotoxic shock likely extends to human sepsis, given the evolutionary conservation of TSG-6 catalyzing HC-HA in all vertebrates [3, 72]. Additionally, the presence of TSG-6 in the serum of healthy patients systemically injected with LPS and hospitalized patients with sepsis has been reported as unpublished observation [185]. This induction of TSG-6 secretion would be carried out by both circulating myeloid cells and endothelial cells stimulated directly by bacterial LPS or the pro-inflammatory cytokines of the septic cytokine storm, which we investigated (Chapter 2.3 Results). During the clinical course of sepsis, the initial pro-inflammatory response to bacteremia is quickly followed by a counterregulatory anti-inflammatory response [112]. Thus, intravascular TSG-6 secretion may peak shortly after the height of the septic cytokine storm and then drop precipitously. This presents an opportunity for identifying an optimal window to intravenously infuse TSG-6 as a therapeutic intervention to generate circulating HC-HA that may confer protection during the particularly vulnerable period after the initial admission of the septic patient.

One caveat of interpreting our survival results was the recent demonstration in chicken and mouse that HC-HA plays an important developmental role in initiating vertebrate midgut rotation and that HC-HA deficient mice (*TSG-6* or *IaI* KO mice) exhibit midgut malrotation [80]. While it was suggested that *TSG-6* KO murine embryos may exhibit impaired viability due to midgut malrotation, we did not observe any impaired viability with *TSG-6* KO mice pups (Chapter 1.2.2 TNF α Stimulated Gene-6) and two reports also independently confirmed that *IaI* KO mice pups exhibited normal Mendelian inheritance ratios [76, 82], which suggest that HC-HA does not reduce viability. These results agree with the clinical finding that most cases of intestinal malrotation do not lead

to life-threatening volvulus and strangulation [83, 84]. While our results suggest no deficits at baseline, these findings do not definitively rule out physiological impairments that may manifest during severe injury and stress, which may be encountered during endotoxic shock.

The TSG-6 generation of HC-HA is ideally spatio-temporally situated in the ECM to signal and direct the inflammatory response to infection and injury [186]. HC-HA can interact with a multitude of cellular effectors of inflammation, because expression of the HA receptor CD44 is either constitutively expressed or inducible in most hematopoietic cells [11] and non-hematopoietic cells including epithelial [187], stromal [188], and endothelial cells [189]. In the vasculature, HA abundance is the greatest in the liver sinusoids, over 500-600 times more than the lung vasculature, which is second in HA abundance [133]. The high concentration of HA in the liver sinusoids may be due to its accumulation there as it awaits clearance by the sinusoidal endothelium *via* endocytosis and lysosomal degradation [51] [52]. Not surprisingly, liver sinusoids are also the location where HC-HA has been implicated in regulating neutrophil trafficking during endotoxic shock [134]. Intravascular HA likely undergoes dramatic changes during endotoxic shock due to increase in amounts of HA fragments of all sizes and covalent modification of all HA fragments, from HMW to those as small as 8-oligosaccharides [190]. While the inflammatory consequence of generating a large amount of intravascular HA repeatedly modified with the HC is relatively unclear, lal's HC moiety may also be acting on other systemic processes, as evidenced by the findings that HC can regulate systemic complement pathway [64, 65] and neutrophil activation [66]. In this context, HA may serve as the scaffold for bringing together CD44 expressing cells for interacting with HC and undergoing HC-mediated effects.

It is important to note that TSG-6 has putative functions besides its evolutionarily conserved role of covalently modifying HA. For example in ALI and endotoxic shock,

TSG-6 has been shown to bind and inhibit human neutrophilic CXCL8 [165, 166]. However, the same studies revealed the ability of TSG-6 to bind to a large number of CXC and CC family chemokines (CXCL4, CXCL12, CCL2, CCL5, CCL7, CCL19, CCL21, and CCL27), which raises the question of the *in vivo* significance of TSG-6 binding any one particular chemokine during inflammation. The *in vivo* contribution of chemokine binding by TSG-6 is likely overshadowed by the predominance of GAGs, which are present in much greater quantities in the endothelial glycocalyx and have been demonstrated to bind and present chemokines to hematopoietic cells during inflammation [191-193].

A key unanswered question is the potential role of HC-HA in the bone marrow during sepsis and endotoxic shock. Immunosuppression can occur in septic patients and bone marrow dysfunction may contribute to neutropenia and inability to fully clear remaining septic foci [112, 113]. While the role of HC-HA is unclear, HA interactions with its CD44 receptor appear to play an important role in promoting hematopoietic progenitor cell proliferation during conditions of bone marrow stress such as accelerating transplant engraftment following irradiation [117]. Additionally, our lab reported that exogenous TSG-6 supplementation can improve hematopoietic progenitor cell function after cigarette smoke-induced myelosuppression [118]. Other labs have shown using TSG-6 supplementation or *TSG-6* KO mice that TSG-6 can regulate bone marrow stromal cell differentiation [119-121]. Together, these findings indicate a potential role of TSG-6 and HC-HA in the bone marrow during sepsis and underscore the need to study potential bone marrow roles during conditions of systemic inflammation, which will be proposed in Chapter 5.2 Future directions.

Chapter 5. Conclusion

5.1 Summary

The inflammation-induced secreted enzyme TSG-6 mediates the sole covalent modification HA can undergo. Formed in the ECM during inflammation, HC-HA is spatio-temporally positioned to regulate the inflammatory response to injury and infection. This thesis provides the first characterization of the remarkable kinetics and role of HC-HA during localized IT and systemic IP LPS exposures. In Chapter 2, we established the potential cellular sources of TSG-6 enzyme that would catalyze HC-HA formation in human lung and plasma during LPS-induced injury. Using *TSG-6* KO mice, we next investigated the kinetics and role of HC-HA during IT LPS- and *PA*-induced ALI in Chapter 3. Lastly in Chapter 4, we pursued comparative studies of systemic vs. localized IT LPS exposure in mice to understand the unique roles of TSG-6 and HC-HA during endotoxic shock.

Our finding that HC-HA is rapidly induced and cleared during two models (IT LPS and gram negative *PA*) of respiratory infection-induced ALI highlights the dynamic nature of HA turnover in the lung. While lung HA undergoes continuous turnover during homeostatic conditions, LPS injury uncovered a remarkable induction of HMW HA breakdown and increase in medium molecular weight fragments, suggestive of increased rate of turnover and/or de novo synthesis, which are likely both occurring due to the recruitment of neutrophils that can release HA-degrading ROS, initial increase in BALF HA levels, and upregulation of whole lung HA synthase transcripts. Following LPS injury, the lamellar and wavy pattern of HA staining of uninjured lung sections became punctuated and more rough, suggestive of active HA remodeling. Our results regarding the induction and clearance of HC-HA during ALI have since been replicated during influenza A-induced lung infection [172], which involved a longer time course due to the time it takes influenza A virus to propagate in the respiratory tract (peak inflammation by

8 day post injury and significant resolution without fibrotic complications by 14 days post injury).

Pursuing comparative IT and IP LPS studies, we discovered how intravascular TSG-6 and HC-HA were specifically induced during endotoxic shock, whereas lung parenchymal HC-HA was non-specifically induced by both IT and IP LPS. Using *TSG-6* KO mice, we confirmed TSG-6's protective role against endotoxic shock and expanded on a previous endotoxemic study with *TSG-6* KO mice [135] that had focused exclusively on the lung tissue and lung macrophage polarization by investigating potential differences in the vasculature, which is the key site of physiologic dysfunction during endotoxic shock. We discovered that the presence of intravascular HC-HA was associated with decreased numbers of circulating neutrophils and plasma levels of TNF α suggestive of less vascular inflammation that may explain the greater protection noted during endotoxic shock.

Our finding of intravascular TSG-6 during murine model of endotoxic shock is consistent with the unpublished observation that TSG-6 is present in the serum of healthy patients injected with LPS and hospitalized patients with bacteremia [185]. We further established the relevance of TSG-6 in human lung and vascular inflammation by using primary human cells and human cell lines to define potential sources of TSG-6. Our findings are the first to describe robust intravascular HC-HA induction during acute systemic inflammation. Intravascular HC-HA has only been previously shown in the serum of patients suffering from rheumatoid arthritis [194] and chronic liver disease [195], which are both associated with systemic vascular inflammation and dysfunction [196, 197] that would be expected to provide the appropriate inflammatory signals to induce TSG-6 to catalyze HC-HA formation. In the case of chronic liver diseases, there may also be deficits in liver HA clearance leading to the accumulation of HC-HA, which may occur acutely during sepsis when endotoxic shock causes end-organ damage to

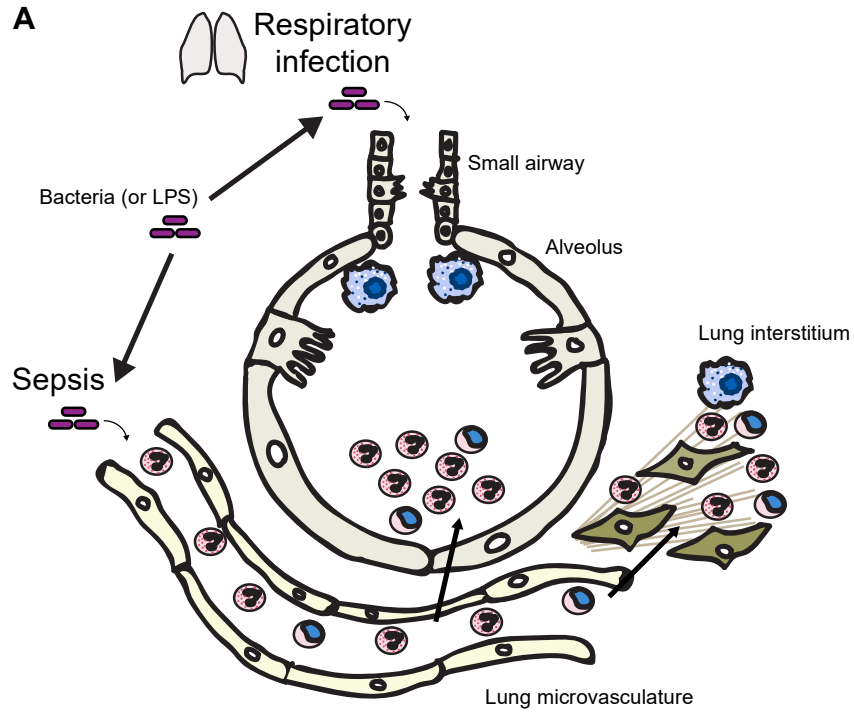
metabolically active organs. Considering the effects of HC-HA on liver sinusoidal neutrophil adhesion during endotoxic shock, it may be useful to quantitatively compare the levels of HC-HA induced during sepsis vs. these chronic inflammatory diseases. We propose that there may be threshold of HC-HA needed for sequestering neutrophils in the liver that is more easily reached during sepsis due to the robust cytokine storm induction of TSG-6 secretion.

In this thesis, we utilized two routes of LPS or bacteria administration, local IT or systemic IP, to model respiratory infection and sepsis (**Figure 5.1A**). In this acute inflammatory context, LPS, TNF α , and IL1 β were examined as potential inflammatory stimuli that upregulated TSG-6 secretion. We examined both myeloid and non-hematopoietic cellular sources (**Figure 5.1B**). Our findings in Chapter 2, together with previous results [68, 140], were used to establish the cell-specific inflammatory stimuli and localization (vasculature, lung interstitium, and respiratory tract) of TSG-6's potential cellular sources.

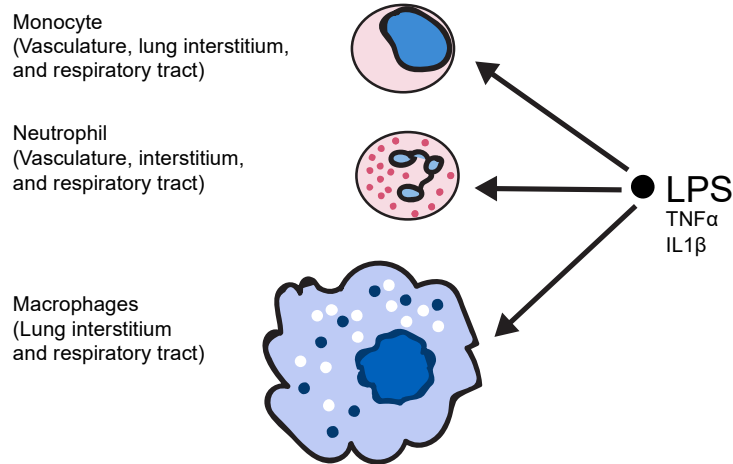
Our results in Chapter 3 suggest that HC-HA has a minimal role on outcomes of localized lung injury by LPS or gram negative bacterial infection including neutrophil recruitment into the respiratory tract. These results are consistent with previous results implicating CD11b/CD18 integrin as a key mediator of neutrophil adhesion, crawling, and emigration during gram negative lung infection [103, 198] and suggest a HC-HA/CD44 independent regulation of neutrophil trafficking in the lung microvasculature (**Figure 5.2A**). Similar to localized lung injury, interaction between CD11b/CD18 integrin and ICAM-1 is the key mediator of neutrophil adhesion, crawling, and emigration during localized liver injury (topically applied N-formyl peptide to liver surface [109]) (**Figure 5.2B**). In contrast, interaction between HC-HA and CD44, not CD11b/CD18 and ICAM-1, regulate liver sinusoidal sequestration of neutrophils during systemic LPS and *E. coli* exposure, which is characterized by lack of emigration into liver tissue [109, 133, 134]

(**Figure 5.2C**). These findings reveal the complex role of adhesion molecules in careful regulation of neutrophil trafficking and localization to the site of infection and avoidance of off-target sites, where neutrophils would not only confer no bacterial defense, but also cause unnecessary tissue injury.

The implications of the neutrophil adhesion and trapping in the liver for the outcomes of sepsis and endotoxic shock are not clearly defined. We have provided four potential mechanisms by which retaining the neutrophils in the liver sinusoids may be beneficial during endotoxic shock and sepsis (**Figure 5.3**). Since neutrophils are important effectors of the vascular inflammation during sepsis [199], their sequestration in the liver may potentially minimize systemic vascular dysfunction and life-threatening shock (**Figure 5.3A**). During systemic inflammation, the liver sinusoids can reprogram neutrophils by secreting anti-inflammatory IL-10 cytokine that downregulates neutrophil CD11b/CD18 expression and emigration (**Figure 5.3B**) [109]. Retaining neutrophils in the liver sinusoids instead of depletion by extravasation is likely ideal for successfully clearing bacteremia. While adherent neutrophils in the liver sinusoids during systemic LPS or *E. coli* exposure are relatively static and not crawling [109], in contrast to the lung microvasculature [103], they may be extruding neutrophil extracellular traps to ensnare and kill bacteria (**Figure 5.3C**) [137, 184]. Because neutrophils have a relatively short half-life, circulating neutrophils that are damaged or apoptotic need to be cleared. Kupffer cells are resident macrophages residing in the liver sinusoids that may play an important role in clearing neutrophils, which can minimize unnecessary neutrophil-mediated vascular or tissue damage [110, 111] (**Figure 5.3D**). Investigating these potential mechanisms in the context of experimental sepsis is highlighted in Chapter 5.2 Future directions.



B Myeloid sources of TSG-6



Non-hematopoietic sources of TSG-6

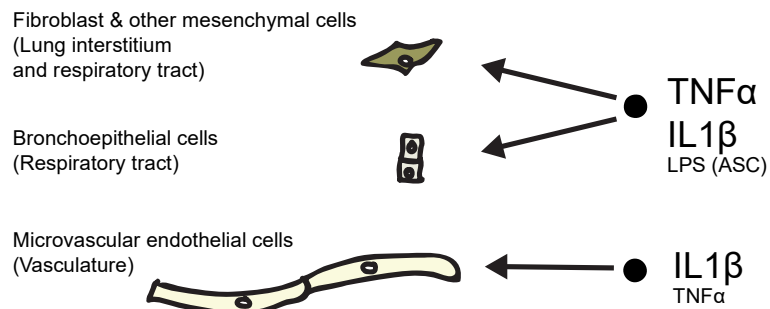


Figure 5.1. Sources of TSG-6 during respiratory infection and sepsis

A. Schematic of the two routes of bacterial or LPS exposure used to model respiratory infection and sepsis. Respiratory infection was induced by IT instillation of LPS or *PA*. Endotoxic shock was induced by systemic IP LPS exposure. Both routes of injury lead to ALI and are characterized by impaired alveolar barrier function, neutrophil recruitment, and vascular leak into the alveoli and lung interstitium that impair breathing (gas exchange). **B.** Cellular sources of TSG-6 during inflammation can be divided into myeloid and non-hematopoietic. Stimuli presented in larger font were found to more effectively stimulate TSG-6 secretion. LPS is the most potent stimulus in myeloid-derived cells. In contrast, TNF α and IL1 β are the most potent inflammatory stimuli in non-hematopoietic cells. In the lung, TSG-6 can be secreted by various cell types in both the respiratory tract (airway and alveolus) and interstitial compartments, which then facilitates HC-HA formation. During inflammation, circulating myeloid cells (neutrophil and monocytes) can transmigrate into the lung interstitium and alveoli. In the vasculature, endothelial cells and myeloid cells can contribute to TSG-6 secretion.

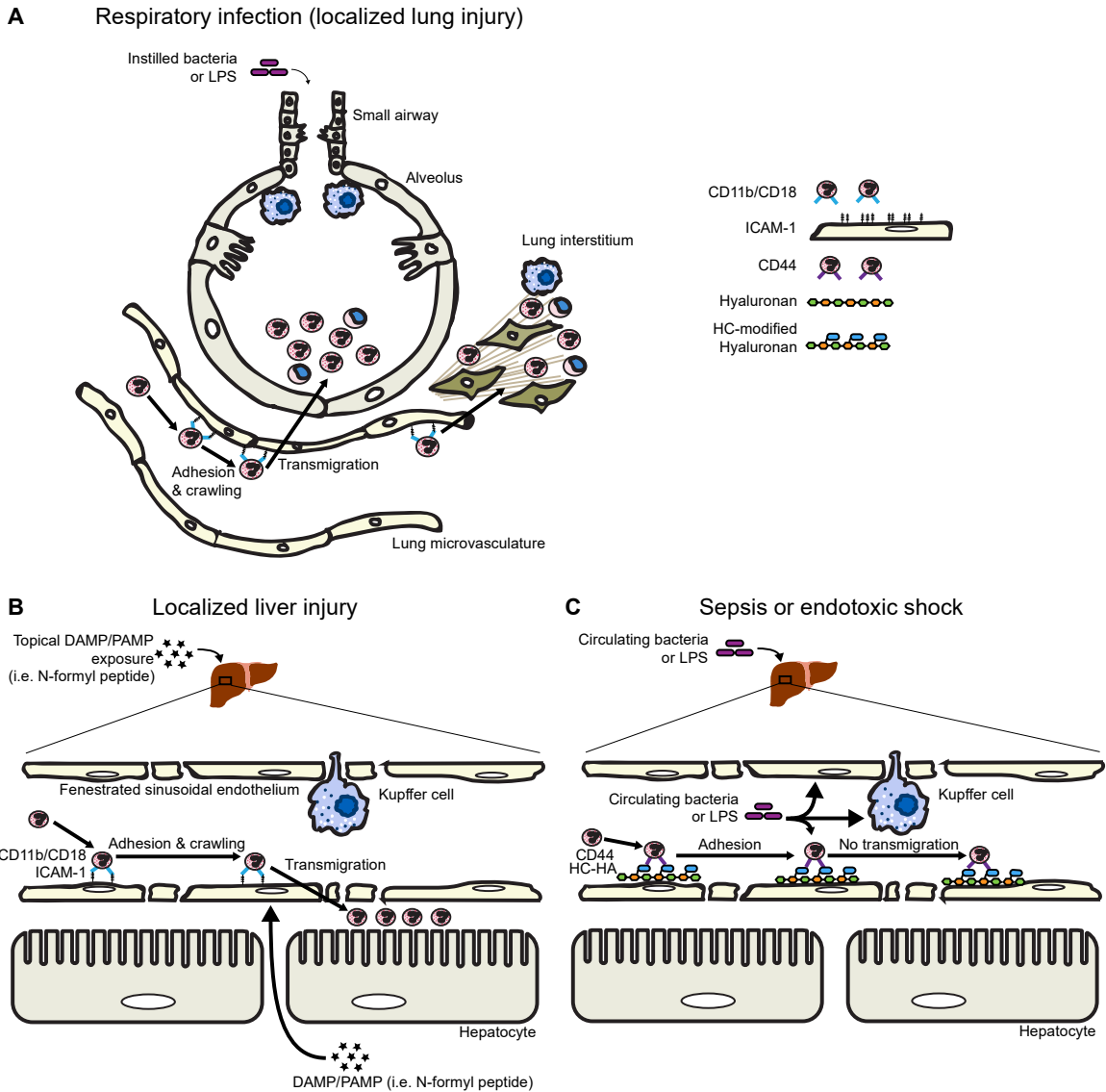


Figure 5.2. Schematic of PMN trafficking during localized vs. systemic infection

Interactions between CD11b/CD18 integrin and ICAM-1, but not HC-HA and CD44, play an important role in neutrophil adhesion, crawling, and extravascular transmigration during localized lung (A) and liver injury (B). In contrast, interactions between HC-HA and CD44 play a central role in the integrin-independent neutrophil adhesion in the liver sinusoids during systemic LPS and *E. coli* exposure (C).

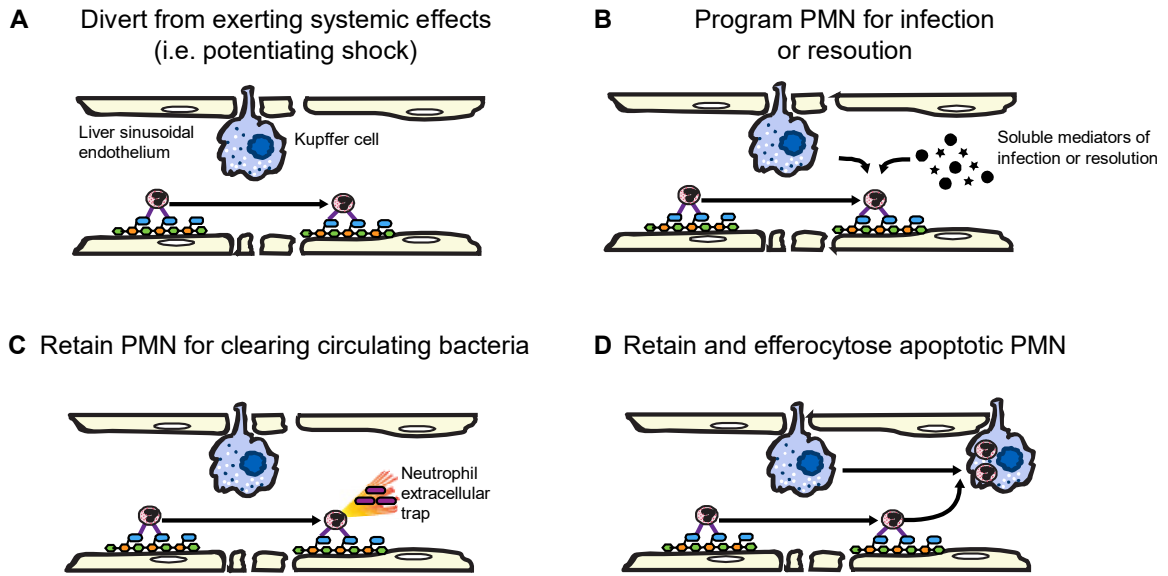


Figure 5.3. Potential mechanisms of HC-HA's protective effects during sepsis/shock

Systemic exposure to LPS or *E. coli* induces HC-HA/CD44-dependent PMN sequestration in the liver sinusoids [109, 133, 134] and is associated with improved survival during endotoxic shock. Proposed mechanisms by which sequestered PMN can act protectively during sepsis and endotoxic shock (**A-D**).

5.2 Future directions

While we only found modest protective effects of TSG-6 in our IT LPS and *PA* respiratory infection models, this may have been due to the rapid clearance of lung parenchymal HC-HA in our murine model system. We performed these experiments in WT control littermates of our *TSG-6* KO mice (BALB/c background), which exhibit less robust neutrophilic response to LPS and *PA* than C57BL/6 mice. This can be appreciated in the 12-day time course that was used for the RNA-seq data of AM isolated from C57BL/6 mice exposed to same dose of LPS (Chapter 2). Consequently, in response to either LPS or non-lethal *PA* dose, inflammation resolved very rapidly in BALB/c, which we assessed over a shorter 6-day time course (Chapter 3). We predict that *TSG-6* KO mice backcrossed to C57BL/6 background would exhibit a more robust and persistent lung parenchymal HC-HA induction, which may provide more time for HC-HA to exert its effects on injury and recovery outcomes. On a similar note, the prolonged 14-day time-course of resolving viral lung infection and resolution presents a valuable opportunity for investigating the effects of more persistent lung parenchymal HC-HA on ALI outcomes.

Besides the effect of strain background on the magnitude of response to LPS, there may be strain differences in HA clearance that would affect the extent of HC-HA accumulation and persistence. In the context of endotoxic shock, where HC-HA has been implicated in liver neutrophil adhesion and promoting survival, testing the effects of TSG-6 on different background, may also be extremely fruitful. Regarding which strain background to select, it is important to note that the HC-HA dependent neutrophil adhesion results were obtained using *IaI* mice on a C57BL/6 background [134]. We would predict that *TSG-6* KO mice backcrossed to C57BL/6 background would show greater magnitude of survival differences in response to endotoxic shock than what we

observed (Chapter 4) due to potential differences in HC-HA accumulation and persistence.

Neutrophils have complex roles during sepsis [200]. While they are crucial for eliminating bacterial infection, their exact role in contributing to vascular dysfunction and end-organ damage during sepsis remains poorly defined. But there is increasing evidence that neutrophils may have both protective and harmful effects in this context [167]. With the advances in intravital microscopy, more work is needed to understand the careful regulation of neutrophil trafficking and localization during sepsis. Our work highlights the need for more studies on the effect of HC-HA on neutrophil trafficking in the context of endotoxic shock and sepsis, which have thus far been completed only in the liver sinusoids with *Ial* KO mice. Completing these studies using *TSG-6* KO mice would be important to rule out any HC-HA independent effects of *Ial*, which is an abundant serum protein that not only has two HC domains, but also features a protease inhibitor whose physiological role has been assumed to be minimal. Nonetheless, the evidence that the HC-HA/CD44 axis regulates neutrophil adhesion in the liver sinusoids is very strong due to the additional use of hyaluronidase and anti-CD44 antibody experiments to specifically confirm HA's role [133].

Thus far, all sepsis studies with *TSG-6* KO mice and *Ial* KO mice have been performed using systemic LPS administration with either IV LPS [133, 134] or IP LPS induced endotoxic shock [135, 136]. Therefore, it remains unclear what are the effects of HC-HA formation during septic bacteremia, which is most commonly modeled in mouse using cecal ligation and puncture. As discussed (Chapter 5.1 Summary), the HC-HA-dependent sequestration of neutrophils in the liver sinusoids may regulate systemic neutrophil numbers and serve to trap and eliminate circulating bacteria. Therefore, cecal ligation and puncture or systemic injections of defined gram negative bacteria in *TSG-6* and *Ial* KO mice are sorely needed to define the role of HC-HA during bacteremia.

While the recent discovery that HC-HA is required for initiating midgut rotation has raised questions regarding the embryonic fitness of *TSG-6* KO mice and *Ial* KO mice [80], we and others have noted no baseline viability or gross deficits with *TSG-6* and *Ial* KO mice. Our findings of minimal differences in respiratory ALI outcomes between *TSG-6* KO and control (Chapter 3) further supports the absence of any deficits. However, these findings cannot definitively rule out any physiological impairments resulting from midgut malrotation during severe injury and stress such as during endotoxic shock or sepsis. Therefore, intestinal inflammation should be assessed in future investigations with *TSG-6* and *Ial* KO mice to control for potential differences arising from midgut malrotation.

For our *TSG-6* KO endotoxic shock studies, while the bone marrow was not investigated, this compartment is high priority for future studies due to its potential effects on outcomes of sepsis and endotoxic shock and the potential role of TSG-6 and HC-HA in the bone marrow during severe systemic inflammation. Immune dysfunction and neutropenia are frequent in the patient populations (infant and elderly) most vulnerable to sepsis-related mortality [112, 113]. Experimental models of sepsis in mice are characterized by myelosuppression and functional deficits in hematopoietic stem and progenitor cells that may be applicable to humans [114, 115]. A recent report highlighted the role of HA/CD44 interactions during conditions of bone marrow stress by demonstrating that HA/CD44 promoted hematopoietic progenitor cell proliferation following irradiation and engraftment [117]. Our lab has previously shown that exogenous TSG-6 supplementation can improve hematopoietic cell cycling and functionality (clonogenic capacity) and LSK (bone marrow population enriched in hematopoietic stem and progenitor cells) counts following cigarette smoke-induced myelosuppression [118]. Other labs have shown that TSG-6 can regulate bone marrow stromal cell differentiation [119-121]. These findings underscore the need to characterize

the bone marrow following endotoxic shock and sepsis in both *TSG-6* and *I α I* KO mice to clearly define whether TSG-6, HC-HA, or both are acting protectively in the bone marrow.

References

1. Yamada S, Sugahara K, Ozbek S: Evolution of glycosaminoglycans: Comparative biochemical study. *Commun Integr Biol* 2011, 4(2):150-158.
2. DeAngelis PL: Evolution of glycosaminoglycans and their glycosyltransferases: Implications for the extracellular matrices of animals and the capsules of pathogenic bacteria. *Anat Rec* 2002, 268(3):317-326.
3. Yoneda M, Nakamura T, Murai M, Wada H: Evidence for the heparin-binding ability of the ascidian Xlink domain and insight into the evolution of the Xlink domain in chordates. *J Mol Evol* 2010, 71(1):51-59.
4. Weigel PH: Hyaluronan Synthase: The Mechanism of Initiation at the Reducing End and a Pendulum Model for Polysaccharide Translocation to the Cell Exterior. *Int J Cell Biol* 2015, 2015:367579.
5. Higman VA, Briggs DC, Mahoney DJ, Blundell CD, Sattelle BM, Dyer DP, Green DE, DeAngelis PL, Almond A, Milner CM *et al*: A refined model for the TSG-6 link module in complex with hyaluronan: use of defined oligosaccharides to probe structure and function. *The Journal of biological chemistry* 2014, 289(9):5619-5634.
6. Higman VA, Blundell CD, Mahoney DJ, Redfield C, Noble ME, Day AJ: Plasticity of the TSG-6 HA-binding loop and mobility in the TSG-6-HA complex revealed by NMR and X-ray crystallography. *J Mol Biol* 2007, 371(3):669-684.
7. Kohda D, Morton CJ, Parkar AA, Hatanaka H, Inagaki FM, Campbell ID, Day AJ: Solution structure of the link module: a hyaluronan-binding domain involved in extracellular matrix stability and cell migration. *Cell* 1996, 86(5):767-775.
8. Bastow ER, Byers S, Golub SB, Clarkin CE, Pitsillides AA, Fosang AJ: Hyaluronan synthesis and degradation in cartilage and bone. *Cell Mol Life Sci* 2008, 65(3):395-413.
9. Tien JY, Spicer AP: Three vertebrate hyaluronan synthases are expressed during mouse development in distinct spatial and temporal patterns. *Dev Dyn* 2005, 233(1):130-141.
10. Camenisch TD, Spicer AP, Brehm-Gibson T, Biesterfeldt J, Augustine ML, Calabro A, Jr., Kubalak S, Klewer SE, McDonald JA: Disruption of hyaluronan synthase-2 abrogates normal cardiac morphogenesis and hyaluronan-mediated transformation of epithelium to mesenchyme. *The Journal of clinical investigation* 2000, 106(3):349-360.
11. Lee-Sayer SS, Dong Y, Arif AA, Olsson M, Brown KL, Johnson P: The Where, When, How, and Why of Hyaluronan Binding by Immune Cells. *Frontiers in Immunology* 2015, 6:150.
12. Csoka AB, Stern R: Hypotheses on the evolution of hyaluronan: a highly ironic acid. *Glycobiology* 2013, 23(4):398-411.
13. Noble PW: Hyaluronan and its catabolic products in tissue injury and repair. *Matrix biology : journal of the International Society for Matrix Biology* 2002, 21(1):25-29.
14. Henderson EB, Grootveld M, Farrell A, Smith EC, Thompson PW, Blake DR: A pathological role for damaged hyaluronan in synovitis. *Ann Rheum Dis* 1991, 50(3):196-200.
15. Chowdhury B, Hemming R, Faiyaz S, Triggs-Raine B: Hyaluronidase 2 (HYAL2) is expressed in endothelial cells, as well as some specialized epithelial cells, and is required for normal hyaluronan catabolism. *Histochem Cell Biol* 2016, 145(1):53-66.

16. Soltes L, Mendichi R, Kogan G, Schiller J, Stankovska M, Arnhold J: Degradative action of reactive oxygen species on hyaluronan. *Biomacromolecules* 2006, 7(3):659-668.
17. Spicer AP, McDonald JA: Characterization and molecular evolution of a vertebrate hyaluronan synthase gene family. *The Journal of biological chemistry* 1998, 273(4):1923-1932.
18. Itano N, Sawai T, Yoshida M, Lenas P, Yamada Y, Imagawa M, Shinomura T, Hamaguchi M, Yoshida Y, Ohnuki Y *et al*: Three isoforms of mammalian hyaluronan synthases have distinct enzymatic properties. *The Journal of biological chemistry* 1999, 274(35):25085-25092.
19. Rilla K, Oikari S, Jokela TA, Hyttinen JM, Karna R, Tammi RH, Tammi MI: Hyaluronan synthase 1 (HAS1) requires higher cellular UDP-GlcNAc concentration than HAS2 and HAS3. *The Journal of biological chemistry* 2013, 288(8):5973-5983.
20. Torronen K, Nikunen K, Karna R, Tammi M, Tammi R, Rilla K: Tissue distribution and subcellular localization of hyaluronan synthase isoenzymes. *Histochem Cell Biol* 2014, 141(1):17-31.
21. Matsumoto K, Li Y, Jakuba C, Sugiyama Y, Sayo T, Okuno M, Dealy CN, Toole BP, Takeda J, Yamaguchi Y *et al*: Conditional inactivation of Has2 reveals a crucial role for hyaluronan in skeletal growth, patterning, chondrocyte maturation and joint formation in the developing limb. *Development* 2009, 136(16):2825-2835.
22. Arranz AM, Perkins KL, Irie F, Lewis DP, Hrabe J, Xiao F, Itano N, Kimata K, Hrabetova S, Yamaguchi Y: Hyaluronan deficiency due to Has3 knock-out causes altered neuronal activity and seizures via reduction in brain extracellular space. *J Neurosci* 2014, 34(18):6164-6176.
23. Weigel PH: Functional characteristics and catalytic mechanisms of the bacterial hyaluronan synthases. *IUBMB Life* 2002, 54(4):201-211.
24. Laurent TC, Laurent UB, Fraser JR: Serum hyaluronan as a disease marker. *Ann Med* 1996, 28(3):241-253.
25. Lebel L, Smith L, Risberg B, Laurent TC, Gerdin B: Increased lymphatic elimination of interstitial hyaluronan during E. coli sepsis in sheep. *Am J Physiol* 1989, 256(6 Pt 2):H1524-1531.
26. Lebel L, Smith L, Risberg B, Gerdin B, Laurent TC: Effect of increased hydrostatic pressure on lymphatic elimination of hyaluronan from sheep lung. *J Appl Physiol (1985)* 1988, 64(4):1327-1332.
27. Fraser JR, Laurent TC, Engstrom-Laurent A, Laurent UG: Elimination of hyaluronic acid from the blood stream in the human. *Clin Exp Pharmacol Physiol* 1984, 11(1):17-25.
28. Fraser JR, Laurent TC, Pertoft H, Baxter E: Plasma clearance, tissue distribution and metabolism of hyaluronic acid injected intravenously in the rabbit. *Biochem J* 1981, 200(2):415-424.
29. Bourguignon V, Flamion B: Respective roles of hyaluronidases 1 and 2 in endogenous hyaluronan turnover. *FASEB journal : official publication of the Federation of American Societies for Experimental Biology* 2016, 30(6):2108-2114.
30. Jadin L, Bookbinder LH, Frost GI: A comprehensive model of hyaluronan turnover in the mouse. *Matrix biology : journal of the International Society for Matrix Biology* 2012, 31(2):81-89.
31. Laurent UBG, Reed RK: Turnover of hyaluronan in the tissues. *Advanced Drug Delivery Reviews* 1991, 7(2):237-256.

32. Stern R: Devising a pathway for hyaluronan catabolism: are we there yet? *Glycobiology* 2003, 13(12):105R-115R.
33. Bourguignon LY, Singleton PA, Diedrich F, Stern R, Gilad E: CD44 interaction with Na⁺-H⁺ exchanger (NHE1) creates acidic microenvironments leading to hyaluronidase-2 and cathepsin B activation and breast tumor cell invasion. *The Journal of biological chemistry* 2004, 279(26):26991-27007.
34. Harada H, Takahashi M: CD44-dependent intracellular and extracellular catabolism of hyaluronic acid by hyaluronidase-1 and -2. *The Journal of biological chemistry* 2007, 282(8):5597-5607.
35. Duterme C, Mertens-Strijthagen J, Tammi M, Flamion B: Two novel functions of hyaluronidase-2 (Hyal2) are formation of the glycocalyx and control of CD44-ERM interactions. *The Journal of biological chemistry* 2009, 284(48):33495-33508.
36. Hida D, Danielson BT, Knudson CB, Knudson W: CD44 knock-down in bovine and human chondrocytes results in release of bound HYAL2. *Matrix biology : journal of the International Society for Matrix Biology* 2015, 48:42-54.
37. Muggenthaler MM, Chowdhury B, Hasan SN, Cross HE, Mark B, Harlalka GV, Patton MA, Ishida M, Behr ER, Sharma S *et al*: Mutations in HYAL2, Encoding Hyaluronidase 2, Cause a Syndrome of Orofacial Clefting and Cor Triatriatum Sinister in Humans and Mice. *PLoS Genet* 2017, 13(1):e1006470.
38. Chowdhury B, Hemming R, Hombach-Klonisch S, Flamion B, Triggs-Raine B: Murine hyaluronidase 2 deficiency results in extracellular hyaluronan accumulation and severe cardiopulmonary dysfunction. *The Journal of biological chemistry* 2013, 288(1):520-528.
39. Jadin L, Wu X, Ding H, Frost GI, Onclinx C, Triggs-Raine B, Flamion B: Skeletal and hematological anomalies in HYAL2-deficient mice: a second type of mucopolysaccharidosis IX? *FASEB journal : official publication of the Federation of American Societies for Experimental Biology* 2008, 22(12):4316-4326.
40. Frost GI, Csoka AB, Wong T, Stern R: Purification, cloning, and expression of human plasma hyaluronidase. *Biochemical and biophysical research communications* 1997, 236(1):10-15.
41. Gasingirwa MC, Thirion J, Mertens-Strijthagen J, Wattiaux-De Coninck S, Flamion B, Wattiaux R, Jadot M: Endocytosis of hyaluronidase-1 by the liver. *Biochem J* 2010, 430(2):305-313.
42. Natowicz MR, Short MP, Wang Y, Dickersin GR, Gebhardt MC, Rosenthal DI, Sims KB, Rosenberg AE: Clinical and biochemical manifestations of hyaluronidase deficiency. *The New England journal of medicine* 1996, 335(14):1029-1033.
43. Triggs-Raine B, Salo TJ, Zhang H, Wicklow BA, Natowicz MR: Mutations in HYAL1, a member of a tandemly distributed multigene family encoding disparate hyaluronidase activities, cause a newly described lysosomal disorder, mucopolysaccharidosis IX. *Proceedings of the National Academy of Sciences of the United States of America* 1999, 96(11):6296-6300.
44. Martin DC, Atmuri V, Hemming RJ, Farley J, Mort JS, Byers S, Hombach-Klonisch S, Csoka AB, Stern R, Triggs-Raine BL: A mouse model of human mucopolysaccharidosis IX exhibits osteoarthritis. *Hum Mol Genet* 2008, 17(13):1904-1915.
45. Imundo L, Leduc CA, Guha S, Brown M, Perino G, Gushulak L, Triggs-Raine B, Chung WK: A complete deficiency of Hyaluronoglucosaminidase 1 (HYAL1) presenting as familial juvenile idiopathic arthritis. *J Inherit Metab Dis* 2011, 34(5):1013-1022.

46. Gushulak L, Hemming R, Martin D, Seyrantepe V, Pshezhetsky A, Triggs-Raine B: Hyaluronidase 1 and beta-hexosaminidase have redundant functions in hyaluronan and chondroitin sulfate degradation. *The Journal of biological chemistry* 2012, 287(20):16689-16697.
47. Yamamoto H, Tobisawa Y, Inubushi T, Irie F, Ohyama C, Yamaguchi Y: A mammalian homolog of the zebrafish transmembrane protein 2 (TMEM2) is the long-sought-after cell-surface hyaluronidase. *The Journal of biological chemistry* 2017, 292(18):7304-7313.
48. Yoshida H, Nagaoka A, Kusaka-Kikushima A, Tobiishi M, Kawabata K, Sayo T, Sakai S, Sugiyama Y, Enomoto H, Okada Y *et al*: KIAA1199, a deafness gene of unknown function, is a new hyaluronan binding protein involved in hyaluronan depolymerization. *Proceedings of the National Academy of Sciences of the United States of America* 2013, 110(14):5612-5617.
49. Yoshida H, Nagaoka A, Nakamura S, Tobiishi M, Sugiyama Y, Inoue S: N-Terminal signal sequence is required for cellular trafficking and hyaluronan-depolymerization of KIAA1199. *FEBS Lett* 2014, 588(1):111-116.
50. De Angelis JE, Lagendijk AK, Chen H, Tromp A, Bower NI, Tunny KA, Brooks AJ, Bakkers J, Francois M, Yap AS *et al*: Tmem2 Regulates Embryonic Vegf Signaling by Controlling Hyaluronic Acid Turnover. *Dev Cell* 2017, 40(2):123-136.
51. Weigel JA, Raymond RC, McGary C, Singh A, Weigel PH: A blocking antibody to the hyaluronan receptor for endocytosis (HARE) inhibits hyaluronan clearance by perfused liver. *The Journal of biological chemistry* 2003, 278(11):9808-9812.
52. Schledzewski K, Geraud C, Arnold B, Wang S, Grone HJ, Kempf T, Wollert KC, Straub BK, Schirmacher P, Demory A *et al*: Deficiency of liver sinusoidal scavenger receptors stabilin-1 and -2 in mice causes glomerulofibrotic nephropathy via impaired hepatic clearance of noxious blood factors. *The Journal of clinical investigation* 2011, 121(2):703-714.
53. Sandson J, Hamerman D, Schwick G: Altered properties of pathological hyaluronate due to a bound inter-alpha trypsin inhibitor. *Trans Assoc Am Physicians* 1965, 78:304-313.
54. Sanggaard KW, Sonne-Schmidt CS, Krogager TP, Kristensen T, Wisniewski HG, Thogersen IB, Enghild JJ: TSG-6 transfers proteins between glycosaminoglycans via a Ser28-mediated covalent catalytic mechanism. *The Journal of biological chemistry* 2008, 283(49):33919-33926.
55. Zhao M, Yoneda M, Ohashi Y, Kurono S, Iwata H, Ohnuki Y, Kimata K: Evidence for the covalent binding of SHAP, heavy chains of inter-alpha-trypsin inhibitor, to hyaluronan. *The Journal of biological chemistry* 1995, 270(44):26657-26663.
56. Ni K, Gill A, Tseng V, Mikosz AM, Koike K, Beatman EL, Xu CY, Cao D, Gally F, Mould KJ *et al*: Rapid clearance of heavy chain-modified hyaluronan during resolving acute lung injury. *Respiratory research* 2018, 19(1):107.
57. Rugg MS, Willis AC, Mukhopadhyay D, Hascall VC, Fries E, Fulop C, Milner CM, Day AJ: Characterization of complexes formed between TSG-6 and inter-alpha-inhibitor that act as intermediates in the covalent transfer of heavy chains onto hyaluronan. *The Journal of biological chemistry* 2005, 280(27):25674-25686.
58. Briggs DC, Birchenough HL, Ali T, Rugg MS, Waltho JP, Ievoli E, Jowitt TA, Enghild JJ, Richter RP, Salustri A *et al*: Metal Ion-dependent Heavy Chain Transfer Activity of TSG-6 Mediates Assembly of the Cumulus-Oocyte Matrix. *The Journal of biological chemistry* 2015, 290(48):28708-28723.
59. Sanggaard KW, Sonne-Schmidt CS, Jacobsen C, Thogersen IB, Valnickova Z, Wisniewski HG, Enghild JJ: Evidence for a two-step mechanism involved in the

- formation of covalent HC x TSG-6 complexes. *Biochemistry* 2006, 45(24):7661-7668.
60. Zhuo L, Kimata K: Structure and function of inter-alpha-trypsin inhibitor heavy chains. *Connect Tissue Res* 2008, 49(5):311-320.
 61. Potempa J, Kwon K, Chawla R, Travis J: Inter-alpha-trypsin inhibitor. Inhibition spectrum of native and derived forms. *The Journal of biological chemistry* 1989, 264(25):15109-15114.
 62. Whittaker CA, Hynes RO: Distribution and evolution of von Willebrand/integrin A domains: widely dispersed domains with roles in cell adhesion and elsewhere. *Mol Biol Cell* 2002, 13(10):3369-3387.
 63. Adair JE, Stober V, Sobhany M, Zhuo L, Roberts JD, Negishi M, Kimata K, Garantziotis S: Inter-alpha-trypsin inhibitor promotes bronchial epithelial repair after injury through vitronectin binding. *The Journal of biological chemistry* 2009, 284(25):16922-16930.
 64. Okroj M, Holmquist E, Sjolander J, Corrales L, Saxne T, Wisniewski HG, Blom AM: Heavy chains of inter alpha inhibitor (Ialpal) inhibit the human complement system at early stages of the cascade. *The Journal of biological chemistry* 2012, 287(24):20100-20110.
 65. Garantziotis S, Hollingsworth JW, Ghanayem RB, Timberlake S, Zhuo L, Kimata K, Schwartz DA: Inter-alpha-trypsin inhibitor attenuates complement activation and complement-induced lung injury. *Journal of immunology* 2007, 179(6):4187-4192.
 66. Htwe SS, Wake H, Liu K, Teshigawara K, Stonestreet BS, Lim YP, Nishibori M: Inter-alpha inhibitor proteins maintain neutrophils in a resting state by regulating shape and reducing ROS production. *Blood Adv* 2018, 2(15):1923-1934.
 67. Lee TH, Wisniewski HG, Vilcek J: A novel secretory tumor necrosis factor-inducible protein (TSG-6) is a member of the family of hyaluronate binding proteins, closely related to the adhesion receptor CD44. *J Cell Biol* 1992, 116(2):545-557.
 68. Wisniewski HG, Maier R, Lotz M, Lee S, Klampfer L, Lee TH, Vilcek J: TSG-6: a TNF-, IL-1-, and LPS-inducible secreted glycoprotein associated with arthritis. *Journal of immunology* 1993, 151(11):6593-6601.
 69. Klampfer L, Chen-Kiang S, Vilcek J: Activation of the TSG-6 gene by NF-IL6 requires two adjacent NF-IL6 binding sites. *The Journal of biological chemistry* 1995, 270(8):3677-3682.
 70. Klampfer L, Lee TH, Hsu W, Vilcek J, Chen-Kiang S: NF-IL6 and AP-1 cooperatively modulate the activation of the TSG-6 gene by tumor necrosis factor alpha and interleukin-1. *Mol Cell Biol* 1994, 14(10):6561-6569.
 71. Wisniewski HG, Burgess WH, Oppenheim JD, Vilcek J: TSG-6, an arthritis-associated hyaluronan binding protein, forms a stable complex with the serum protein inter-alpha-inhibitor. *Biochemistry* 1994, 33(23):7423-7429.
 72. Sanggaard KW, Hansen L, Scavenius C, Wisniewski HG, Kristensen T, Thogersen IB, Enghild JJ: Evolutionary conservation of heavy chain protein transfer between glycosaminoglycans. *Biochim Biophys Acta* 2010, 1804(4):1011-1019.
 73. Lesley J, English NM, Gal I, Mikecz K, Day AJ, Hyman R: Hyaluronan binding properties of a CD44 chimera containing the link module of TSG-6. *The Journal of biological chemistry* 2002, 277(29):26600-26608.
 74. Yingsung W, Zhuo L, Morgelin M, Yoneda M, Kida D, Watanabe H, Ishiguro N, Iwata H, Kimata K: Molecular heterogeneity of the SHAP-hyaluronan complex. Isolation and characterization of the complex in synovial fluid from patients with

- rheumatoid arthritis. *The Journal of biological chemistry* 2003, 278(35):32710-32718.
75. Baranova NS, Nileback E, Haller FM, Briggs DC, Svedhem S, Day AJ, Richter RP: The inflammation-associated protein TSG-6 cross-links hyaluronan via hyaluronan-induced TSG-6 oligomers. *The Journal of biological chemistry* 2011, 286(29):25675-25686.
 76. Zhuo L, Yoneda M, Zhao M, Yingsung W, Yoshida N, Kitagawa Y, Kawamura K, Suzuki T, Kimata K: Defect in SHAP-hyaluronan complex causes severe female infertility. A study by inactivation of the bikunin gene in mice. *The Journal of biological chemistry* 2001, 276(11):7693-7696.
 77. Fulop C, Szanto S, Mukhopadhyay D, Bardos T, Kamath RV, Rugg MS, Day AJ, Salustri A, Hascall VC, Glant TT *et al*: Impaired cumulus mucification and female sterility in tumor necrosis factor-induced protein-6 deficient mice. *Development* 2003, 130(10):2253-2261.
 78. Varani S, Elvin JA, Yan C, DeMayo J, DeMayo FJ, Horton HF, Byrne MC, Matzuk MM: Knockout of pentraxin 3, a downstream target of growth differentiation factor-9, causes female subfertility. *Mol Endocrinol* 2002, 16(6):1154-1167.
 79. Salustri A, Garlanda C, Hirsch E, De Acetis M, Maccagno A, Bottazzi B, Doni A, Bastone A, Mantovani G, Beck Peccoz P *et al*: PTX3 plays a key role in the organization of the cumulus oophorus extracellular matrix and in in vivo fertilization. *Development* 2004, 131(7):1577-1586.
 80. Sivakumar A, Mahadevan A, Lauer ME, Narvaez RJ, Ramesh S, Demler CM, Souchet NR, Hascall VC, Midura RJ, Garantziotis S *et al*: Midgut Laterality Is Driven by Hyaluronan on the Right. *Dev Cell* 2018, 46(5):533-551 e535.
 81. Bedford JM: Puzzles of mammalian fertilization--and beyond. *Int J Dev Biol* 2008, 52(5-6):415-426.
 82. Sato H, Kajikawa S, Kuroda S, Horisawa Y, Nakamura N, Kaga N, Kakinuma C, Kato K, Morishita H, Niwa H *et al*: Impaired fertility in female mice lacking urinary trypsin inhibitor. *Biochemical and biophysical research communications* 2001, 281(5):1154-1160.
 83. Pelayo JC, Lo A: Intestinal Rotation Anomalies. *Pediatr Ann* 2016, 45(7):e247-250.
 84. Langer JC: Intestinal Rotation Abnormalities and Midgut Volvulus. *Surg Clin North Am* 2017, 97(1):147-159.
 85. Sheu CC, Gong MN, Zhai R, Chen F, Bajwa EK, Clardy PF, Gallagher DC, Thompson BT, Christiani DC: Clinical characteristics and outcomes of sepsis-related vs non-sepsis-related ARDS. *Chest* 2010, 138(3):559-567.
 86. Erickson SE, Martin GS, Davis JL, Matthay MA, Eisner MD, Network NNA: Recent trends in acute lung injury mortality: 1996-2005. *Critical care medicine* 2009, 37(5):1574-1579.
 87. Randolph AG: Management of acute lung injury and acute respiratory distress syndrome in children. *Critical care medicine* 2009, 37(8):2448-2454.
 88. Matthay MA, McAuley DF, Ware LB: Clinical trials in acute respiratory distress syndrome: challenges and opportunities. *Lancet Respir Med* 2017, 5(6):524-534.
 89. Beutz MA, Abraham E: Community-acquired pneumonia and sepsis. *Clinics in chest medicine* 2005, 26(1):19-28.
 90. Marshall JC: Why have clinical trials in sepsis failed? *Trends Mol Med* 2014, 20(4):195-203.

91. Reinhart K, Karzai W: Anti-tumor necrosis factor therapy in sepsis: update on clinical trials and lessons learned. *Critical care medicine* 2001, 29(7 Suppl):S121-125.
92. Opal SM, Fisher CJ, Jr., Dhainaut JF, Vincent JL, Brase R, Lowry SF, Sadoff JC, Slotman GJ, Levy H, Balk RA *et al*: Confirmatory interleukin-1 receptor antagonist trial in severe sepsis: a phase III, randomized, double-blind, placebo-controlled, multicenter trial. The Interleukin-1 Receptor Antagonist Sepsis Investigator Group. *Critical care medicine* 1997, 25(7):1115-1124.
93. Opal SM, Laterre PF, Francois B, LaRosa SP, Angus DC, Mira JP, Wittebole X, Dugernier T, Perrotin D, Tidswell M *et al*: Effect of eritoran, an antagonist of MD2-TLR4, on mortality in patients with severe sepsis: the ACCESS randomized trial. *JAMA* 2013, 309(11):1154-1162.
94. Matute-Bello G, Downey G, Moore BB, Groshong SD, Matthay MA, Slutsky AS, Kuebler WM, Acute Lung Injury in Animals Study G: An official American Thoracic Society workshop report: features and measurements of experimental acute lung injury in animals. *American journal of respiratory cell and molecular biology* 2011, 44(5):725-738.
95. Rehm SR, Gross GN, Pierce AK: Early bacterial clearance from murine lungs. Species-dependent phagocyte response. *The Journal of clinical investigation* 1980, 66(2):194-199.
96. Tsai WC, Strieter RM, Mehrad B, Newstead MW, Zeng X, Standiford TJ: CXC chemokine receptor CXCR2 is essential for protective innate host response in murine *Pseudomonas aeruginosa* pneumonia. *Infect Immun* 2000, 68(7):4289-4296.
97. Skerrett SJ, Liggitt HD, Hajjar AM, Wilson CB: Cutting edge: myeloid differentiation factor 88 is essential for pulmonary host defense against *Pseudomonas aeruginosa* but not *Staphylococcus aureus*. *Journal of immunology* 2004, 172(6):3377-3381.
98. D'Alessio FR, Craig JM, Singer BD, Files DC, Mock JR, Garibaldi BT, Fallica J, Tripathi A, Mandke P, Gans JH *et al*: Enhanced resolution of experimental ARDS through IL-4-mediated lung macrophage reprogramming. *American journal of physiology Lung cellular and molecular physiology* 2016, 310(8):L733-746.
99. D'Alessio FR, Tsushima K, Aggarwal NR, West EE, Willett MH, Britos MF, Pipeling MR, Brower RG, Tudor RM, McDyer JF *et al*: CD4+CD25+Foxp3+ Tregs resolve experimental lung injury in mice and are present in humans with acute lung injury. *The Journal of clinical investigation* 2009, 119(10):2898-2913.
100. Cabrera-Benitez NE, Laffey JG, Parotto M, Spieth PM, Villar J, Zhang H, Slutsky AS: Mechanical ventilation-associated lung fibrosis in acute respiratory distress syndrome: a significant contributor to poor outcome. *Anesthesiology* 2014, 121(1):189-198.
101. Burnham EL, Janssen WJ, Riches DW, Moss M, Downey GP: The fibroproliferative response in acute respiratory distress syndrome: mechanisms and clinical significance. *The European respiratory journal* 2014, 43(1):276-285.
102. Clark SR, Ma AC, Tavener SA, McDonald B, Goodarzi Z, Kelly MM, Patel KD, Chakrabarti S, McAvoy E, Sinclair GD *et al*: Platelet TLR4 activates neutrophil extracellular traps to ensnare bacteria in septic blood. *Nature medicine* 2007, 13(4):463-469.
103. Yipp BG, Kim JH, Lima R, Zbytniuk LD, Petri B, Swanlund N, Ho M, Szeto VG, Tak T, Koenderman L *et al*: The Lung is a Host Defense Niche for Immediate Neutrophil-Mediated Vascular Protection. *Sci Immunol* 2017, 2(10).

104. Andonegui G, Zhou H, Bullard D, Kelly MM, Mullaly SC, McDonald B, Long EM, Robbins SM, Kubes P: Mice that exclusively express TLR4 on endothelial cells can efficiently clear a lethal systemic Gram-negative bacterial infection. *The Journal of clinical investigation* 2009, 119(7):1921-1930.
105. Anghileri E, Marconi S, Pignatelli A, Cifelli P, Galie M, Sbarbati A, Krampera M, Belluzzi O, Bonetti B: Neuronal differentiation potential of human adipose-derived mesenchymal stem cells. *Stem Cells Dev* 2008, 17(5):909-916.
106. Dong Y, Arif A, Olsson M, Cali V, Hardman B, Dosanjh M, Lauer M, Midura RJ, Hascall VC, Brown KL *et al*: Endotoxin free hyaluronan and hyaluronan fragments do not stimulate TNF-alpha, interleukin-12 or upregulate co-stimulatory molecules in dendritic cells or macrophages. *Sci Rep* 2016, 6:36928.
107. Shi J, Gilbert GE, Kokubo Y, Ohashi T: Role of the liver in regulating numbers of circulating neutrophils. *Blood* 2001, 98(4):1226-1230.
108. Wang J, Kubes P: A Reservoir of Mature Cavity Macrophages that Can Rapidly Invade Visceral Organs to Affect Tissue Repair. *Cell* 2016, 165(3):668-678.
109. Menezes GB, Lee WY, Zhou H, Waterhouse CC, Cara DC, Kubes P: Selective down-regulation of neutrophil Mac-1 in endotoxemic hepatic microcirculation via IL-10. *Journal of immunology* 2009, 183(11):7557-7568.
110. Poon IK, Lucas CD, Rossi AG, Ravichandran KS: Apoptotic cell clearance: basic biology and therapeutic potential. *Nature reviews Immunology* 2014, 14(3):166-180.
111. Fadok VA, Bratton DL, Konowal A, Freed PW, Westcott JY, Henson PM: Macrophages that have ingested apoptotic cells in vitro inhibit proinflammatory cytokine production through autocrine/paracrine mechanisms involving TGF-beta, PGE2, and PAF. *The Journal of clinical investigation* 1998, 101(4):890-898.
112. Hotchkiss RS, Monneret G, Payen D: Immunosuppression in sepsis: a novel understanding of the disorder and a new therapeutic approach. *Lancet Infect Dis* 2013, 13(3):260-268.
113. Delano MJ, Ward PA: Sepsis-induced immune dysfunction: can immune therapies reduce mortality? *The Journal of clinical investigation* 2016, 126(1):23-31.
114. Zhang H, Rodriguez S, Wang L, Wang S, Serezani H, Kapur R, Cardoso AA, Carlesso N: Sepsis Induces Hematopoietic Stem Cell Exhaustion and Myelosuppression through Distinct Contributions of TRIF and MYD88. *Stem Cell Reports* 2016, 6(6):940-956.
115. Rodriguez S, Chora A, Goumnerov B, Mumaw C, Goebel WS, Fernandez L, Baydoun H, HogenEsch H, Dombkowski DM, Karlewicz CA *et al*: Dysfunctional expansion of hematopoietic stem cells and block of myeloid differentiation in lethal sepsis. *Blood* 2009, 114(19):4064-4076.
116. Elting LS, Rubenstein EB, Rolston KV, Bodey GP: Outcomes of bacteremia in patients with cancer and neutropenia: observations from two decades of epidemiological and clinical trials. *Clin Infect Dis* 1997, 25(2):247-259.
117. Lee-Sayer SSM, Dougan MN, Cooper J, Sanderson L, Dosanjh M, Maxwell CA, Johnson P: CD44-mediated hyaluronan binding marks proliferating hematopoietic progenitor cells and promotes bone marrow engraftment. *PLoS one* 2018, 13(4):e0196011.
118. Xie J, Broxmeyer HE, Feng D, Schweitzer KS, Yi R, Cook TG, Chitteti BR, Barwinska D, Traktuev DO, Van Demark MJ *et al*: Human adipose-derived stem cells ameliorate cigarette smoke-induced murine myelosuppression via secretion of TSG-6. *Stem cells* 2015, 33(2):468-478.

119. Lee RH, Yu JM, Foskett AM, Peltier G, Reneau JC, Bazhanov N, Oh JY, Prockop DJ: TSG-6 as a biomarker to predict efficacy of human mesenchymal stem/progenitor cells (hMSCs) in modulating sterile inflammation in vivo. *Proceedings of the National Academy of Sciences of the United States of America* 2014, 111(47):16766-16771.
120. Mahoney DJ, Mikecz K, Ali T, Mabileau G, Benayahu D, Plaas A, Milner CM, Day AJ, Sabokbar A: TSG-6 regulates bone remodeling through inhibition of osteoblastogenesis and osteoclast activation. *The Journal of biological chemistry* 2008, 283(38):25952-25962.
121. Tsukahara S, Ikeda R, Goto S, Yoshida K, Mitsumori R, Sakamoto Y, Tajima A, Yokoyama T, Toh S, Furukawa K *et al*: Tumour necrosis factor alpha-stimulated gene-6 inhibits osteoblastic differentiation of human mesenchymal stem cells induced by osteogenic differentiation medium and BMP-2. *Biochem J* 2006, 398(3):595-603.
122. Lauer ME, Aytakin M, Comhair SA, Loftis J, Tian L, Farver CF, Hascall VC, Dweik RA: Modification of hyaluronan by heavy chains of inter-alpha-inhibitor in idiopathic pulmonary arterial hypertension. *The Journal of biological chemistry* 2014, 289(10):6791-6798.
123. Lauer ME, Majors AK, Comhair S, Ruple LM, Matuska B, Subramanian A, Farver C, Dworski R, Grandon D, Laskowski D *et al*: Hyaluronan and its heavy chain modification in asthma severity and experimental asthma exacerbation. *The Journal of biological chemistry* 2015.
124. Matuska B, Comhair S, Farver C, Chmiel J, Midura RJ, Bonfield T, Lauer ME: Pathological Hyaluronan Matrices in Cystic Fibrosis Airways and Secretions. *American journal of respiratory cell and molecular biology* 2016, 55(4):576-585.
125. Garantziotis S, Zudaire E, Trempus CS, Hollingsworth JW, Jiang D, Lancaster LH, Richardson E, Zhuo L, Cuttitta F, Brown KK *et al*: Serum inter-alpha-trypsin inhibitor and matrix hyaluronan promote angiogenesis in fibrotic lung injury. *American journal of respiratory and critical care medicine* 2008, 178(9):939-947.
126. Swaidani S, Cheng G, Lauer ME, Sharma M, Mikecz K, Hascall VC, Aronica MA: TSG-6 protein is crucial for the development of pulmonary hyaluronan deposition, eosinophilia, and airway hyperresponsiveness in a murine model of asthma. *The Journal of biological chemistry* 2013, 288(1):412-422.
127. Stober VP, Johnson CG, Majors A, Lauer ME, Cali V, Midura RJ, Wisniewski HG, Aronica MA, Garantziotis S: TNF-stimulated gene 6 promotes formation of hyaluronan-inter-alpha-inhibitor heavy chain complexes necessary for ozone-induced airway hyperresponsiveness. *The Journal of biological chemistry* 2017, 292(51):20845-20858.
128. Garantziotis S, Li Z, Potts EN, Kimata K, Zhuo L, Morgan DL, Savani RC, Noble PW, Foster WM, Schwartz DA *et al*: Hyaluronan mediates ozone-induced airway hyperresponsiveness in mice. *The Journal of biological chemistry* 2009, 284(17):11309-11317.
129. Cheng G, Swaidani S, Sharma M, Lauer ME, Hascall VC, Aronica MA: Hyaluronan deposition and correlation with inflammation in a murine ovalbumin model of asthma. *Matrix biology : journal of the International Society for Matrix Biology* 2011, 30(2):126-134.
130. Evanko SP, Potter-Perigo S, Petty LJ, Workman GA, Wight TN: Hyaluronan Controls the Deposition of Fibronectin and Collagen and Modulates TGF-beta1 Induction of Lung Myofibroblasts. *Matrix biology : journal of the International Society for Matrix Biology* 2015, 42:74-92.

131. Li Y, Jiang D, Liang J, Meltzer EB, Gray A, Miura R, Wogensen L, Yamaguchi Y, Noble PW: Severe lung fibrosis requires an invasive fibroblast phenotype regulated by hyaluronan and CD44. *The Journal of experimental medicine* 2011, 208(7):1459-1471.
132. Li Y, Liang J, Yang T, Monterrosa Mena J, Huan C, Xie T, Kurkciyan A, Liu N, Jiang D, Noble PW: Hyaluronan synthase 2 regulates fibroblast senescence in pulmonary fibrosis. *Matrix biology : journal of the International Society for Matrix Biology* 2016, 55:35-48.
133. McDonald B, McAvoy EF, Lam F, Gill V, de la Motte C, Savani RC, Kubes P: Interaction of CD44 and hyaluronan is the dominant mechanism for neutrophil sequestration in inflamed liver sinusoids. *The Journal of experimental medicine* 2008, 205(4):915-927.
134. McDonald B, Jenne CN, Zhuo L, Kimata K, Kubes P: Kupffer cells and activation of endothelial TLR4 coordinate neutrophil adhesion within liver sinusoids during endotoxemia. *American journal of physiology Gastrointestinal and liver physiology* 2013, 305(11):G797-806.
135. Mittal M, Tirupathi C, Nepal S, Zhao YY, Grzych D, Soni D, Prockop DJ, Malik AB: TNFalpha-stimulated gene-6 (TSG6) activates macrophage phenotype transition to prevent inflammatory lung injury. *Proceedings of the National Academy of Sciences of the United States of America* 2016, 113(50):E8151-E8158.
136. Wakahara K, Kobayashi H, Yagyu T, Matsuzaki H, Kondo T, Kurita N, Sekino H, Inagaki K, Suzuki M, Kanayama N *et al*: Bikunin suppresses lipopolysaccharide-induced lethality through down-regulation of tumor necrosis factor- alpha and interleukin-1 beta in macrophages. *J Infect Dis* 2005, 191(6):930-938.
137. Gregory SH, Wing EJ: Neutrophil-Kupffer cell interaction: a critical component of host defenses to systemic bacterial infections. *Journal of leukocyte biology* 2002, 72(2):239-248.
138. Lee RH, Pulin AA, Seo MJ, Kota DJ, Ylostalo J, Larson BL, Semprun-Prieto L, Delafontaine P, Prockop DJ: Intravenous hMSCs improve myocardial infarction in mice because cells embolized in lung are activated to secrete the anti-inflammatory protein TSG-6. *Cell stem cell* 2009, 5(1):54-63.
139. Li C, Li M, Li S, Xing Y, Yang CY, Li A, Borok Z, De Langhe S, Minoo P: Progenitors of secondary crest myofibroblasts are developmentally committed in early lung mesoderm. *Stem cells* 2015, 33(3):999-1012.
140. Maina V, Cotena A, Doni A, Nebuloni M, Pasqualini F, Milner CM, Day AJ, Mantovani A, Garlanda C: Coregulation in human leukocytes of the long pentraxin PTX3 and TSG-6. *Journal of leukocyte biology* 2009, 86(1):123-132.
141. Traktuev DO, Merfeld-Clauss S, Li J, Kolonin M, Arap W, Pasqualini R, Johnstone BH, March KL: A population of multipotent CD34-positive adipose stromal cells share pericyte and mesenchymal surface markers, reside in a periendothelial location, and stabilize endothelial networks. *Circ Res* 2008, 102(1):77-85.
142. Lu H, Poirier C, Cook T, Traktuev DO, Merfeld-Clauss S, Lease B, Petrache I, March KL, Bogatcheva NV: Conditioned media from adipose stromal cells limit lipopolysaccharide-induced lung injury, endothelial hyperpermeability and apoptosis. *J Transl Med* 2015, 13:67.
143. Ni K, Mian MUM, Meador C, Gill A, Bawrinska D, Cao D, Justice MJ, Jiang D, Schaefer N, Schweitzer KS *et al*: Oncostatin M and TNF-a induce alpha-1 antitrypsin production in undifferentiated adipose stromal cells. *Stem Cell and Development* 2017.

144. Wisniewski HG, Colon E, Liublinska V, Karia RJ, Stabler TV, Attur M, Abramson SB, Band PA, Kraus VB: TSG-6 activity as a novel biomarker of progression in knee osteoarthritis. *Osteoarthritis and cartilage / OARS, Osteoarthritis Research Society* 2014, 22(2):235-241.
145. Mould KJ, Barthel L, Mohning MP, Thomas SM, McCubbrey AL, Danhorn T, Leach SM, Fingerlin TE, O'Connor BP, Reisz JA *et al*: Cell Origin Dictates Programming of Resident versus Recruited Macrophages during Acute Lung Injury. *American journal of respiratory cell and molecular biology* 2017, 57(3):294-306.
146. Vaure C, Liu Y: A comparative review of toll-like receptor 4 expression and functionality in different animal species. *Front Immunol* 2014, 5:316.
147. Cannon JG, Tompkins RG, Gelfand JA, Michie HR, Stanford GG, van der Meer JW, Endres S, Lonnemann G, Corsetti J, Chernow B *et al*: Circulating interleukin-1 and tumor necrosis factor in septic shock and experimental endotoxin fever. *J Infect Dis* 1990, 161(1):79-84.
148. O'Connell KE, Mikkola AM, Stepanek AM, Vernet A, Hall CD, Sun CC, Yildirim E, Staropoli JF, Lee JT, Brown DE: Practical murine hematopathology: a comparative review and implications for research. *Comp Med* 2015, 65(2):96-113.
149. Vigetti D, Genasetti A, Karousou E, Viola M, Moretto P, Clerici M, Deleonibus S, De Luca G, Hascall VC, Passi A: Proinflammatory cytokines induce hyaluronan synthesis and monocyte adhesion in human endothelial cells through hyaluronan synthase 2 (HAS2) and the nuclear factor-kappaB (NF-kappaB) pathway. *The Journal of biological chemistry* 2010, 285(32):24639-24645.
150. Qi Y, Jiang D, Sindrilaru A, Stegemann A, Schatz S, Treiber N, Rojewski M, Schrezenmeier H, Vander Beken S, Wlaschek M *et al*: TSG-6 released from intradermally injected mesenchymal stem cells accelerates wound healing and reduces tissue fibrosis in murine full-thickness skin wounds. *The Journal of investigative dermatology* 2014, 134(2):526-537.
151. Choi H, Lee RH, Bazhanov N, Oh JY, Prockop DJ: Anti-inflammatory protein TSG-6 secreted by activated MSCs attenuates zymosan-induced mouse peritonitis by decreasing TLR2/NF-kappaB signaling in resident macrophages. *Blood* 2011, 118(2):330-338.
152. Lauer ME, Loftis J, de la Motte C, Hascall VC: Analysis of the heavy-chain modification and TSG-6 activity in pathological hyaluronan matrices. *Methods in molecular biology* 2015, 1229:543-548.
153. Cavaleri FM, Balbach ST, Gentile L, Jauch A, Bohm-Steuer B, Han YM, Scholer HR, Boiani M: Subsets of cloned mouse embryos and their non-random relationship to development and nuclear reprogramming. *Mech Dev* 2008, 125(1-2):153-166.
154. Li Q, Pangas SA, Jorgez CJ, Graff JM, Weinstein M, Matzuk MM: Redundant roles of SMAD2 and SMAD3 in ovarian granulosa cells in vivo. *Mol Cell Biol* 2008, 28(23):7001-7011.
155. Cheng G, Swaidani S, Sharma M, Lauer ME, Hascall VC, Aronica MA: Correlation of hyaluronan deposition with infiltration of eosinophils and lymphocytes in a cockroach-induced murine model of asthma. *Glycobiology* 2013, 23(1):43-58.
156. Ouyang X, Panetta NJ, Talbott MD, Payumo AY, Halluin C, Longaker MT, Chen JK: Hyaluronic acid synthesis is required for zebrafish tail fin regeneration. *PLoS one* 2017, 12(2):e0171898.

157. Forteza RM, Casalino-Matsuda SM, Falcon NS, Valencia Gattas M, Monzon ME: Hyaluronan and layilin mediate loss of airway epithelial barrier function induced by cigarette smoke by decreasing E-cadherin. *The Journal of biological chemistry* 2012, 287(50):42288-42298.
158. Bhilocha S, Amin R, Pandya M, Yuan H, Tank M, LoBello J, Shytuhina A, Wang W, Wisniewski HG, de la Motte C *et al*: Agarose and polyacrylamide gel electrophoresis methods for molecular mass analysis of 5- to 500-kDa hyaluronan. *Analytical biochemistry* 2011, 417(1):41-49.
159. Yuan H, Amin R, Ye X, de la Motte CA, Cowman MK: Determination of hyaluronan molecular mass distribution in human breast milk. *Analytical biochemistry* 2015, 474:78-88.
160. Schindelin J, Arganda-Carreras I, Frise E, Kaynig V, Longair M, Pietzsch T, Preibisch S, Rueden C, Saalfeld S, Schmid B *et al*: Fiji: an open-source platform for biological-image analysis. *Nat Methods* 2012, 9(7):676-682.
161. Lange DA, Jennings HM, Shah SP: Analysis of surface roughness using confocal microscopy. *Journal of Materials Science* 1993, 28(14):3879-3884.
162. Chinga G, Johnsen PO, Dougherty R, Berli EL, Walter J: Quantification of the 3D microstructure of SC surfaces. *J Microsc* 2007, 227(Pt 3):254-265.
163. Haserodt S, Aytakin M, Dweik RA: A comparison of the sensitivity, specificity, and molecular weight accuracy of three different commercially available Hyaluronan ELISA-like assays. *Glycobiology* 2011, 21(2):175-183.
164. Culty M, Nguyen HA, Underhill CB: The hyaluronan receptor (CD44) participates in the uptake and degradation of hyaluronan. *J Cell Biol* 1992, 116(4):1055-1062.
165. Dyer DP, Thomson JM, Hermant A, Jowitt TA, Handel TM, Proudfoot AE, Day AJ, Milner CM: TSG-6 inhibits neutrophil migration via direct interaction with the chemokine CXCL8. *Journal of immunology* 2014, 192(5):2177-2185.
166. Dyer DP, Salanga CL, Johns SC, Valdambriini E, Fuster MM, Milner CM, Day AJ, Handel TM: The Anti-inflammatory Protein TSG-6 Regulates Chemokine Function by Inhibiting Chemokine/Glycosaminoglycan Interactions. *The Journal of biological chemistry* 2016, 291(24):12627-12640.
167. Reber LL, Gillis CM, Starkl P, Jonsson F, Sibilano R, Marichal T, Gaudenzio N, Berard M, Rogalla S, Contag CH *et al*: Neutrophil myeloperoxidase diminishes the toxic effects and mortality induced by lipopolysaccharide. *The Journal of experimental medicine* 2017, 214(5):1249-1258.
168. Kolls JK, Lei D, Nelson S, Summer WR, Greenberg S, Beutler B: Adenovirus-mediated blockade of tumor necrosis factor in mice protects against endotoxic shock yet impairs pulmonary host defense. *J Infect Dis* 1995, 171(3):570-575.
169. Wagner JG, Roth RA: Neutrophil migration during endotoxemia. *Journal of leukocyte biology* 1999, 66(1):10-24.
170. Jiang D, Liang J, Fan J, Yu S, Chen S, Luo Y, Prestwich GD, Mascarenhas MM, Garg HG, Quinn DA *et al*: Regulation of lung injury and repair by Toll-like receptors and hyaluronan. *Nature medicine* 2005, 11(11):1173-1179.
171. Liang J, Zhang Y, Xie T, Liu N, Chen H, Geng Y, Kurkciyan A, Mena JM, Stripp BR, Jiang D *et al*: Hyaluronan and TLR4 promote surfactant-protein-C-positive alveolar progenitor cell renewal and prevent severe pulmonary fibrosis in mice. *Nature medicine* 2016, 22(11):1285-1293.
172. Bell TJ, Brand OJ, Morgan DJ, Salek-Ardakani S, Jagger C, Fujimori T, Cholewa L, Tilakaratna V, Ostling J, Thomas M *et al*: Defective lung function following influenza virus is due to prolonged, reversible hyaluronan synthesis. *Matrix biology : journal of the International Society for Matrix Biology* 2018.

173. Ormiston ML, Slaughter GR, Deng Y, Stewart DJ, Courtman DW: The enzymatic degradation of hyaluronan is associated with disease progression in experimental pulmonary hypertension. *American journal of physiology Lung cellular and molecular physiology* 2010, 298(2):L148-157.
174. Greenwald RA, Moy WW: Effect of oxygen-derived free radicals on hyaluronic acid. *Arthritis and rheumatism* 1980, 23(4):455-463.
175. Michishita E, Garces G, Barrett JC, Horikawa I: Upregulation of the KIAA1199 gene is associated with cellular mortality. *Cancer Lett* 2006, 239(1):71-77.
176. Pure E, Cuff CA: A crucial role for CD44 in inflammation. *Trends Mol Med* 2001, 7(5):213-221.
177. Brown KL, Maiti A, Johnson P: Role of sulfation in CD44-mediated hyaluronan binding induced by inflammatory mediators in human CD14(+) peripheral blood monocytes. *Journal of immunology* 2001, 167(9):5367-5374.
178. Katoh S, Miyagi T, Taniguchi H, Matsubara Y, Kadota J, Tominaga A, Kincade PW, Matsukura S, Kohno S: Cutting edge: an inducible sialidase regulates the hyaluronic acid binding ability of CD44-bearing human monocytes. *Journal of immunology* 1999, 162(9):5058-5061.
179. Teder P, Heldin P: Mechanism of impaired local hyaluronan turnover in bleomycin-induced lung injury in rat. *American journal of respiratory cell and molecular biology* 1997, 17(3):376-385.
180. Teder P, Vandivier RW, Jiang D, Liang J, Cohn L, Pure E, Henson PM, Noble PW: Resolution of lung inflammation by CD44. *Science* 2002, 296(5565):155-158.
181. Ni K, Gill A, Cao D, Koike K, Schweitzer KS, Garantziotis S, Petrache I: Intravascular heavy chain-modification of hyaluronan during endotoxic shock. *Biochem Biophys Rep* 2019, 17:114-121.
182. Deitch EA: Animal models of sepsis and shock: a review and lessons learned. *Shock* 1998, 9(1):1-11.
183. Souza DG, Vieira AT, Soares AC, Pinho V, Nicoli JR, Vieira LQ, Teixeira MM: The essential role of the intestinal microbiota in facilitating acute inflammatory responses. *Journal of immunology* 2004, 173(6):4137-4146.
184. Honda M, Kubes P: Neutrophils and neutrophil extracellular traps in the liver and gastrointestinal system. *Nat Rev Gastroenterol Hepatol* 2018, 15(4):206-221.
185. Lee TH, Wisniewski HG, Klampfer L, Klampfer L, Oppenheim JD, Vilcek J: TSG-6: A Novel Secretory Protein Inducible by Tumor Necrosis Factor or Interleukin-1 in Fibroblasts and Mononuclear Cells. In: *Tumor Necrosis Factor: Molecular and Cellular Biology and Clinical Relevance*. edn. Edited by Fiers W, Buurman WA. Basel: Karger; 1993: 90-95.
186. Day AJ, de la Motte CA: Hyaluronan cross-linking: a protective mechanism in inflammation? *Trends in immunology* 2005, 26(12):637-643.
187. Kasper M, Gunthert U, Dall P, Kayser K, Schuh D, Haroske G, Muller M: Distinct expression patterns of CD44 isoforms during human lung development and in pulmonary fibrosis. *American journal of respiratory cell and molecular biology* 1995, 13(6):648-656.
188. Svee K, White J, Vaillant P, Jessurun J, Roongta U, Krumwiede M, Johnson D, Henke C: Acute lung injury fibroblast migration and invasion of a fibrin matrix is mediated by CD44. *The Journal of clinical investigation* 1996, 98(8):1713-1727.
189. Mohamadzadeh M, DeGrendele H, Arizpe H, Estess P, Siegelman M: Proinflammatory stimuli regulate endothelial hyaluronan expression and CD44/HA-dependent primary adhesion. *The Journal of clinical investigation* 1998, 101(1):97-108.

190. Lauer ME, Glant TT, Mikecz K, DeAngelis PL, Haller FM, Husni ME, Hascall VC, Calabro A: Irreversible heavy chain transfer to hyaluronan oligosaccharides by tumor necrosis factor-stimulated gene-6. *The Journal of biological chemistry* 2013, 288(1):205-214.
191. Parish CR: The role of heparan sulphate in inflammation. *Nature reviews Immunology* 2006, 6(9):633-643.
192. Haeger SM, Yang Y, Schmidt EP: Heparan Sulfate in the Developing, Healthy, and Injured Lung. *American journal of respiratory cell and molecular biology* 2016, 55(1):5-11.
193. Wang L, Fuster M, Sriramarao P, Esko JD: Endothelial heparan sulfate deficiency impairs L-selectin- and chemokine-mediated neutrophil trafficking during inflammatory responses. *Nat Immunol* 2005, 6(9):902-910.
194. Kida D, Yoneda M, Miyaura S, Ishimaru T, Yoshida Y, Ito T, Ishiguro N, Iwata H, Kimata K: The SHAP-HA complex in sera from patients with rheumatoid arthritis and osteoarthritis. *J Rheumatol* 1999, 26(6):1230-1238.
195. Shen L, Zhuo L, Okumura A, Ishikawa T, Miyachi M, Owa Y, Ishizawa T, Sugiura N, Nagata Y, Nonami T *et al*: The SHAP-hyaluronan complex in serum from patients with chronic liver diseases caused by hepatitis virus infection. *Hepato Res* 2006, 34(3):178-186.
196. Metsios GS, Stavropoulos-Kalinoglou A, Sandoo A, van Zanten JJ, Toms TE, John H, Kitas GD: Vascular function and inflammation in rheumatoid arthritis: the role of physical activity. *Open Cardiovasc Med J* 2010, 4:89-96.
197. Iwakiri Y, Shah V, Rockey DC: Vascular pathobiology in chronic liver disease and cirrhosis - current status and future directions. *J Hepatol* 2014, 61(4):912-924.
198. Doerschuk CM, Tasaka S, Wang Q: CD11/CD18-dependent and -independent neutrophil emigration in the lungs: how do neutrophils know which route to take? *American journal of respiratory cell and molecular biology* 2000, 23(2):133-136.
199. Phillipson M, Kubes P: The neutrophil in vascular inflammation. *Nature medicine* 2011, 17(11):1381-1390.
200. Silvestre-Roig C, Hidalgo A, Soehnlein O: Neutrophil heterogeneity: implications for homeostasis and pathogenesis. *Blood* 2016, 127(18):2173-2181.

Curriculum vitae

Kevin Chen Ni

Education

2012-2021	Indiana University	M.D. (in progress)
2014-2019	Indiana University	Ph.D.: Biochemistry Minor: Life Sciences
2007-2012	Harvard University	A.B.: Chemical and Physical Biology Foreign language citation: Spanish

Peer-reviewed publications

1. **Ni K**, Serban KA, Batra C, and Petrache I. Alpha-1 Antitrypsin Investigations Using Animal Models of Emphysema. *Annals of the American Thoracic Society*, 13 Suppl 4 (2016) S311-316.
2. **Ni K**, Mukhtar MU, Meador C, Gill A, Cao D, Justice MJ, Schweitzer KS, March KL, Petrache I. Proinflammatory stimuli induce functional A1AT expression and secretion in adipose stem cells. *Stem Cells and Development*, 26 (2017) 1468-1476.
3. **Ni K**, Gill A, Tseng V, Mikosz AM, Koike K, Beatman EL, Xu CY, Cao D, Gally F, Mould KJ, Serban KA, Schweitzer KS, March KL, Janssen WJ, Grayck EN, Garantziotis S, Petrache I. Rapid clearance of heavy chain-modified hyaluronan during resolving acute lung injury. *Respiratory Research*, 19 (2018) 107.
4. Koike K, Beatman EL, Schweitzer KS, Justice MJ, Mikosz AM, **Ni K**, Clauss MA, and Petrache I. Subcutaneous administration of neutralizing antibodies to endothelial monocyte-activating protein II attenuates cigarette smoke-induced lung injury in mice. *American journal of physiology. Lung cellular and molecular physiology*, 316 (2019) L558-L566.
5. **Ni K**, Gill A, Cao D, Koike K, Schweitzer KS, Garantziotis S, Petrache I. Intravascular heavy chain-modification of hyaluronan during endotoxic shock. *Biochemistry and Biophysics Reports*, 17 (2019) 114-121.
6. Tseng V, Prohaska C, **Ni K**, Hernandez-Lagunas L, Elajaili H, Cali V, Midura R, Hascall V, Petrache I, and Grayck EN. Hypoxic pulmonary hypertension involves early vascular hyaluronan remodeling regulated by extracellular superoxide dismutase. Manuscript submitted to *FASEB J*.

Awards

2006	Martin Luther King Jr. Youth Leadership Award, University of Utah
2007	US Presidential Scholar
2007	International Summer Science Institute Summer Research Fellow, Weizmann Institute
2008	Harvard Life Sciences and Culture in Bonn Summer Research Fellow, University of Bonn
2010	Pechet Family Award for summer research, Harvard University, MA
2010	Harvard College Research Program (HCRP) Fellow, Harvard University, MA
2011	Pechet Family Award for summer research, Harvard University, MA

- 2012 Program for Research in Science and Engineering (PRISE) Fellow, Harvard University, MA
- 2012 Foreign Language Citation in Spanish, Harvard University, MA
- 2012 Senior thesis with recommendation for highest honors, Harvard University, MA
- 2012 A.B. *cum laude* in Chemical Physical Biology, Harvard University, MA
- 2013 Lois Letzter Fellowship for outstanding MD/PhD student, IU School of Medicine, IN
- 2016 T32 Fellowship Training program in Lung Disease, IU School of Medicine, IN
- 2017 Amer. Assn. of Immunologists (AAI) Young Investigator Award, Colorado Immunology Retreat
- 2018 F30 NRSA/Predocctoral Fellowship (NHLBI), 1F30HL136169-01A1

Teaching and research mentoring

- 2011 Facilitator, Life Sci 1a (Introduction to Life Sciences), Harvard University
- 2011 Teaching Fellow in Statistics, Stat 104 (Introduction to Quantitative Methods for Economics), Harvard University
- 2015 Supervised a MD (international medical graduate, currently pediatric critical care fellow), Indiana University. Co-author on one publication.
- 2015 Supervised a high school student, Indiana University. Co-author on one publication.
- 2016 Supervised a UC Denver undergraduate (University Honors and Leadership research experience), National Jewish Health.
- 2016-2018 Supervised a UC Denver BA/BS-MD undergraduate (BA/BS-MD Longitudinal Experiential research experience), National Jewish Health. Co-author on three publications.

Presentations

1. Role of TSG-6 during acute lung injury. American Thoracic Society Student Scholar Program, 3 Minute Thesis (3MT) Competition, May 20, 2018.

Published abstracts (2018-present)

1. Schweitzer KS, **Ni K**, Petrache I. Crosstalk Between Tetraspanin-Interacting Protein Igsf3 and Sphingolipid Metabolism. Poster at Experimental Biology, April 2018.
2. **Ni K**, Gill A, March KL, Petrache I. Lung Cell Origin of Endogenous TSG-6 Secretion in Response to Inflammatory Stimuli. Poster at American Thoracic Society, May 2018.
3. Beatman E, **Ni K**, Koike K, Berdyshev EV, Bronova IA, Schweitzer KS, Petrache I. Targeting Sphingosine-1-Phosphate (S1P) Lyase to Reduce Lung Injury Following Cigarette Smoke Exposure. Poster at American Thoracic Society, May 2018.
4. Scruggs A, Beatman E, **Ni K**, Koike K, Cao D, Berdyshev EV, Bronova IA, Schweitzer KS, Petrache I. Enzymatic Control of Lung Sphingosine-1 Phosphate

(S1P) During Cigarette Smoke Exposure. Poster at American Thoracic Society, May 2018.

5. Tseng V, **Ni K**, Prohaska C, Trumpie A, Hernandez A, Maltzahn J, Midura R, Petrache I, Grayck EN. Vascular Hyaluronan Remodeling and Regulation of Lung Hyaluronidases in Hypoxic Pulmonary Hypertension. Poster at American Thoracic Society, May 2018.
6. Prohaska C, Tseng V, Allawzi A, Haeger S, **Ni K**, Linhardt RJ, Petrache I, Schmidt EP, Grayck EN. Hyaluronan Shedding and Clearance During Experimental Sepsis and Acute Lung Injury. Poster at American Thoracic Society, May 2018.